

RESILIENT MODULUS AND DYNAMIC POISSON'S RATIO
OF ASPHALTIC CONCRETE MIXES

RESILIENT MODULUS AND DYNAMIC POISSON'S RATIO
OF ASPHALTIC CONCRETE MIXES

by

MICHAEL A. LEE, B.ENG.

A Thesis

Submitted to the Faculty of Graduate Studies
in Partial Fulfilment of the Requirements
for the Degree
Master of Engineering

MCMASTER UNIVERSITY

HAMILTON, ONTARIO


CANADA

DECEMBER 1976

MASTER OF ENGINEERING (1976)
(CIVIL ENGINEERING)

McMASTER UNIVERSITY
HAMILTON, ONTARIO

TITLE: RESILIENT MODULUS AND DYNAMIC POISSON'S
RATIO OF ASPHALTIC CONCRETE MIXES

AUTHOR:  MICHAEL A. LEE, B.ENG. (McMASTER
UNIVERSITY)

SUPERVISOR: DR. JOHN J. EMERY

NUMBER OF PAGES: xii, 128

ABSTRACT

Increased interest in rational approaches to flexible pavement design, rather than the usual empirical methods, has brought about an urgent need for a better understanding of the material properties involved. In this study, laboratory equipment capable of providing reliable measurements of the material properties for asphaltic concrete mixes, under variable stress and temperature conditions has been developed. The basic material properties obtained from these measurements are the resilient modulus (M_R) and dynamic Poisson's ratio (ν), which are the required inputs for the elastic analysis of flexible pavement structures.

Tests have indicated that temperature is the main parameter affecting the resilient modulus of asphaltic concrete mixes, with deviator stress and confining pressure secondary in effect. Based on tests performed on a few samples, the dynamic Poisson's ratio was found to increase with temperature from about 0.24 at 10°C (50°F) to approximately 0.46 at 42°C (108°F). Confining pressure was found to have little or no effect on the dynamic ν .

Analysis using a linear elastic flexible pavement computer programme has indicated a significant reduction in M_R by using a mix with

a higher M_R value. This demonstrates the advantage of utilizing the structural analysis approach to flexible pavement design for more efficient use of materials.

ACKNOWLEDGEMENTS

I wish to express my sincere gratitude to Dr. John J. Emery for his careful guidance and encouragement throughout the course of this research.

I am grateful to Mr. W. Sherriff and Mr. R. Winterle for their help in the construction of the equipment. The careful preparation of this text by Miss D. Pitkin is also gratefully acknowledged.

Finally, a special thank you to my family for their encouragement and support throughout my education at McMaster University.

| | Page |
|--|------|
| Acknowledgements | v |
| Table of Contents | vi |
| List of Figures | ix |
| List of Tables | xii |
| Chapter 1 Introduction | |
| 1.1 Purpose and Scope | 1 |
| 1.2 Current Methods of Flexible Pavement Design | 3 |
| 1.3 Flexible Pavement Distress Modes and Indicators | 7 |
| 1.4 Design Using the Structural Approach | 8 |
| 1.5 Summary of Objectives | 15 |
| Chapter 2 Theoretical Considerations | |
| 2.1 Resilient Modulus by the Diametral Method | 16 |
| 2.2 Poisson's Ratio by Direct Compression Tests | 26 |
| 2.3 Parameters for Test Programme | |
| 2.3.1 Vertical and Horizontal Stress Levels for Testing | 28 |
| 2.3.2 Pulse Time for Repeated Loading | 36 |
| 2.3.3 Pulse Shapes for Repeated Loading | 38 |
| 2.3.4 Temperature Levels for Testing | 39 |
| Chapter 3 Test Equipment and Procedures | |
| 3.1 Apparatus Development | |
| 3.1.1 General Layout | 40 |
| | 42 |

| | | | |
|-----------|-------|--|-----|
| | 3.1.3 | Poisson's Ratio Measuring Device | 46 |
| | 3.1.4 | Temperature Control | 50 |
| | 3.1.5 | Confining Pressure Control | 54 |
| | 3.1.6 | Axial Load Control | 56 |
| | 3.1.7 | Monitoring and Recording of Output Signals | 58 |
| | 3.2 | Calibration of Equipment | 64 |
| | 3.3 | Sample Preparation | 68 |
| | 3.4 | Equipment Operation | 70 |
| Chapter 4 | | Experimental Findings | |
| | 4.1 | Asphalt Mix Designs for Test Programme | 75 |
| | 4.2 | Effect of Varying Diametral Stress on M_R | 76 |
| | 4.3 | Effect of Varying Temperature on M_R | 80 |
| | 4.4 | Effect of Varying Confining Pressure on M_R | 90 |
| | 4.5 | Effect of Varying Temperature on Dynamic v | 95 |
| | 4.6 | Effect of Varying Confining Pressure on Dynamic v | 95 |
| Chapter 5 | | Influence of Asphaltic Concrete M_R and v on Rational Flexible Pavement Designs | |
| | 5.1 | Preliminary Design Considerations | 98 |
| | 5.2 | Limiting Stress and Strain Conditions | |
| | 5.2.1 | Tensile Strain at Bottom of Lowest Asphalt Cement Bound Layer | 101 |
| | 5.2.2 | Compressive Strain at Top of the Subgrade | 102 |
| | 5.2.3 | Horizontal Tensile Stress at the Bottom of the Unbound Layer | 102 |
| | 5.3 | Computer Runs Comparing Designs for Various Mixes | 103 |

| | | |
|------------|---|-----|
| Chapter 6 | Conclusions | 105 |
| References | | 108 |
| Appendix A | Computer Programme for Calculating DELA and DELB | 114 |
| Appendix B | Electrical Circuit Diagrams | 115 |
| Appendix C | Testing Programme and Physical Charact- eristics of Asphaltic Concrete Mixes | 120 |

LIST OF FIGURES

| Number | | Page |
|--------|---|------|
| 1.1 | Typical Flexible Pavement Section | 4 |
| 1.2 | Three-Layer Flexible Pavement System Showing Governing Conditions | 11 |
| 1.3 | Flow Diagram of Typical Structural Design System for Flexible Pavements | 13 |
| 1.4 | Load Equivalency Factors for Loads Equal to or Greater than 10K | 14 |
| 2.1 | The Indirect Tensile Test | 17 |
| 2.2 | Stress Distributions on X-Axis | 19 |
| 2.3 | Notation for Polar Stress Components in a Circular Element Compressed by Short Strip Loadings | 23 |
| 2.4 | Measurements for Determination of Poisson's Ratio | 27 |
| 2.5 | Single Wheel Loadings for Boussinesq and Chevron Calculations | 31 |
| 2.6 | Dual Wheel Loading for 'Bistro' Calculations | 35 |
| 2.7a | Relationship Between Loading Time and Depth for Various Vehicle Speeds | 37 |
| 2.7b | Relationship Between Mean Loading Time and Thickness of Asphaltic Concrete Layer for Various Vehicle Speeds | 37 |
| 3.1 | General Schematic of Equipment | 41 |
| 3.2 | General Layout of Equipment | 43 |
| 3.3 | Resilient Modulus Measuring Device | 44 |
| 3.4 | Specimen Mounted in Resilient Modulus Device | 47 |
| | Poi Ra Dev | 48 |

| Number | | Page |
|--------|---|------|
| 3.6 | Specimen Mounted in Poisson's Ratio Device | 51 |
| 3.7 | Temperature Control System | 52 |
| 3.8 | Confining Pressure Control System | 55 |
| 3.9 | Axial Load Control System | 57 |
| 3.10 | Monitoring of Axial Load | 60 |
| 3.11 | Data Acquisition System | 63 |
| 3.12 | Calibration of Resilient Modulus Strain Gauge | 66 |
| 3.13 | Triaxial Apparatus Showing Final Connections before Testing | 71 |
| 4.1 | M_R - Diametral Stress Relationship | 81 |
| 4.2 | Relationship Between M_R and Temperature for HM-3 (Steel Slag) and HM-3 (Limestone) Mixes | 82 |
| 4.3 | Relationship Between M_R and Temperature for Steel Slag (OH-STELCO) Mixes | 83 |
| 4.4 | Relationship Between M_R and Temperature for HM-3 Mixes | 84 |
| 4.5 | Relationship Between M_R and Temperature for HM-5 Mixes | 85 |
| 4.6 | Relationship Between M_R and Temperature for Type C Field Mix | 86 |
| 4.7 | Comparison of M_R - Temperature Relationship for HM-3, HM-5, and Steel Slag (OH-STELCO) Mixes for Asphalt Contents Close to Maximum Marshall Designs | 87 |
| 4.8 | $M_R - \sigma_{CON} / (\sigma_{DM} - \sigma_{CON})$ Relationship for HM-3 | |

| Number | | Page |
|--------|--|------|
| 4.9 | $M_R - \sigma_{CON} / (\sigma_{DM} - \sigma_{CON})$ Relationship for Steel Slag (OH-STELCO) Lab Mixes | 92 |
| 4.10 | M_R - Confining Pressure Relationship for HM-5 Mix | 93 |
| 4.11 | $M_R - \sigma_{CON} / (\sigma_{DM} - \sigma_{CON})$ for HM-3, HM-3 (Steel Slag), HM-5, and Steel (OH-STELCO) at 5% AC | 94 |
| 4.12 | Relationship Between Dynamic Poisson's Ratio and Temperature | 96 |
| 5.1 | Temperature Prediction Graph for Pavement Greater than 2 Inches Thick | 99 |
| B.1 | Typical Strain Gauge Cantilever Beam | 116 |
| B.2 | Circuit Diagram for Main and Phase Lab Timers | 117 |
| B.3 | Diagram of Typical Amplifier Circuit for 5-Channel Amplifier | 118 |
| B.4 | Circuit Diagram for Temperature Probe Amplifier | 119 |

LIST OF TABLES

| Number | | Page |
|--------|---|------|
| 2.1 | Stress Distributions for Boussinesq Analysis | 31 |
| 2.2 | Stress Distributions for Chevron Computer Analysis | 33 |
| 2.3 | Stress Distributions for 'Bistro' Computer Analysis | 35 |
| 4.1 | Resilient Moduli of HM-3 and Steel Slag (OH-STELCO) Mixes for Various Diametral Stress Levels | 77 |
| 4.2 | Fitted Straight Line Equations for HM-3 and Steel Slag (OH-STELCO) Mixes | 79 |
| 5.1 | Final Analysis for Hypothetical Design Examples | 104 |
| C.1 | Gradation and Physical Properties of HM-3 Mixes | 121 |
| C.2 | Gradation and Physical Properties of HM-3 (Steel Slag) Mixes | 122 |
| C.3 | Gradation and Physical Properties of Steel Slag (OH-STELCO) Mixes | 123 |
| C.4 | Gradation and Physical Properties of HM-5 Mixes | 124 |
| C.5 | Physical Properties of Type C Mix | 125 |
| C.6 | Testing Programme for Various Asphalt Mixes | 126 |
| C.7 | Typical Calculations for Finding M_R | 127 |
| C.8 | Typical Calculations for Finding v | 128 |

CHAPTER 1

INTRODUCTION

1.1 Purpose and Scope

The rational approach to flexible pavement design is based on treating the layered pavement system as a structure, and replacing previous empirical methods by analytical methods, in which each material's behaviour under traffic loadings and environmental influences is considered. This rational approach has been facilitated by the development of sophisticated computer programmes, typically by large oil companies (1-4), which provide solutions for the stresses and strains in combined pavement structures, based on linear elastic behaviour. These computer programmes require as basic inputs the elastic modulus, Poisson's ratio, and thickness of each layer, including the subgrade properties. Although asphaltic concrete, and soils forming the subgrade display nonlinear and somewhat time-dependent stress-strain characteristics, it is generally considered that linear elastic analysis provides adequate solutions for design purposes (5). While the parameters currently utilized are based on elastic behaviour, the methods developed, and basic data obtained in this study are also applicable to nonlinear approaches.

This study is mainly concerned with the laboratory testing of asphaltic concrete samples to determine their resilient modulus (M_R), and Poisson's ratio (ν) (the two material properties required as programme inputs) under conditions representative of the field environment. These field conditions were simulated by tests conducted in a special triaxial system developed for this study, under controlled temperature and pressure levels, for repeated dynamic loadings. In simple terms, the resilient modulus was determined by means of the diametral tensile test method, that has been adopted previously to study various materials (6-18). While the resilient modulus measuring device is essentially of the same basic design as that developed by Schmidt (6), extensive modifications and additions were necessary. Measurement of lateral deformations were based on a simple strain gauged cantilever beam technique developed by Gonsalves in previous studies at McMaster University and extended in the current study.

Measurements of Poisson's ratio were conducted on specimens using a simple direct compression test technique. The deformation measurements were made using the cantilever beam technique developed for the resilient modulus apparatus. Full details on all of the experimental equipment and techniques are given in the following chapters.

The experimental programme entailed the investigation of the influence of various parameters on the resilient modulus and Poisson's ratio, in particular: (1) vertical

stress; (2) confining pressure; and (3) temperature. Previous studies on asphaltic concrete have indicated that the resilient modulus is highly affected by changes in temperature, and confining pressure (7, 19). The results of these tests on various asphaltic concrete mixes are presented with an evaluation of the fundamental characteristics observed.

This information is then used to examine some typical flexible pavement sections using computer programmes to determine the sensitivity of designs to material properties. It is shown that increased stiffness as given by the resilient modulus can be an advantage since pavement sections can be reduced in design thickness. This should be contrasted with empirical methods where the stiffness is not considered.

1.2 Current Methods of Flexible Pavement Design

Flexible pavements consist of one or more base courses of suitable granular material, with or without asphalt binder, and an asphaltic concrete surfacing (binder course(s) and/or surface course) as shown in Figure 1.1. They are essentially layered systems with little beam strength, and carry the imposed traffic loads by distributing them through the layers which generally decrease in strength and quality with depth. The prime function of the layers is to reduce the load intensity to a level that may be carried safely by the next underlying layer and ultimately by the subgrade.

There are many methods for flexible pavement design, each claiming some "fundamental" criteria as its basis.

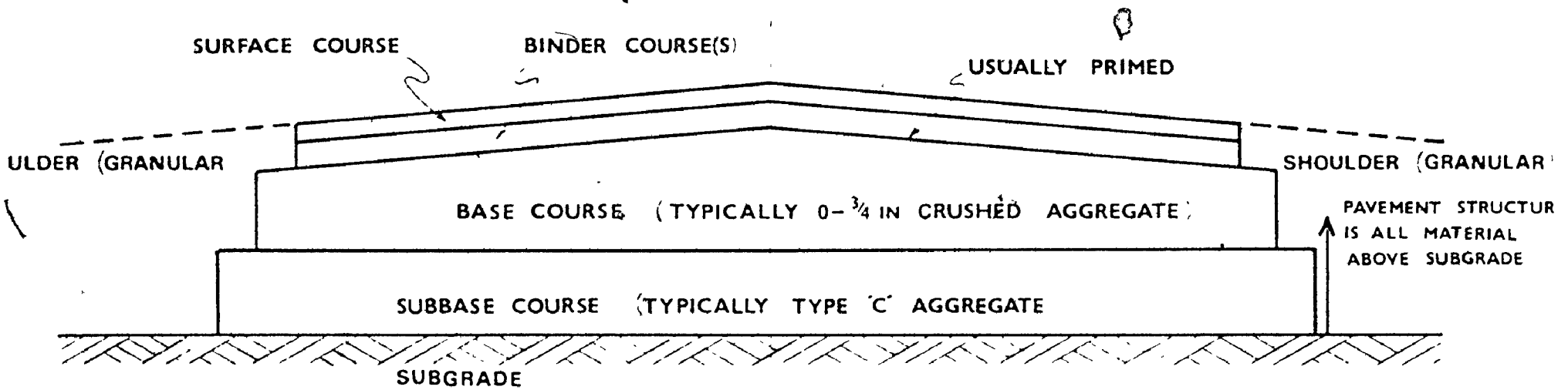


FIGURE 1.1 — TYPICAL FLEXIBLE PAVEMENT SECTION

Some of these have been adapted as standard design procedures by various agencies, however, many remain as scattered information in journals and technical reports. One attempt to group all recognized design methods was undertaken by the Highway Research Board (HRB, now TRB) in 1966 (20). According to this HRB committee, flexible pavement design may be divided into four groups:

- 1) Ultimate strength methods;
- 2) Semi-empirical and statistical methods;
- 3) Empirical and environmental methods; and
- 4) Elasticity methods.

The ultimate strength methods are based on pavement performance at failure. Their main design criterion is that the pavement system must possess an adequate safety factor against shear failure. Semi-empirical and statistical methods are based almost exclusively upon accumulated experience and on assembled design performance information. These methods have sought credence through statistical analysis of past and existing field test data, using servicibility-performance concepts. Empirical strength tests, such as the Marshall and Hveem methods (21) are frequently used to determine the adequacy of mix designs, however, no theoretical consideration is given to actual pavement mechanics. The empirical and environmental methods are based on the soil characteristics and environmental conditions of the proposed site. No highway material properties apart from those needed for soil classification, are used for estimating the support characteristics of the pavement subgrade.

Elasticity methods are based on predicting the actual deformation behaviour of flexible pavements under expected working and environmental conditions, using layered elastic theories. The basic design procedure involves adjusting layer thicknesses and materials so that certain limiting values of stresses or strains (displacements) at designated points within the pavement are not exceeded. A rational design system adopts such elasticity methods as part of the total design procedure. The rational design concept, developed in recent years, has embraced not only the structural aspects, but also road performance to user relationships and economic considerations. This study is concerned exclusively with the structural design aspects of rational systems.

By far the most widely used design procedures today are the empirical and semi-empirical methods, which are used with some degree of success throughout the world. The continued use of such procedures would be quite satisfactory if we could be assured that traffic, materials, construction, etc. will remain the same. However, conditions are constantly changing, the most dramatic example being a trend towards much heavier axle loadings for more energy efficient and economic commercial transport (22). Rational design systems offer the flexibility to consider such changes, and there is a growing trend to utilize them for both current designs and in management systems for the maintenance of existing road networks (23).

1.3 Flexible Pavement Distress Modes and Indicators

Due to material influences, flexible pavement design is generally a far more complex problem compared to most concrete and steel structural design. Steel and concrete exhibit material properties that are generally homogeneous, isotropic, and relatively stable with time. On the other hand, pavement materials are nonlinear and time-dependent at working stress levels, and their behaviour depends on a number of variables such as: temperature; rate and nature of loading; density; stress history; and stress state. Unlike concrete and steel construction, "servicibility" rather than "sudden catastrophic failure" governs pavement design. Because of these and other inherent differences, a new structural design philosophy must be formulated for flexible pavements.

The successful design of a flexible pavement structure is measured by its actual performance in the field during the expected life. In recent years, the performance has been evaluated using a servicibility-performance concept, similar to that initially developed by Carey and Irick(24). This system assumes that pavements display certain distress modes that can be organized into three main categories: fracture; distortion; and disintegration. In general, disintegration is caused by a reactive aggregate or by poor bonding between aggregate and binder. This is not itself a part of the structural design, and while very important during materials selection, will not be included here.

Fracture and distortion manifest themselves in three different ways: (1) permanent deformation (distortion mode); (2) load induced fatigue cracking (fracture mode); and (3) thermal induced cracking (fracture mode). It should be recognized that permanent deformation is also a fatigue phenomenon, in the sense that it depends on the accumulation of inelastic deflections due to repeated wheel load applications.

The type and severity of pavement failure is dependent on a number of factors, which includes environmental and traffic conditions, as well as the characteristics of local construction materials. For example, in the United Kingdom, failure takes place most commonly in the form of excessive permanent deformation (rutting). On the other hand, in the United States, loss of servicibility is due mainly to fatigue cracking.

1.4 Design Using the Structural Approach

The fundamental structural design procedure adopted in this study was first presented by Brown and Pell (5). This method is based on treating the pavement structure as a layered elastic system, which may be analyzed using available computer programmes (1-4). As indicated previously, the assumption of linear elastic behaviour is adequate for design purposes. This design procedure is similar to a design method developed by the Shell Oil Company (25), except that resilient moduli values are derived from laboratory testing, rather than from the stiffness nomograph suggested by the Shell method (25, 26).

The basis of the Shell nomograph is that mix properties are controlled by the properties of the asphalt binder. The asphalt properties, in turn, are functions of origin, hardness (which includes effects due to aging), rate and duration of loading, and temperature. This method suggests that the stiffness of asphaltic concrete mixes is insensitive to aggregate characteristics, and is influenced only by the volumetric ratio of asphalt to aggregate.

Triaxial testing was used in this study in order to derive the mix characteristics from actual measured responses. Besides providing an alternate and direct method, the laboratory derived values can be used to evaluate the accuracy of the Shell nomograph method. Direct measurements were also desirable, since the Shell nomograph method does not incorporate the influence of confining pressure on the modulus. Another advantage of laboratory testing is that samples or cores from existing pavements may be conveniently tested to investigate aging effects.

The structural approach adapted in this study, like the Shell method, assumes that the flexible pavement structure consists essentially of the three layers:

1. An asphaltic concrete layer or layers;
2. A granular unbound layer or layers; and
3. the subgrade.

In the case of a full depth asphaltic concrete pavement, the granular unbound layer(s) is of course disregarded as it is replaced by asphalt cement bound layers.

In the structural design method, it is generally considered that the critical pavement conditions are (5):

1. The horizontal tensile strain at the bottom of the lowest asphalt cement bound layer;
2. The vertical compressive strain on the surface of the subgrade; and
3. The horizontal tensile stress at the bottom of the unbound base.

The first two criteria are directed towards the fatigue and permanent deformation failure modes, respectively. The third condition is aimed at preventing local "decompaction" and consequent reduction in the effective stiffness of the unbound layer. A typical pavement section, showing these critical points is presented in Figure 1.2.

Laboratory derived fatigue criteria for the tensile strain at the bottom of the asphalt cement bound layer have been developed by Pell (27, 28). This is given in the form of the fitted equation:

$$N_s = K(1/\epsilon_m)^n$$

where N_s = number of applications of equivalent 18 kip (80 kN) load to initiate a fatigue crack.

ϵ_m = maximum induced tensile strain.

n and k = factors depending on the composition of the asphaltic concrete mix.

The vertical subgrade strain criteria can be taken from design charts developed by Dormon and Metcalf (29), using elastic layered system theory. However, a major criticism of these charts is that they do

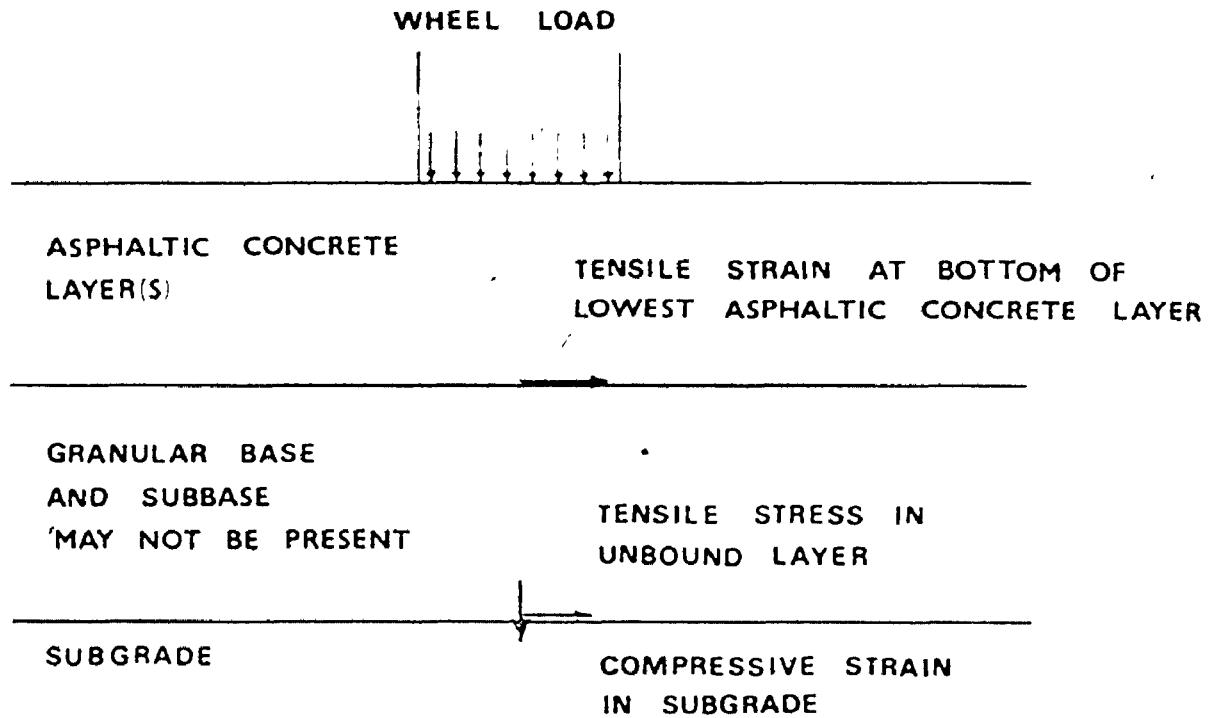


FIGURE 1-2 — THREE-LAYER FLEXIBLE PAVEMENT SYSTEM
SHOWING GOVERNING CONDITIONS

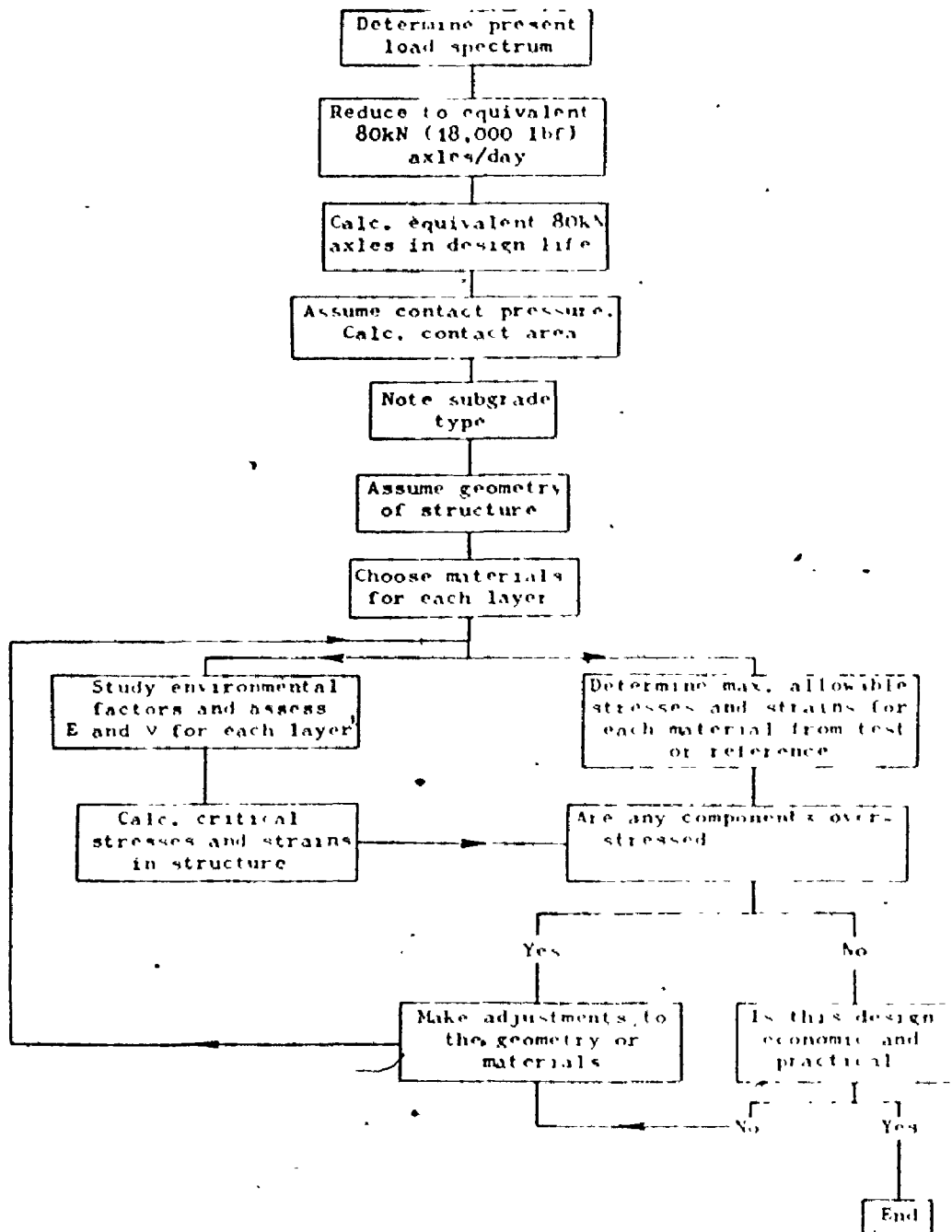
(AFTER REF 25)

age considerations (30).

In the case where a granular unbound layer is used, the horizontal tensile stress design criterion is that it should not exceed 0.5 times the vertical stress plus the horizontal overburden pressure. The horizontal overburden pressure is the stress induced in the horizontal direction by the weight of the material above the point concerned. (5)

The full design procedure, as shown in Figure 1.3, first entails reducing the expected truck loading data to the equivalent 18 kip (80 kN) standard axle load applications using charts such as in Figure 1.4. The next step involves determining the limiting stresses and strains within the pavement for the 18 kip (80 kN) axle load. Analysis of the pavement structure is carried out using a dual wheel arrangement of the 18 kip (80 kN) equivalent axle loading. The pavement is assumed to be statically loaded by two 4,500 lb (20 kN) loads. These are uniformly distributed over 4.23 in (10.74 cm) radius circular areas, located 12 in (30.5 cm) apart centre to centre.

The design is an iterative process as indicated by the flow chart in Figure 1.3, in which the material, and thickness are chosen for each layer, and then analyzed in the combined structure. If the analysis indicates that critical stresses and strains are exceeded, changes are made in layer thickness or materials (or both), until a satisfactory design is achieved. Since an array of alternatives are then available to the designer, economic considerations can readily be incorporated during the selection of the final design.



I OR SIMILAR PROPERTIES SUCH AS M_R AND DYNAMIC ν

FIGURE 1-3 - FLOW DIAGRAM OF TYPICAL STRUCTURAL DESIGN SYSTEM FOR FLEXIBLE PAVEMENTS

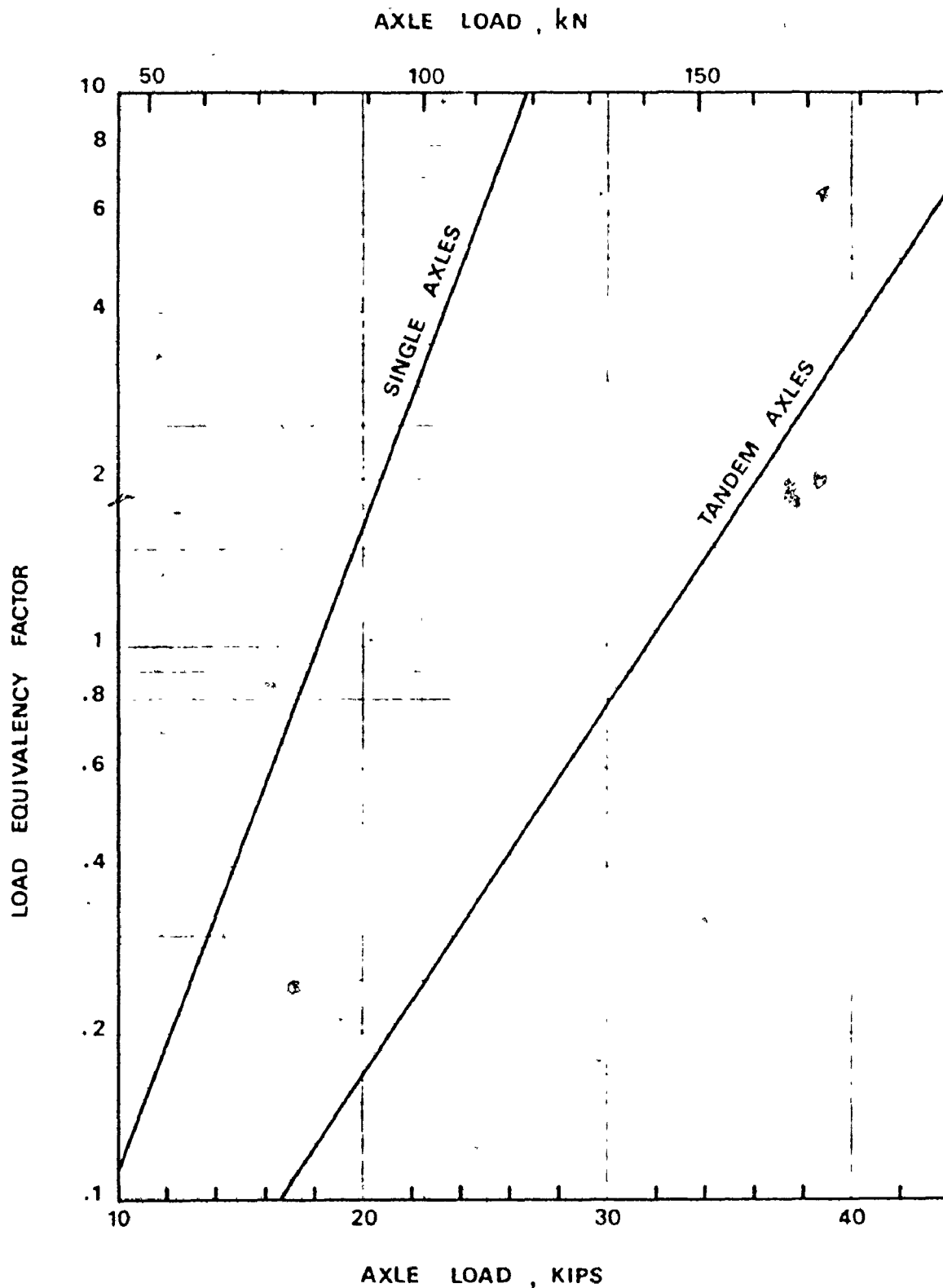


FIGURE 1-4 — LOAD EQUIVALENCY FACTORS FOR LOADS EQUAL TO OR GREATER THAN 10 K (AFTER REF. 31)

At the present time, the determination of material properties for the analysis has not kept up with the ability to perform the actual computations based on theoretical considerations.

1.5 Summary of Objectives

The major purpose of this study is to develop an economic and reliable testing method for, and to determine, the required material characteristics (M_R and ν) for typical asphaltic concrete mixes (City of Hamilton specifications). More specifically, the objective is to investigate the effects on M_R of:

1. confining pressure levels (σ_{CON});
2. diametral stress levels (σ_{DM});
3. temperature;
4. asphalt content; and
5. different aggregate gradation and type.

The effects of the following on the dynamic Poisson's ratio, ν , will also be investigated:

1. confining pressure levels (σ_{CON});
2. temperature; and
3. different aggregate gradation and type.

CHAPTER 2

THEORETICAL CONSIDERATIONS

2.1 Resilient Modulus by the Diametral Method

Development of the indirect tensile test for materials testing is credited to Carniero and Barcellus (16) in Brazil, and Akazawa (17) in Japan. Although originally developed for strength tests on portland cement concrete, this method has been extended to similar tests on asphaltic concrete (10, 11, 14, 15) and lime-soil mixtures (13). Basically, the test entails applying line loads (uniformly distributed loads in practice) to a cylindrical specimen, along two opposite generatrices. Assuming the plane stress condition, it can be shown that a relatively uniform tensile stress results along the diametral plane containing the applied load (32, 33). Failure of the specimen is usually caused by splitting along the loaded plane as indicated in Figure 2.1.

Of particular interest to flexible pavement designers, is the resilient modulus (M_R) which is defined by the equation:

$$M_R = \frac{\sigma_d}{\epsilon_{\text{resil}}}$$

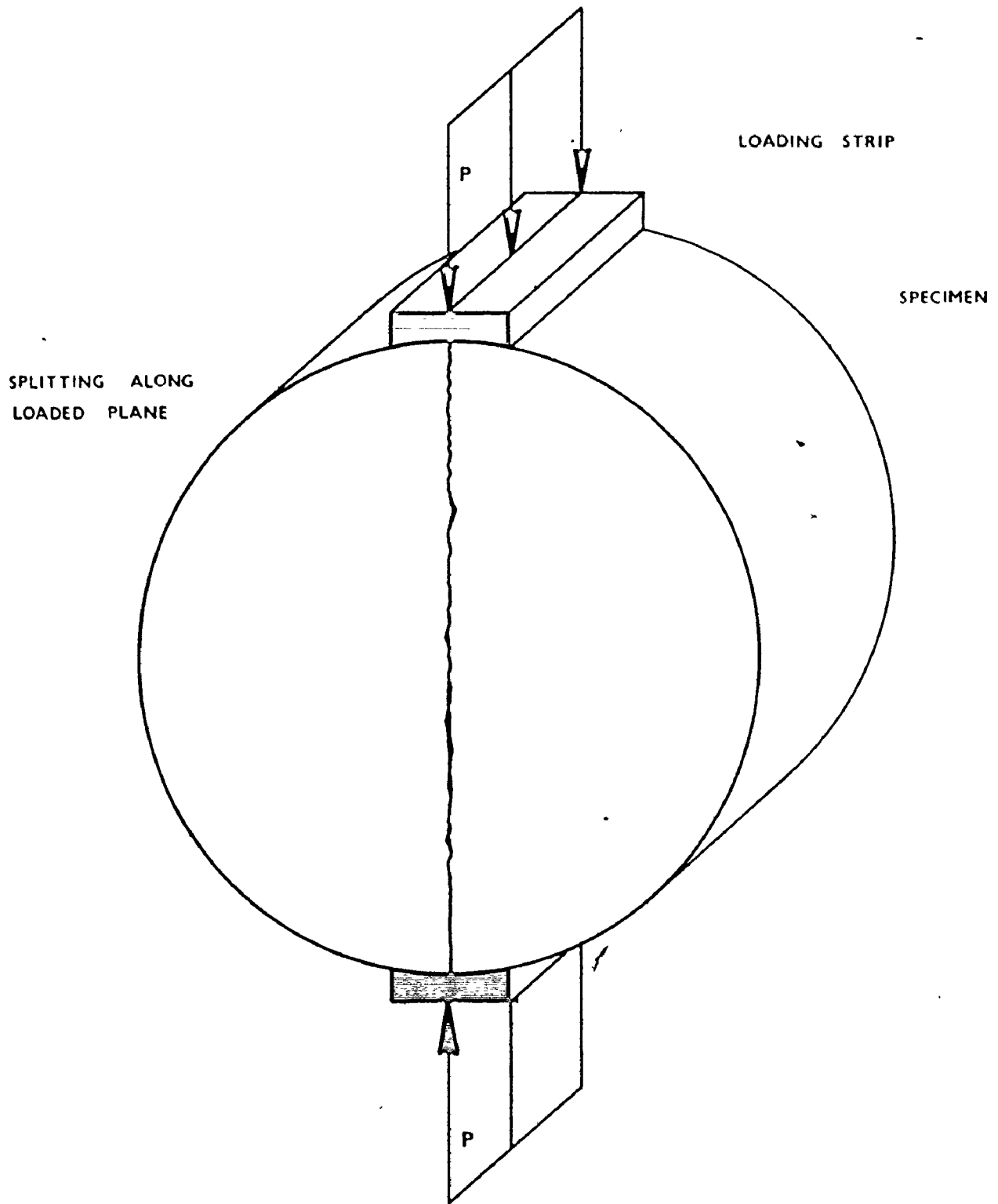


FIGURE 2-1 - THE INDIRECT TENSILE TEST

where

M_R = resilient modulus;

σ_d = repeated axial deviator stress; and

ϵ_{resil} = resilient strain.

Resilient strain is that which is instantaneously recovered after removal of the applied load.

Research by Schmidt (6) has shown that the indirect tensile test is readily adaptable for determining the resilient modulus of asphaltic concrete mixes. This is achieved by applying known repeated loads to the specimen, and measuring the corresponding deformations across the diameter perpendicular to the loading direction. Schmidt (6) developed the equation for M_R using elastic theory and available analytical solutions (32, 33). The stresses across the diameter perpendicular to the loading direction in Figure 2.2 are:

$$\sigma_x = \frac{2P}{\pi t d} \left[\frac{d^2 - 4x^2}{d^2 + 4x^2} \right]^2 \quad (2.1)$$

$$\sigma_y = - \frac{2P}{\pi t d} \left[\frac{4d^4}{(d^2 + 4x^2)^2} - 1 \right] \quad (2.2)$$

where σ_x , σ_y = stresses perpendicular and parallel to direction of loading, respectively;

P = applied load;

t = thickness of cylindrical disc;

d = diameter of disc; and

x = distance along horizontal diameter from centre of disc.

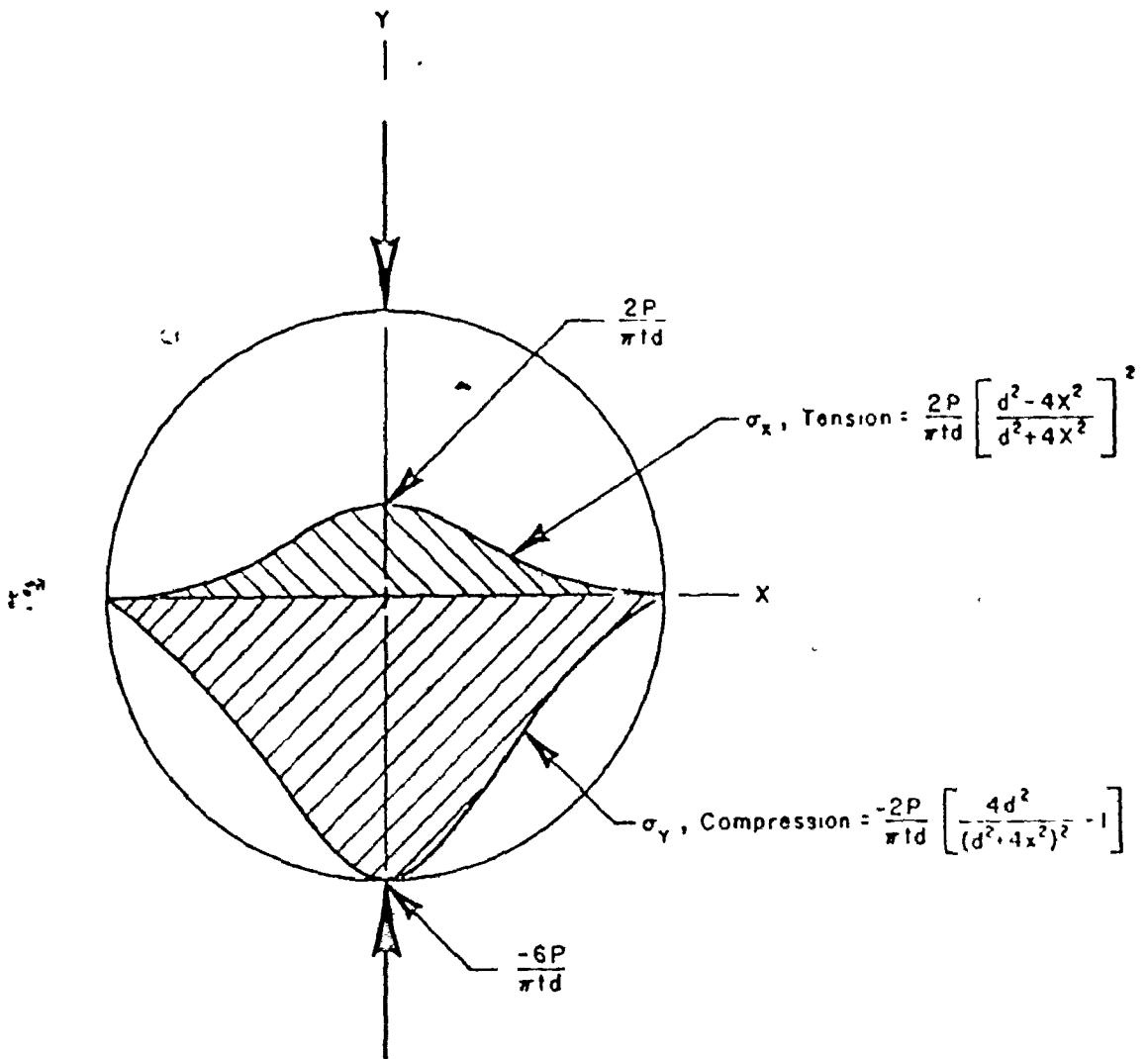


FIGURE 2-2 - STRESS DISTRIBUTIONS ON X-AXIS

(AFTER ")

Assuming plane stress and elastic behaviour, the strain across the horizontal diameter is:

$$\epsilon_x = \frac{1}{E} \left[\sigma_x - \nu \sigma_y \right] \quad (2.3)$$

where: ϵ_x = strain across the horizontal diameter;

E = Young's modulus; and

ν = Poisson's ratio.

Substituting equations (2.1) and (2.2) into equation (2.3) gives:

$$\epsilon_x = \frac{2P}{E\pi t d} \left[\frac{(4d^4 \nu - 16d^2 x^2)}{(d^2 + 4x^2)^2} + (1 - \nu) \right] \quad (2.4)$$

The total deformation across the horizontal diameter is found by integrating the strain, ϵ_x , between the limits $\pm d/2$:

$$\Delta = \int_{-d/2}^{d/2} \epsilon_x dx \quad (2.5)$$

where Δ = total deformation across the diameter. Substituting equation (2.4) into equation (2.5) and integrating yields:

$$\Delta = \frac{P}{tE} \left[(4/\pi) + \nu - 1 \right]$$

or in terms of E :

$$E = \frac{P(\nu + 0.2732)}{t\Delta} \quad (2.6a)$$

It should be noted that equation (2.6a) was derived using elastic theory, and is applicable for both static and dynamic loadings. In the case of viscoelastic materials such as asphaltic concrete, deformations are time dependent, approaching elastic behaviour for asphaltic concrete if the

loading time (pulse) is of short duration. Thus, if the repeated loading time is short enough, equation (2.6a) will apply to asphaltic concrete within the bounds of experimental measurements (6). The apparent Young's modulus, E , is then simply the asphaltic concrete's resilient modulus, M_R , discussed earlier:

$$M_R = \frac{P(\nu + 0.2732)}{t\Delta} \quad (2.6b)$$

These equations are for a point load on a thin disc, which corresponds to a line loading along a generator of the cylinder (Figure 2.2). In actual testing, the load is distributed over an area with an appreciable width through a loading strip to ensure proper load distribution (9-12). As shown below by the writer, moduli found by using equation (2.6b), are very close to those based on solutions which consider the finite width of the loading strip. It should also be recognized that actual specimens are of finite length so that the assumption of plane stress is also an approximation, but very reasonable for the geometries involved (8).

The stress analysis of a circular element subjected to short strip loadings has been given by Hondros (8). Body forces are assumed negligible and the stress distributions for plane stress (disc) and plane strain (cylinder) are identical:

$$\sigma_{rx} = \frac{2P}{\pi at} \left[\frac{(1-r^2/R^2) \sin 2\alpha}{1+(2r^2/R^2) (\cos 2\alpha) + (r^4/R^4)} - \tan^{-1} \left(\frac{(1-r^2/R^2)}{(1+r^2/R^2)} \tan \alpha \right) \right] \quad (2.7)$$

$$\sigma_{\theta x} = - \frac{2P}{\pi a t} \left[\frac{(1-r^2/R^2) \sin 2\alpha}{1+(2r^2/R^2) (\cos 2\alpha) + (r^4/R^4)} + \tan^{-1} \left(\frac{(1-r^2/R^2)}{(1+r^2/R^2)} \tan \alpha \right) \right] \quad (2.8)$$

where the subscript x denotes values on the horizontal diameter. The orientation of these stresses in polar coordinates, and definitions of the terms involved are given in Figure 2.3.

Assuming plane stress and elastic behaviour as in the previous case, the expression for ϵ_x across the horizontal diameter is the same as equation (2.3):

$$\epsilon_x = \frac{1}{E} [\sigma_{rx} - \nu \sigma_{\theta x}] \quad (2.3a)$$

Substituting equations (2.7) and (2.8) into (2.3a) yields:

$$\epsilon_x = \frac{2P}{\pi a t E} \left[\frac{(1-r^2/R^2) \sin 2\alpha}{1+(2r^2/R^2) (\cos 2\alpha) + (r^4/R^4)} (1+\nu) - \tan^{-1} \left(\frac{(1-r^2/R^2)}{(1+r^2/R^2)} \tan \alpha \right) (1-\nu) \right] \quad (2.9)$$

The total lateral deformation is thus given by integrating the strain, ϵ_x , between the limits $\pm R$:

$$\Delta = \int_{-R}^R \epsilon_x dr \quad (2.10)$$

Substituting equation (2.9) into (2.10), completing the integration and solving for E, results in:

$$E = \frac{2P}{\pi a t \Delta} [(1+\nu) (2 \times \text{DELA}) - (1-\nu) (2 \times \text{DELB})] \quad (2.11)$$

where

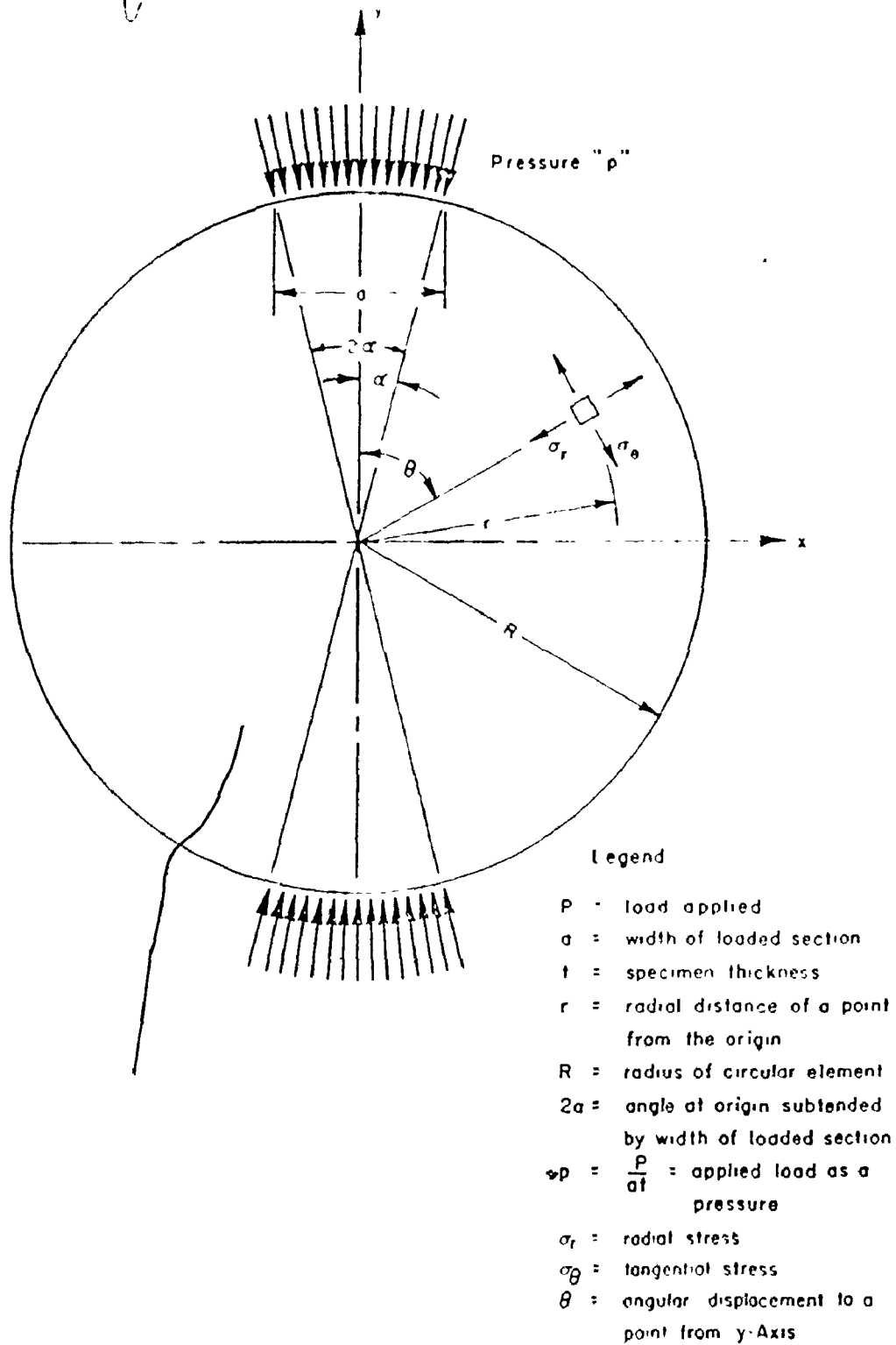


FIGURE 2.3 -NOTATION FOR POLAR STRESS COMPONENTS IN A CIRCULAR ELEMENT COMPRESSED BY SHORT

$$\text{DELA} = \int_0^R \frac{(1-r^2/R^2) \sin 2\alpha \, dr}{1+(2r^2/R^2) \cos 2\alpha + (r^4/R^4)} \quad (2.12)$$

$$\text{DELB} = \int_0^R \tan^{-1} \left(\frac{(1-r^2/R^2)}{(1+r^2/R^2)} \tan \alpha \right) dr \quad (2.13)$$

Due to the relatively complex nature of the integrand, equation (2.11) is written in the above form, which is amenable to numerical integration. Numerical integration of DELA, and DELB, is performed by setting dr as a constant, varying r from zero to R (by constant increments), and then summing all corresponding incremental values. A simple computer programme to perform this tedious summation process is presented in APPENDIX A.

The resilient modulus equipment developed for this study utilized loading strips which were 3/4 in (1.91 cm) wide (ie $a = 3/4$ in). Use of this equipment for testing standard asphaltic concrete Marshall briquettes, measuring 4 inches (10.16 cm) in diameter (ie $R = 2$ in) gives values of DELA and DELB of 0.37061 and 0.21500 respectively. Substituting these values into equation (2.11) yields:

$$M_R = \frac{P}{t\lambda} (0.99416v + 0.26417) \quad (2.11a)$$

In the event that field cores (3.8 inches (9.65 cm) in diameter) from existing pavements are tested, the above values are 0.37013 and 0.21510, and from equation (2.11);

$$M_R = \frac{P}{t\lambda} (0.99353v + 0.26319) \quad (2.11b)$$

By substituting a value of v for asphaltic concrete of 0.35 into equations (2.6b) and (2.11a), a comparison of the difference in theoretical results between the two loading

methods is made:

$$\text{line load, } M_R = \frac{P}{t} (0.35 + 0.2732) = \frac{0.6232P}{t}$$

$$\begin{aligned} \text{distributed load, } M_R &= \frac{P}{t} (0.99416 \times 0.35 + 0.26417) \\ &= \frac{0.6120P}{t} \end{aligned}$$

The difference is only about 1.8 percent. This is of favourable consequence, since the loading strips may not always provide ideal, uniformly distributed loads, due to slight irregularities in some asphaltic concrete specimens. Also, considering the limits of experimental accuracy, no serious error is caused by assuming either of the two theoretical derivations.

Due to the application of vertical loads across a diameter of the specimen, the theory for the determination of vertical stresses is more complex than for direct tensile or compression tests. The total compressive stress along the horizontal diameter of the specimen can be found by substituting values of DELA and DELB into equation (2.8) and dividing by the specimen radius, R , to obtain the average:

$$\begin{aligned} 4 \text{ in diameter, average } \sigma_{\theta x} &= \frac{-2P}{\pi at} \times \frac{[0.37061 + 0.21500]}{2.0} \\ &= -0.24854 \frac{P}{t} \quad (2.8a) \end{aligned}$$

$$\begin{aligned} 3.8 \text{ in diameter, average } \sigma_{\theta x} &= \frac{-2P}{\pi at} \times \frac{[0.37013 + 0.21510]}{1.9} \\ &= -0.26145 \frac{P}{t} \quad (2.8b) \end{aligned}$$

In this study, the average $\sigma_{\theta x}$ as described above is referred to as the diametral stress, σ_{DM} . The sign convention adapted for all equations throughout this study assigns negative values for compressive stresses. Since this convention is awkward for discussion, only absolute

stress values are presented in the text and are taken as compressive, unless otherwise stated.

2.2 Poisson's Ratio by Direct Compression Tests

To date, the experimental determination of Poisson's ratio, ν , for asphaltic concrete mixes has not received enough attention to warrant confident use of commonly assumed values during pavement design. The general practice has been to assume a value of ν between 0.30 to 0.50, without considering effects such as stress levels and temperatures. A few researchers (11, 12, 15) have reported experimental values of ν using the diametral method. However, they have also indicated that there is need for more research in this area as the reliability of the test methods is not adequate and the required equipment is not readily available.

A simple and reliable direct method for finding ν by conventional repeated loading compression tests was developed as part of this study. By definition, Poisson's ratio is the ratio of the strain in the lateral direction to the strain in the axial direction:

$$\nu = - \frac{\epsilon_y}{\epsilon_x} = - \frac{\epsilon_z}{\epsilon_x} = \frac{\text{LATERAL STRAIN}}{\text{AXIAL STRAIN}} \quad (2.12)$$

The required measurements are the axial and radial deformations of 4 in (10.16 cm) diameter by 8 in (20.32 cm) long specimens, as indicated in Figure 2.4. The axial deformation is measured over a known length, x , between variable points A and B (Figure 2.4), while the radial deflections are measured across the 4 in (10.16 cm) diameter.

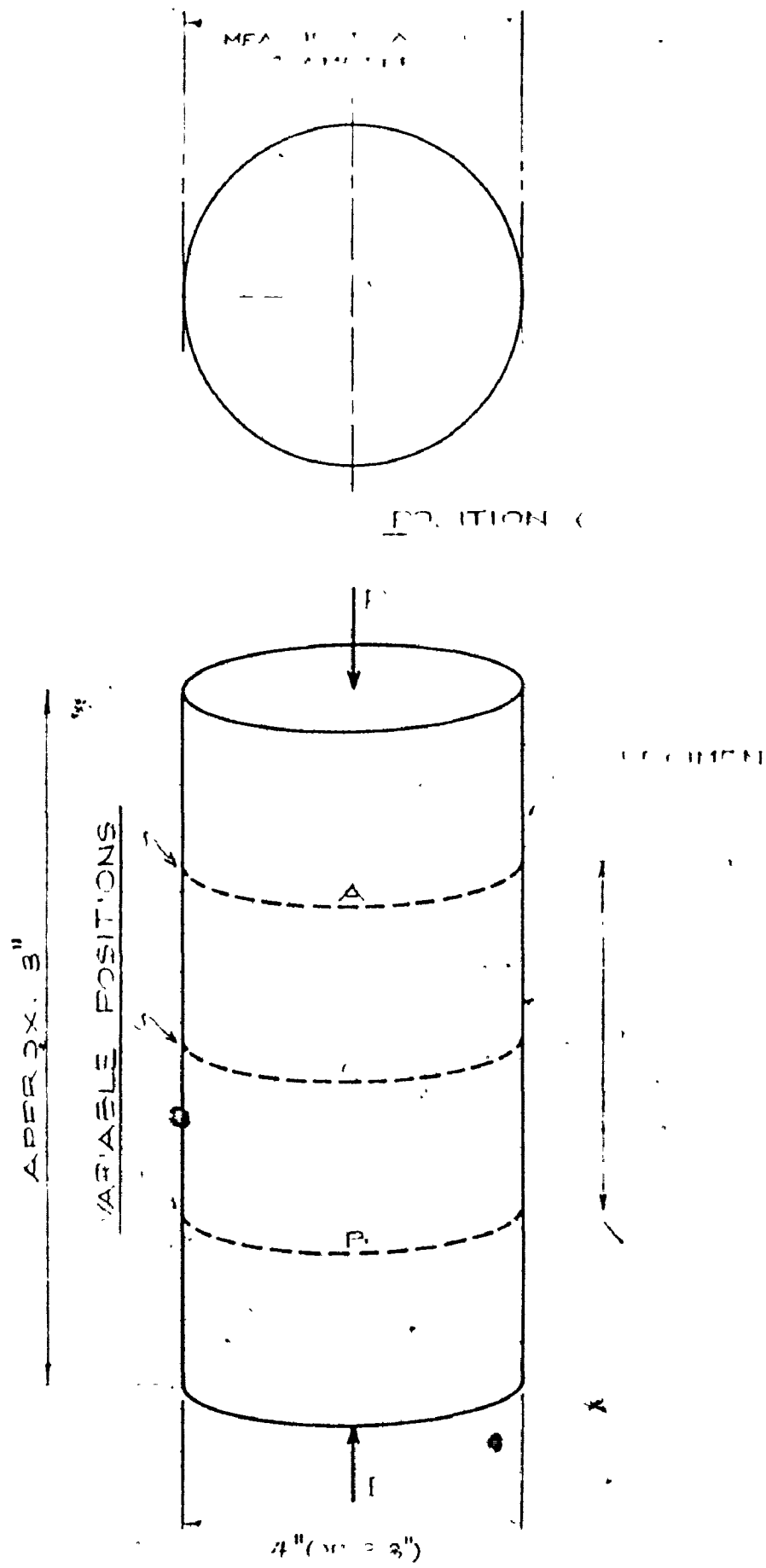


FIGURE 2-4 — MEASUREMENTS FOR DETERMINATION OF POISSON'S RATIO

From these readings the axial and lateral strains, respectively, may be calculated:

$$\text{AXIAL STRAIN} = \frac{\text{AXIAL DEFORMATION OVER AB}}{x} \quad (2.13)$$

$$\text{LATERAL STRAIN} = \frac{\text{RADIAL DEFORMATION}}{4 \text{ in}} \quad (2.14)$$

All measurements are taken under repeated loading conditions, using the same frequency and duration as for the resilient modulus measurements. Details of the apparatus developed for the Poisson's ratio test are given in the next chapter. For field cores having a diameter, D , equal to 3.8 in (9.65 cm), the denominator in equation (2.14) is 3.8 in (9.65 cm).

2.3 Parameters for Test Programme

2.3.1 Vertical and Horizontal Stress Levels for Testing

To reiterate, a major aim of this study was to simulate the expected field stress conditions due to traffic loadings. Besides providing more realistic values for pavement design, such stress levels would ensure that specimens were not tested to destruction, or at levels which would produce excessive permanent deformation. For vertical and horizontal stress levels (σ_v and σ_h , respectively) in pavements, a brief study using various analytical techniques was made in order to determine appropriate values to be used. A range of stress values must be selected as the stress intensity is dependent on the thickness and properties of the layers constituting the pavement structure, none of which are known at this stage.

Since the critical area under consideration within the asphaltic concrete is at the bottom of the layer, it is

only natural that testing should attempt to duplicate stress levels at this point. However, linear elastic analyses indicate that tensile horizontal stresses, σ_{CON} , develop at the bottom of the asphaltic concrete layer which cannot be simulated in the triaxial cell (which can only apply compressive confining stresses). This does not present a problem in the upper half of the asphaltic concrete layer since horizontal stresses in this region are compressive. Brown (34) presents a possible solution to this problem from a mathematical point of view. However, this method suggests applying tensile vertical stresses to the specimen, which is not permitted in the indirect tensile test. Morris (30) uses a "simulative statistically-based approach", however, he concludes that this method also provides unrealistic conditions. He also states that there is no testing technique available at the present time nor in the foreseeable future which is capable of reproducing the desired stress patterns simultaneously.

In view of the foregoing observations, the writer adopts a method whereby horizontal stresses are calculated at different depths within an asphalt pavement of infinite depth. Although this procedure provides solutions that are idealized, the philosophy is to obtain a range of positive horizontal stress values to investigate the influence of confining pressure on both M_R and v .

Although stresses are due to moving wheel loads, the general practice has been to calculate stresses for areas directly beneath a static wheel loading. This loading is

assumed to be due to the standard 18 kip (80 kN) axle load in either single or dual wheel configurations. In both cases, it is assumed that 80 psi (551.6 kPa) tire pressures are appropriate.

For the determination of stresses in the asphalt bound layer(s), the granular base and subbase layers are excluded. This is felt justified since actual pavement geometry is unknown at this stage, furthermore, we are interested only in rough estimates of stress levels for testing. Although flexible pavement construction normally includes more than one layer of asphaltic concrete material, only a single layer (base layer) is considered for stress level determinations. This approximation is considered adequate, since the base layer constitutes the main structural component of the flexible pavements.

The assumed properties of the asphaltic concrete layer are: 0.35 and 250 ksi (1.724 GPa) for ν and M_R , respectively. These are typical HM-5 asphalt mix (City of Hamilton) values at room temperature, as determined during the course of the study. Subgrade properties are assumed to be similar to those of the Brampton Test Road (18), and are taken as: 0.43 and 20 ksi (137.9 MPa) for ν and M_R , respectively.

As a first approximation and upper bound of both vertical and radial stresses at various depths below the pavement surface (Figure 2.5), the modified Boussinesq equations (35) were used:

$$\sigma_v = -q_0 \left[1 - \frac{1}{[1 + (r/z)^2]^{3/2}} \right] \quad (2.15)$$

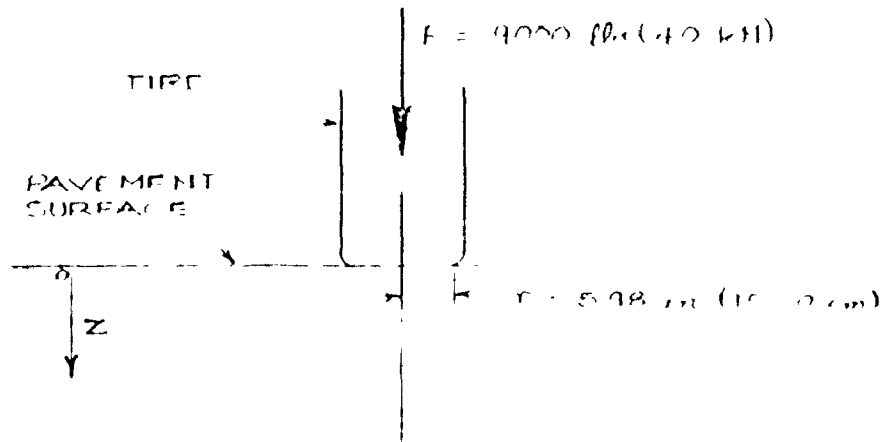


FIGURE 2.5 - SINGLE WHEEL LOADINGS FOR BOUSSINESQ AND CHEVRON CALCULATIONS

| z (ins) | r/z | σ_v (psi) | σ_h (psi) |
|--------------|----------|---------------------|---------------------|
| 0 | ∞ | -80.0 | -68.0 |
| 2 | 2.99 | -77.5 | -35.0 |
| 4 | 1.50 | -66.3 | -14.8 |
| 6 | 1.00 | -51.6 | - 5.7 |
| 8 | 0.75 | -38.9 | - 2.1 |
| 10 | 0.60 | -29.4 | - 0.6 |
| 12 | 0.50 | -22.6 | 0 |
| 14 | 0.43 | -17.8 | 0 |
| 16 | 0.37 | -14.2 | 0 |
| 18 | 0.33 | -11.6 | 0 |

TABLE 2.1: STRESS DISTRIBUTIONS FOR BOUSSINESQ ANALYSIS

$$\sigma_h = -\frac{q_0}{2} \left[1 + 2\nu - \frac{2(1+\nu)z}{(r^2+z^2)^{1/2}} + \frac{z^3}{(a^2+z^2)^{3/2}} \right] \quad (2.16)$$

where σ_v , σ_h = vertical and horizontal stress, respectively,
below the centre line of loading;

a = radius of loaded area (5.98 in (15.20 cm))

for single wheel configuration;

z = vertical depth below surface; and

q_0 = tire pressure at surface (80 psi (551.6 kPa)).

The results using equations (2.15) and (2.16) for σ_v and σ_h for depths up to 18 in (45.72 cm) are presented in Table 2.1. Since the asphaltic concrete in full depth asphalt pavements is normally between 4 to 18 inches (10.16 to 45.72 cm) in thickness, it can be inferred from Table 2.1 that vertical stress values, σ_v , vary from about 11 to 65 psi (76 to 448 kPa); and horizontal stresses, σ_h , vary from 0 to about 15 psi (0 to 103 kPa). However, these values for σ_v , are questionable due to certain basic assumptions in the Boussinesq theory, particularly that the continuum is homogeneous, when it is in fact a layered structure of various materials.

The second method of examining appropriate stress levels for testing involved the use of the CHEVRON N-LAYER computer programme (1). A major advantage of this method over the Boussinesq solution is that the programme treats the structure as a layered system, and influences due to the moduli (E and ν) of each layer are accounted for. Table 2.2 shows the analysis of several typical full depth structures (i.e.

| Depth ' z (ft) | σ_v at bottom of asphalt layer (psi) | σ_h at depth z in infinite asphalt layer (psi) |
|----------------------|---|---|
| 4 | -36.5 | -16.4 |
| 6 | -22.1 | - 7.0 |
| 8 | -14.6 | - 3.1 |
| 10 | -10.3 | - 1.5 |
| 12 | - 7.6 | - 0.8 |
| 14 | - 5.8 | - 0.5 |
| 16 | - 4.5 | - 0.2 |
| 18 | - 3.6 | - 0.1 |

TABLE 2.2: STRESS DISTRIBUTIONS FOR
CHEVRON COMPUTER ANALYSIS

two layers, including subgrade), using the CHEVRON programme. The same single wheel load as in the Boussinesq method was used (Figure 2.5), and the upper pavement layer thickness was varied from 4 to 18 inches (10.16 to 45.72 cm) for vertical stress determinations. The results (Table 2.2) show that the vertical stresses vary from about 4 to 37 psi (28 to 255 kPa) at the bottom of the asphalt layer. Calculation of horizontal stresses, assuming an infinite asphaltic concrete continuum, gives values of σ_h ranging from approximately 0.1 to 16 psi (0 to 110 kPa).

A third method of stress levels determination was made using the BISTRO computer programme (2). An additional feature of this programme is its ability to analyze pavement structures loaded by multi-wheel configurations. Using a dual wheel loading, as shown in Figure 2.6, the same pavement structures as in the previous method were analyzed and presented in Table 2.3. The results indicate that σ_v varies from approximately 3 to 27 psi (21 to 186 kPa), and σ_h ranges from about 0.5 to 14 psi (3 to 97 kPa).

A comparison of the three techniques shows that the Boussinesq method does indeed provide an upper bound for σ_v . As expected, due to the assumption of a homogeneous continuum for the horizontal stress levels, values of σ_h by all three methods were in very close agreement. For this study, the solutions provided by BISTRO were taken as the limiting stresses.

Substituting the maximum allowable value of σ_v (27 psi (186 kPa)) into equation (2.8a), the maximum allowable diametral

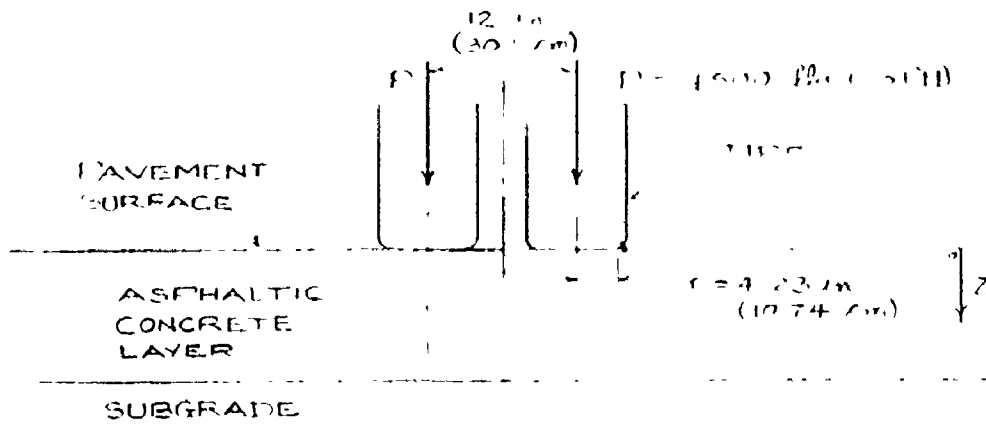


FIGURE 2.6 - DUAL WHEEL LOADING FOR 'BISTRO' CALCULATIONS

| Depth z (ft) | σ_v at bottom of asphalt layer (psi) | | Average σ_h at depth z in infinite asphalt layer (psi) | |
|----------------------|---|------------------|---|------------------|
| | Under 1 Wheel | ¢ of 2 Wheels | Under 1 Wheel | ¢ of 2 Wheels |
| 4 | -26.6 | -21.6 | -10.0 | -13.7 |
| 6 | -16.3 | -15.1 | - 4.8 | - 8.2 |
| 8 | -11.0 | -10.9 | - 2.9 | - 4.9 |
| 10 | - 7.9 | - 8.2 | - 2.0 | - 3.0 |
| 12 | - 6.0 | - 6.3 | - 1.5 | - 1.8 |
| 14 | - 4.7 | - 5.0 | - 1.0 | - 1.2 |
| 16 | - 3.8 | - 4.0 | - 0.7 | - 0.7 |
| 18 | - 3.1 | - 3.3 | - 0.5 | - 0.4 |

TABLE 2.3: STRESS DISTRIBUTIONS FOR 'BISTRO' COMPUTER ANALYSIS

load is found for the typical 2.5 in thick specimen:

$$27 \text{ psi} = 0.24854 \frac{P}{2.5 \text{ in}}$$

i.e.

$$P = 271.6 \text{ lbs.}$$

2.3.2 Pulse Time for Repeated Loading

As previously indicated, due to the viscoelastic nature of flexible pavement materials, load induced deformations are time dependent. The behaviour of such materials is approximately elastic, provided that the loading time is short enough so that viscous effects are small. For this reason, consideration of repeated loading time and frequency for testing is of primary importance if the elastic equations are to be used with any confidence.

Brown (36) indicates that the loading time should be based on the average stress pulses for the vertical, radial and tangential directions. Also, there is no unique loading time for asphaltic materials in situ, as the pulse is dependent on various factors including the depth of the point concerned. An attempt to define the loading time to be used in dynamic triaxial testing of asphaltic materials has been described by Barksdale (37). This method applies only to vertical stresses, however, it is based on a combination of theory and experimental observations. The results of this development have been presented in the form of curves relating loading time to depth for various vehicle speeds. These curves were replotted by Brown (36) (Figure 2.7a) based on the loading time definition:

$$t = \frac{1}{2\pi f} \quad (2.17)$$

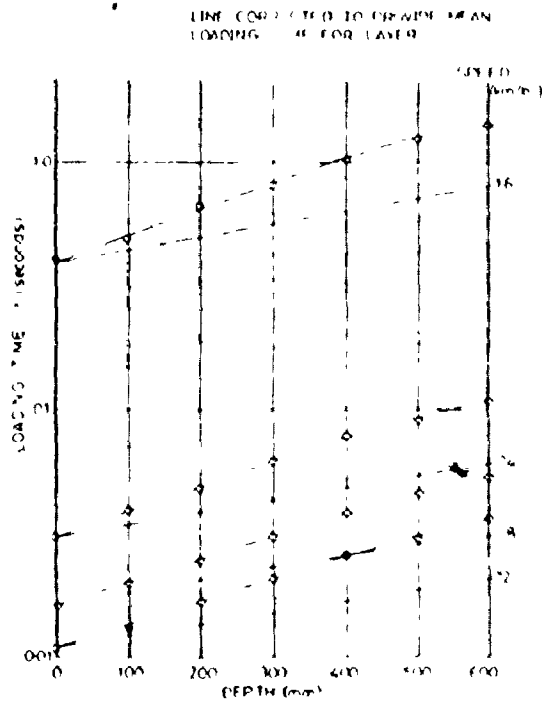


FIGURE 2-7a RELATIONSHIP BETWEEN LOADING TIME AND DEPTH FOR VARIOUS VEHICLE SPEEDS

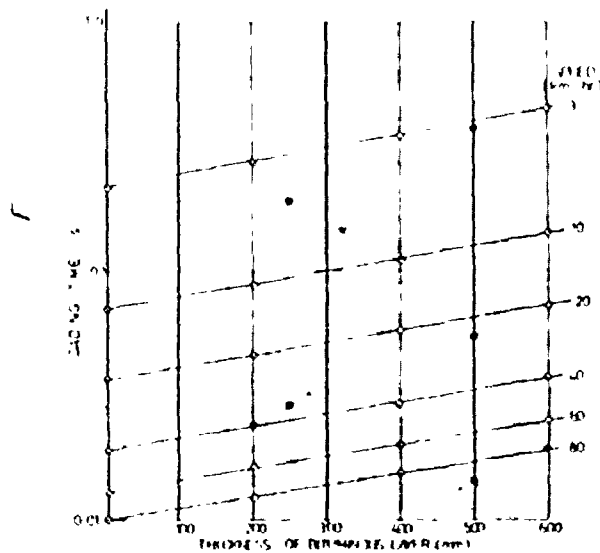


FIGURE 2-7b RELATIONSHIP BETWEEN MEAN LOADING TIME AND THICKNESS OF ASPHALTIC CONCRETE LAYER FOR VARIOUS VEHICLE SPEEDS (AFTER REF. 36)

where t = loading time; and

f = frequency of the sinusoidally applied stress.

Figure 2.7a also shows corrected curves to provide mean loading times for the asphaltic concrete layers. These were derived by taking the loading times at half the depth from Barksdale's curves. Figure 2.7b shows the relationship between mean loading time and thickness of asphaltic concrete layer for various vehicle speeds (36).

For this study, a load duration of 0.1 sec at a frequency of 20 cycles per minute was chosen, since this is the loading adopted by Schmidt and other researchers (6, 7, 38-40). Also a load duration of 0.1 sec is roughly the same as that obtained with the Benkleman beam deflection test (41, 42). Although a loading time of 0.1 sec corresponds to a speed of only about 5 mph (8 km/h), this is representative of creep speeds which are more critical to design. Analysis indicates that a time of loading of 0.05 secs approximates the actual time of loading in the field when a truck passes over the road at about 60 mph (96.6 km/h). The preceding values were obtained from Figure 2.7b assuming a typical 12 in (30.5 cm) asphaltic concrete layer. The 2.9 sec dwell time between repeated loadings permits substantially complete visco-elastic recovery of the specimen.

2.3.3 Pulse Shapes for Repeated Loading

Research on the pulse shapes to simulate moving wheel loads for use in triaxial testing has been reported by Barksdale (37). Based on linear elastic finite element studies, he reported that the load induced pulse shapes varied from

approximately sinusoidal at the surface, to more nearly triangular at depths below approximately the middle of the base.

For this study, only approximately sinusoidal shaped pulses were employed for testing. This was felt justified in view of the deficiencies of the triaxial test. However, future research using similar equipment should focus on investigating the effects of using three widely different waveforms during testing: triangular; sinusoidal; and square. These tests should provide some guidance as to the variations caused by differences in pulse shapes for both indirect tensile and direct compression tests.

2.3.4 Temperature Levels for Testing

Research by many individuals (7, 18) has indicated that the major parameter affecting the resilient modulus of the asphaltic concrete mixes is temperature. For the indirect tensile test, Schmidt (7) indicates that an approximately inverse linear relationship exists between $\log_{10} M_R$ and temperature, between 0 and 50°C. Poisson's ratio is thought to increase towards the upper limit of 0.5 as the temperature increases, although the actual dynamic ν vs temperature relationship is not known. For this study, a temperature range of about 10 to 50°C is used since these levels are easily attained with the developed laboratory equipment. Furthermore, typical pavement temperatures during the critical spring thaw and early summer periods are included in this range. Details of the laboratory equipment will be presented in the next chapter.

CHAPTER 3

TEST EQUIPMENT AND PROCEDURES

3.1 Apparatus Development

3.1.1 General Layout

The laboratory equipment developed for this project is basically an advanced version of the apparatus developed for previous resilient modulus studies by Gonsalves. This previous work at McMaster University was concerned mainly with the development of the resilient modulus and Poisson's ratio measuring devices for investigating material properties under uniaxial, unconfined stress conditions. This study, was directed towards the refining of both of the above devices so that they were able to be mounted within a standard 7 in diameter triaxial cell. In addition, the triaxial cell was modified so that the temperature of the cell could be accurately controlled and a confining pressure applied in a static or dynamic fashion. A schematic of the general testing layout is shown in Figure 3.1.

The schematic shows that there are five main parts to the equipment:

- 1) the triaxial cell containing the appropriate measuring devices;

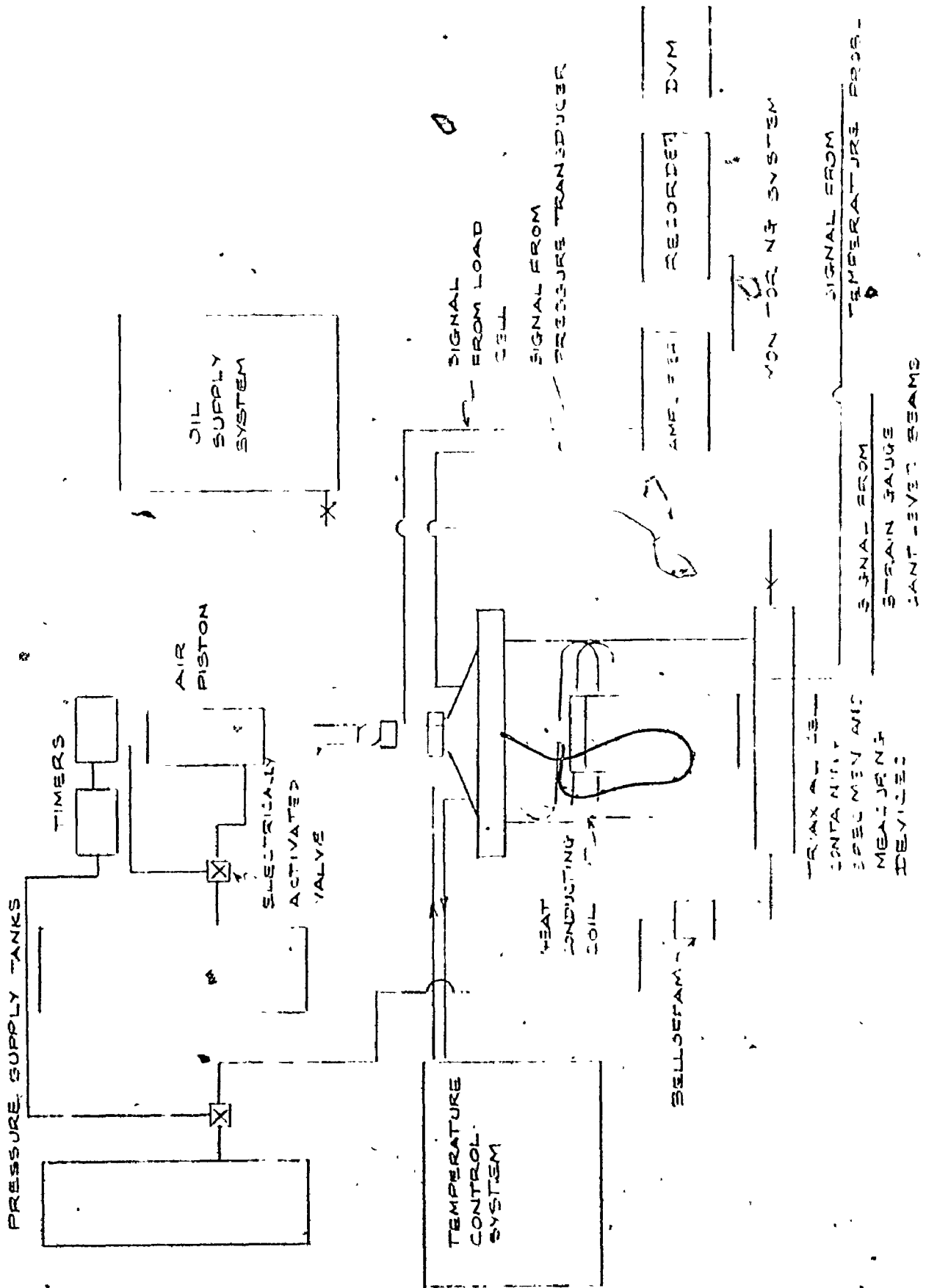


FIGURE 3.1: GENERAL SCHEMATIC OF EQUIPMENT

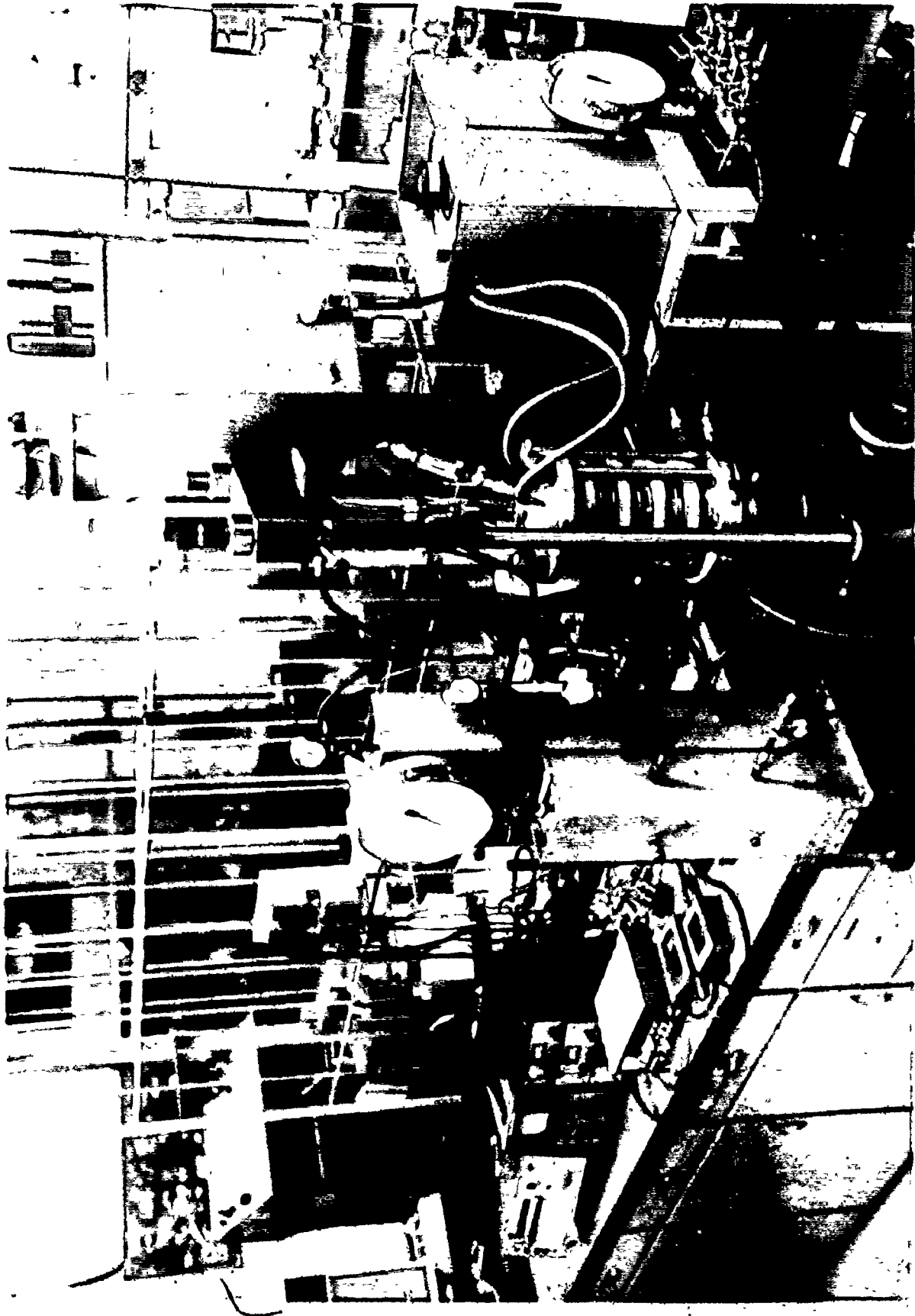
- 2) the oil supply system;
- 3) the temperature control system;
- 4) the load/pressure application control (including timing) system; and
- 5) data acquisition and monitoring system.

A photograph showing the general arrangement of the total system is presented in Figure 3.2.

3.1.2 Resilient Modulus Measuring Device

For the determination of the resilient modulus, M_R , the concept of measuring the lateral deflection of diametrically loaded specimens, as proposed by Schmidt (6) was adopted. Significant modifications had to be made to Schmidt's design since it was necessary to fit the measuring device into the triaxial cell. A major change was the use of full bridge strain gauges mounted on spring steel cantilever beams to measure the horizontal diametral deflection of the specimen as shown in Figure 3.3. These replaced the Statham (UC-3) transducers used by Schmidt, which would have been too bulky to fit into the cell (and are extremely expensive). Details of a typical strain gauge deflection beam, along with the electrical wiring diagram, are given in Figure B.1 of APPENDIX B.

Another significant change was the redesign of the measuring collar and mounting cradle system which facilitated easier set-up and mounting of the specimen prior to testing. The need for this was apparent in the early stages of development, since the positioning and constant readjustment of the specimen (which posed no major problems to earlier open



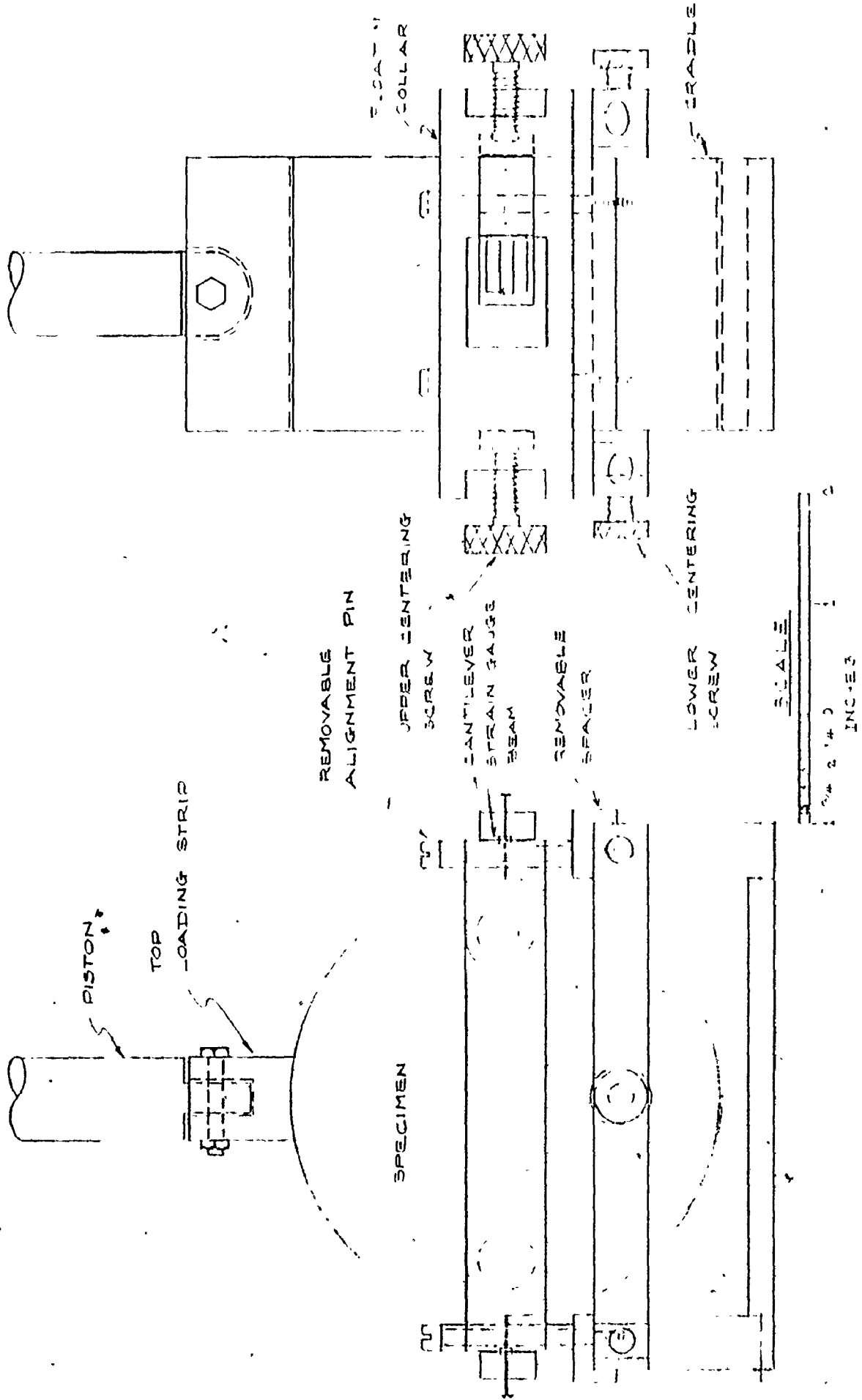


FIGURE 3-3 — RESILIENT MODULUS MEASURING DEVICE

systems) would not be possible once the assembled equipment was inside the triaxial cell. Much time was spent in this aspect of the design, in order to preserve the "free floating collar" concept necessary to obtain realistic results. Details of the final design of the resilient modulus measuring device, including the mounting cradle, are shown in Figure 3.3.

Setting Up Specimen in the Apparatus

Setting up of a specimen is preceded by securing the four alignment pins in the holes provided, and positioning the 3/16 in (0.476 cm) spacers between the collar and the cradle (Figure 3.3). The sample is then placed over the lower loading strip, taking care to ensure that it is properly seated and centered on the strip. Next, the bottom centering screws are adjusted, and tightened just enough that the briquette (test specimen) is held snugly in place. These screws are necessary to stop sliding of the sample during the set-up period, or unavoidable tilting of the triaxial cell. The centering screws on the collar are next adjusted, and tightened two at a time (both screws directly across from each other), such that no movement of the briquette is observed during the sequence. The latter screws should be moderately tight, but not overly tight as to cause any restriction of lateral deformation of the briquette.

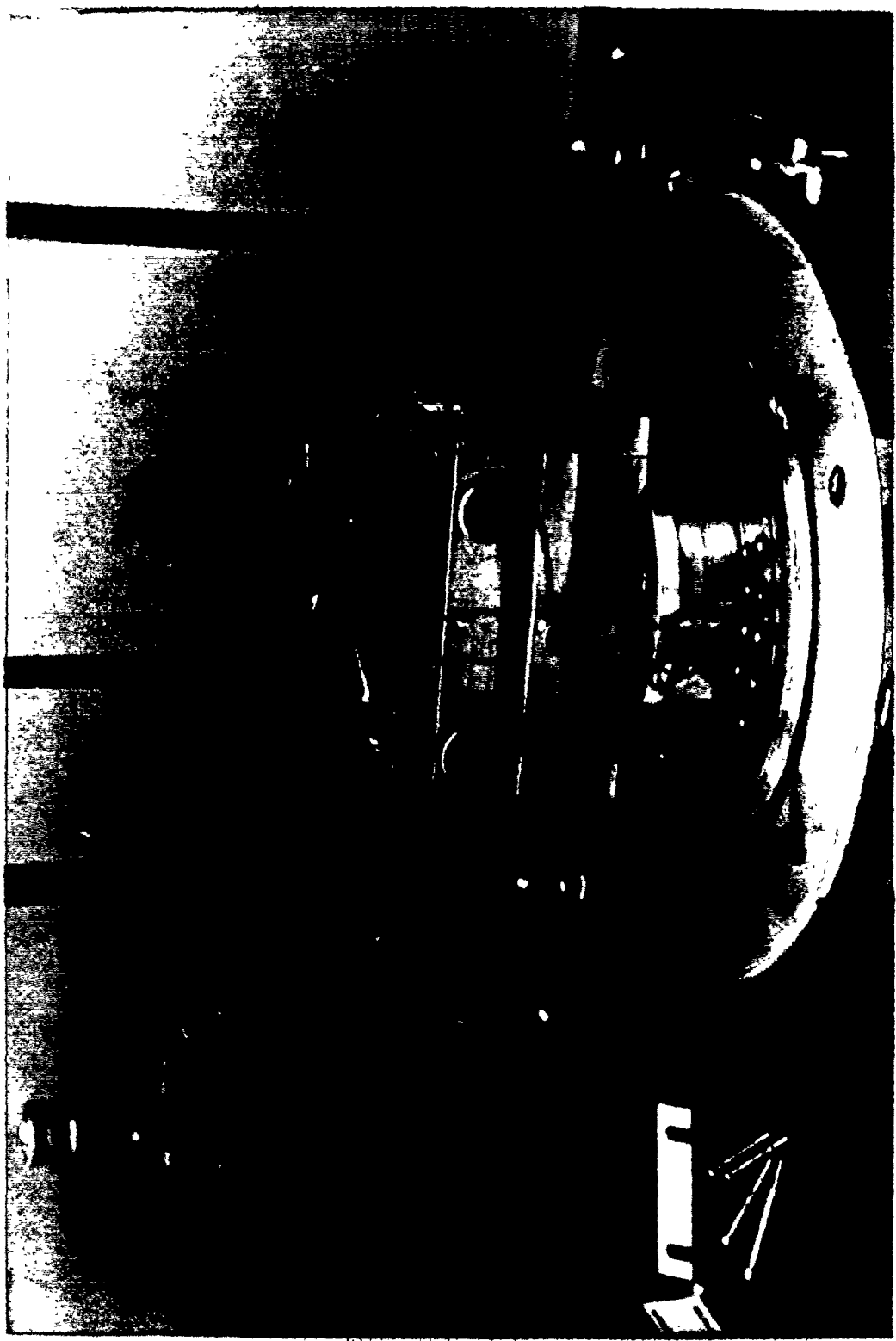
The strain gauge screws are then rotated inwards, until they are just touching the sample, and then rotated clockwise by another half-turn. The final step before placing the apparatus in the triaxial cell is to remove the alignment pins,

and then the spacers, to allow free movement of the measuring collar. A photograph showing a briquette in position is given in Figure 3.4.

3.1.3 Poisson's Ratio Measuring Device

The Poisson's ratio measuring device, in contrast to the resilient modulus apparatus, uses 8 in (20.3 cm) high, 4 in (10.2 cm) diameter, cylindrical specimens, rather than the conventional 2-1/2 in (6.4 cm) thick 4 in (10.2 cm) diameter Marshall briquettes. Triaxial size specimens were used, since it is anticipated that future research will focus on the use of specimens prepared by kneading compaction for both resilient modulus and Poisson's ratio determinations; larger size specimens generally result in less scatter of experimental results; and most important, end restraint influences tend to be minimized, particularly with length to diameter ratios greater than two. In tests conducted with this "Poisson's ratio equipment", compressive loads (static or repeated) are applied vertically along the axis of the cylindrical specimen. The resulting vertical deformations are measured parallel to the loaded axis, and the lateral deformations across the specimen diameter, from which the vertical and horizontal strains, respectively are calculated. To the writer's knowledge, this is the first experimental apparatus that has been specifically developed to determine the Poisson's ratio of asphaltic concretes for various temperatures, confining pressures and repeated loadings.

Figure 3.5 shows the main features of this apparatus, which consists essentially of two measuring collars, A and C,



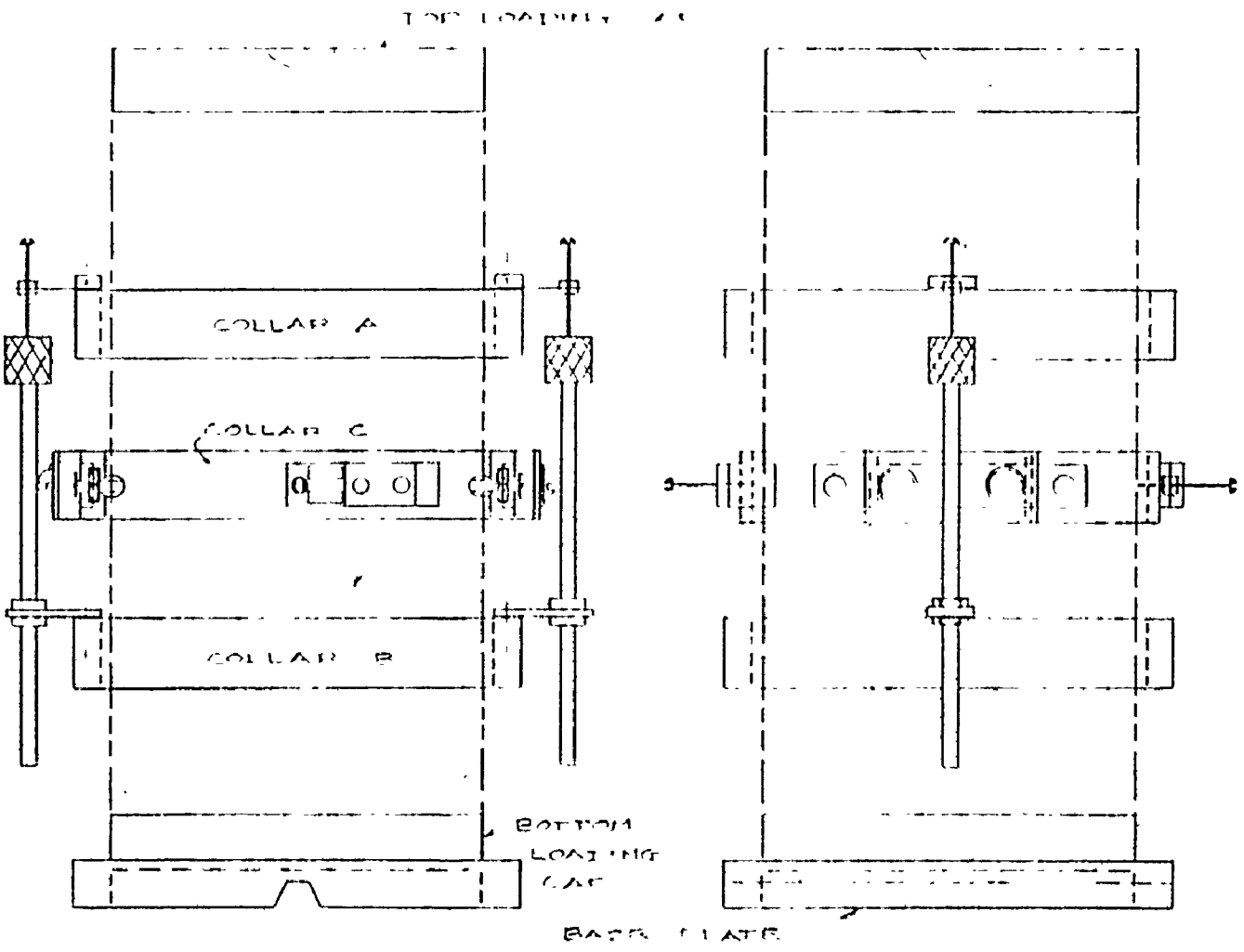
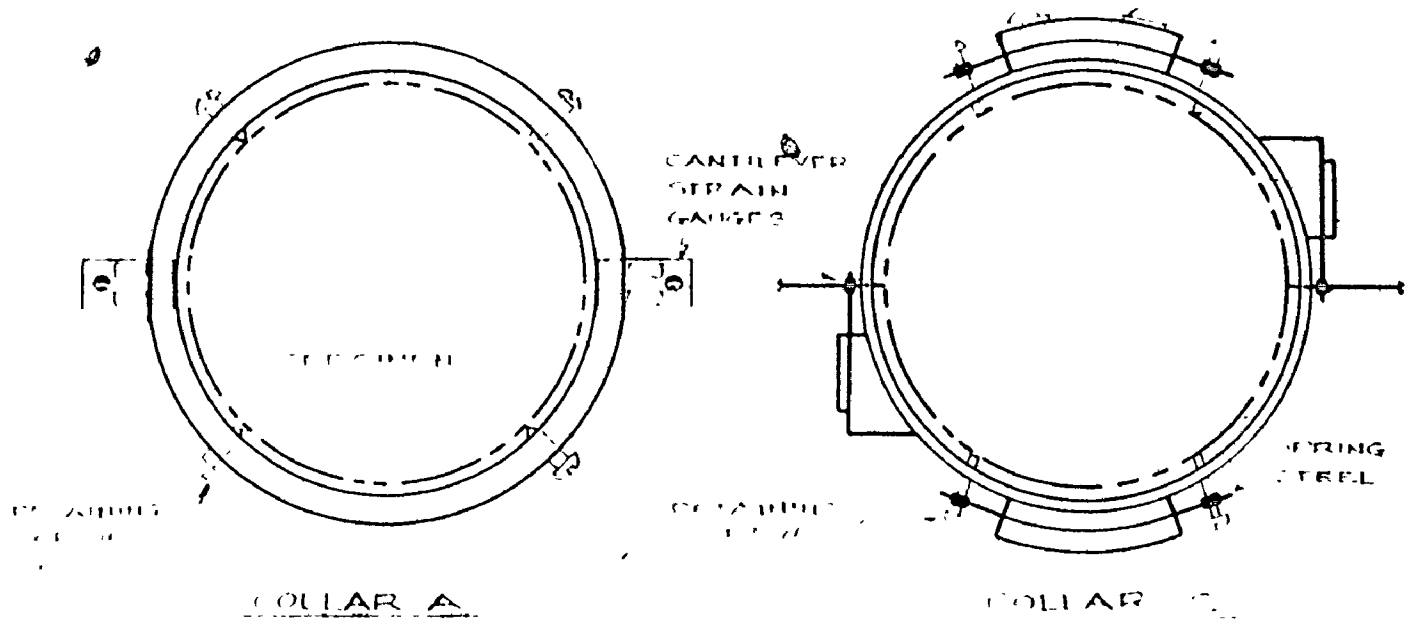


FIGURE 3-5 - POISSON'S RATIO MEASURING DEVICE

and a third collar, B, for supporting the two adjustable vertical rods. Collar B has also been made adjustable, so that the vertical deformations may be measured over any convenient length or section of the cylinder. The operation of this device is best explained with reference to Figure 3.5. Compressive loads applied along the axis of the cylindrical sample cause A and B to move closer together, producing a deflection in both cantilever strain gauge beams mounted on ring A. The average deflection, as measured by the gauges, should reflect the average relative movement between collars A and B, from which the vertical strain is determined. The horizontal deformation, on the other hand, is measured directly by the strain gauge beams, mounted on opposite sides of ring C as shown in Figure 3.5. By using this "floating collar" system, end effects (i.e. the restraining of lateral deformation of the sample by the loading caps) and measuring device restraints are virtually eliminated. Also, this technique assures that movements, due to slight rocking of the sample, are not measured. The strain gauge deflection beams used with this device are the same as those used in the indirect tension resilient modulus test as detailed in Figure B.1 APPENDIX B, and this provides great flexibility in the design of the system and monitoring equipment. *

Setting Up Specimens in the Apparatus

Prior to mounting the triaxial specimen in the apparatus, the sample is checked to ensure that it stands perfectly upright, and the bottom of the specimen is sanded if necessary.

After the sealing procedure (described in following sections) is performed, the specimen is then placed in position on the base of the triaxial cell, and electrical tape is placed around the sample at the expected locations of collars A and B. This is to prevent the securing screws (which hold the collars to the sample) from piercing the sealing membrane. The collars are then located, one at a time (starting from collar B), with the aid of spacers to ensure that they are as level as possible. Securing screws are hand tightened only, but must be tightened enough so that differential movement of collar and sample (i.e. slip) does not occur. The cantilever strain gauge beam screws are then adjusted in the same manner described previously for the resilient modulus apparatus. Due to the variable positions of collars A and B, the average distance between the securing screws on these collars must be measured for vertical strain calculations. A photograph showing a specimen in position is given in Figure 3.6.

3.1.4 Temperature Control

Accurate control and maintenance of temperature was a vital aspect in the development of the equipment. Figure 3.7 shows the main features of the hardware used for controlling the temperature of the specimens during testing. Basically, the system consists of two parts: 1) a temperature control bath for maintaining the desired temperature; and 2) a coil of copper tubing built into the triaxial cell, for conducting heat to the oil in the cell. The principle of this design, is to control the temperature of the cell indirectly

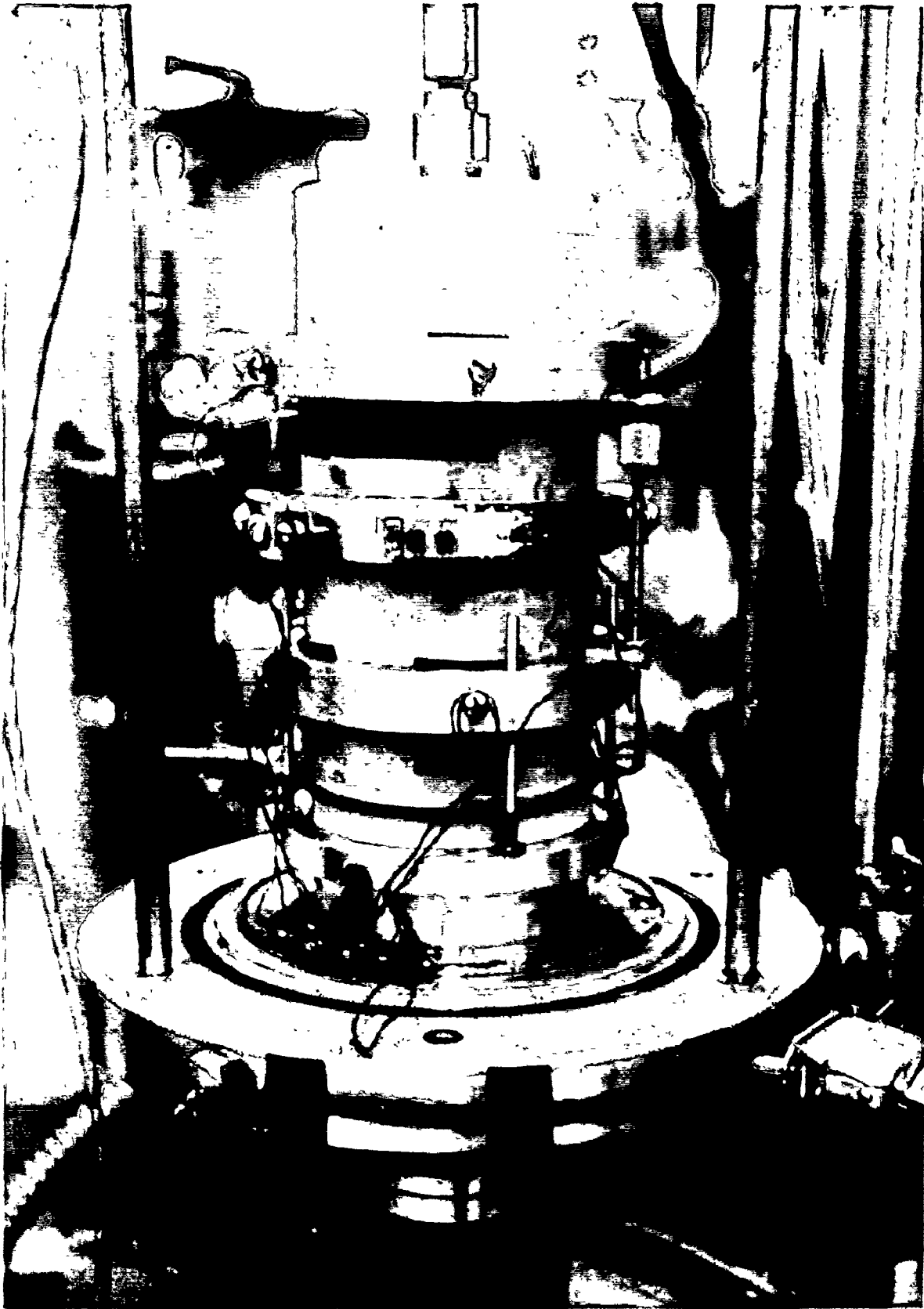
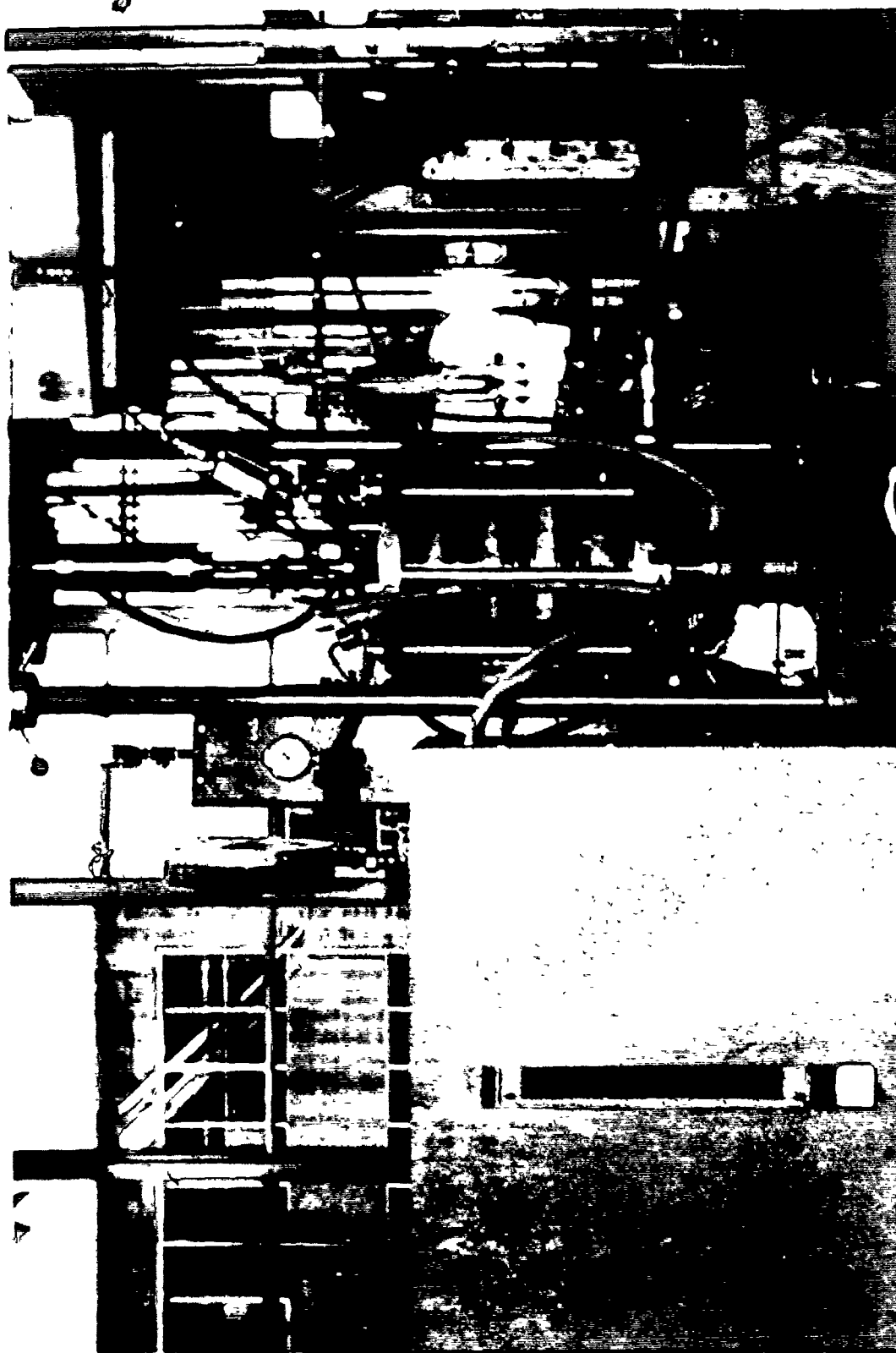


FIGURE 3.6: SPECIMEN MOUNTED IN POISSON'S RATIO DEVICE



F. 3.7: TEMPERATU! CON

by circulating a liquid (water) from the bath through the conducting coil (glycol can be circulated for working at low temperatures).

Heating of the temperature bath was achieved through the use of an adjustable HAAKE E12 constant temperature circulator. By trial and error, the correct settings on the circulator were determined for the corresponding desired temperature levels in the triaxial cell. This was a necessary step since the temperature of the oil in the triaxial cell never attains the same level as that of the bath due to various heat losses.

Cooling of the temperature bath was achieved by simply adding ice from a freezer (approximately -35°C) to the bath. Again, a temperature gradient was inevitable, however the triaxial cell attained equilibrium at about 9°C , depending on the laboratory ambient which was generally maintained at $20 \pm 2^{\circ}\text{C}$. Although a temperature of less than 9°C was never attained (or required for the current study) by using this method, glycol could be added to the system and then circulated from the bath through a second coil placed in a freezer. Control of the much lower temperatures involved would then be achieved by controlling the setting on the freezer.

A major consideration in the temperature control system was the choice of a suitable fluid for use in the triaxial cell. It was obvious that a fluid was necessary, in order to conduct heat and maintain temperature levels, and also to allow for the application of confining pressures to the specimen. Some of the desired fluid properties are:

- 1) must not conduct electricity;
- 2) non-corrosive to any material used in the triaxial cell;
- 3) adequately transparent;
- 4) good conductor of heat; and
- 5) readily available and inexpensive.

Of all the fluids considered, only silicone oil and a special heat conducting oil (petroleum base) proved feasible. The silicone oil was rejected since it is expensive and has an undesirable penetrating power. Heat conducting oil satisfies all of the above conditions, and was locally available at low cost. However, a major drawback to the use of any petroleum base oil is that it attacks asphalt. The problem was readily solved by heat sealing the resilient modulus specimens in plastic bags (described later), which was also a necessary step in order to apply confining pressures. For the larger size triaxial specimens, sealing was achieved by the use of conventional rubber membranes.

3.1.5 Confining Pressure Control

Development of a simple pressure control system for applying pulsating confining pressures to asphaltic concrete specimens was required. This was achieved using the equipment shown in Figure 3.8 consisting essentially of the following components:

- 1) air pressure reservoir tank;
- 2) electrically triggered air valve;
- 3) bellows separating the air/oil interface; and
- 4) solid state timer for triggering the air valve.

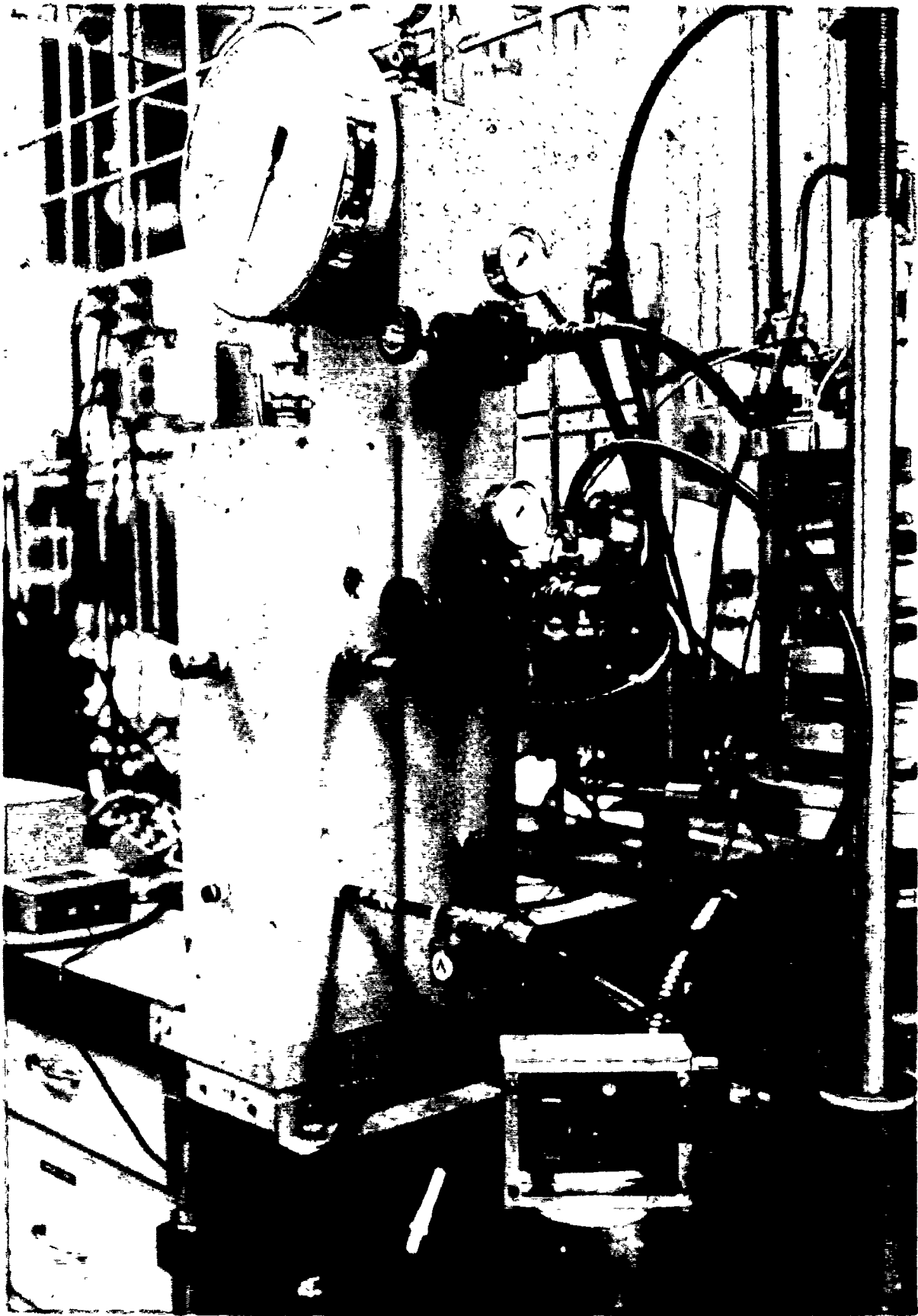


FIGURE 3.8: CONFINING PRESSURE CONTROL SYSTEM

The timer was adjusted to open the valve for one-tenth of a second, twenty times per minute. Within the open interval, air from the reservoir flows to the flexible Bellofram, thereby transferring pressure to the oil in the triaxial cell. As anticipated, there was appreciable "inertia" in the system, preventing full pressure response in the triaxial cell. This inertia, besides depending on the dimensions of the apparatus (i.e. compliance) is also a function of the viscosity of the oil which is temperature dependent. For this reason, it was necessary to monitor the actual pulsating pressure within the cell, using a pressure transducer (Statham model PA208TC-100-350, a strain gauge type) located at the top of the triaxial cell. Control of peak pressures in the triaxial cell was obtained by adjusting the pressure of the reservoir tank. The circuit diagram of the pulse timer is given in APPENDIX B. This timer was especially designed to minimize any electrical noise that would interfere with signal monitoring and involves solid state circuits rather than typical relay circuits. From the initial timer design, a rather sophisticated printed circuit model has been developed by R. Winterle for the resilient modulus studies.

3.1.6 Axial Load Control

Axial loads for indirect tensile (resilient modulus) or direct compression tests are produced by the air and piston system, as shown in Figure 3.9. Basically, the system consists of the following components:

- 1) air pressure reservoir tank;

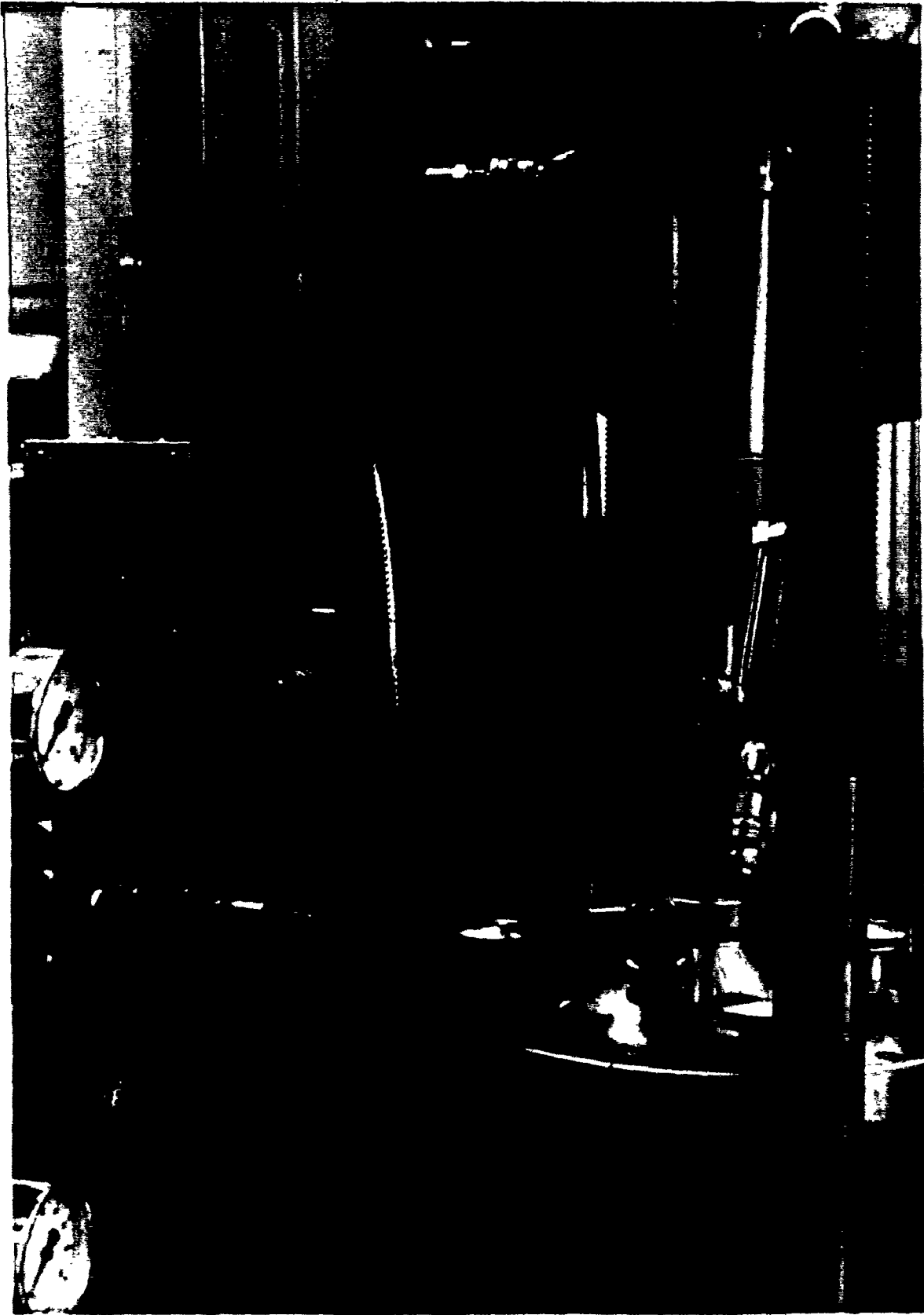


FIGURE 3.9: AXIAL LOAD CONTROL SYSTEM.

- 2) electrically triggered air valve;
- 3) 2-1/2 in diameter (nominal) BIMBA air piston; and
- 4) solid state timer for activating the air valve.

This equipment is quite similar in principle and operation to the previously discussed confining pressure control system. The timer, adjusted to the same 1/10 sec. duration, and 20 cycles per minute, triggers the valve which allows air to activate the piston. However, the axial load system uses a somewhat specialized timer that is triggered by the timer used in the lateral pressure equipment. The purpose of this triggering is to provide an adjustable lag, so that both vertical load and confining pressure "peak" at the same instant. This technique effectively compensates for any lag in developing full confining pressure for each load repetition.

The axial load level is controlled by adjusting the pressure of the reservoir tank in a similar way to the previous system. Except for the timing sequence, both loading systems are completely independent of each other, using separate air pressure reservoir tanks. This allows adjustment of pressure levels to obtain any combination of vertical stress and confining conditions for testing.

The electronics design of the phase-lag timer used for this equipment is given in Figure B.2, APPENDIX B.

3.1.7 Monitoring and Recording of Output Signals

Determination of material properties using both the resilient modulus and Poisson's ratio devices require accurate measurement of:

- 1)
- 2) confining pressure;
- 3) strain gauge outputs from the cantilever beams monitoring deformation at designated points under the applied stress system; and
- 4) sample temperature.

These measurements are explained further in the following sections.

1. Axial Load

Due to the appreciable friction between the vertical ram and the close fitting top seal of the triaxial apparatus (Figure 3.10), it was found necessary to monitor axial loads from within the cell (i.e. below the top seal) to obtain accurate load readings. This was accomplished by using a bolt-type strain gauge, load cell (4,500 lb. capacity), mounted within the piston ram (Figure 3.10). Electrical leads from the load cell were then located within the hollow piston and brought out above the top seal, allowing complete freedom of movement of the piston. Although their size is small enough for this particular set-up, bolt type strain gauges generally lack in monitoring sensitivity. Thus, it was found necessary to amplify the output signal prior to recording. Details of the amplifier used are given in a later section.

2. Confining Pressure

As previously discussed in 3.1.5, due to compliance and temperature effects, accurate determination of applied confining pressures was essential. Confining pressures

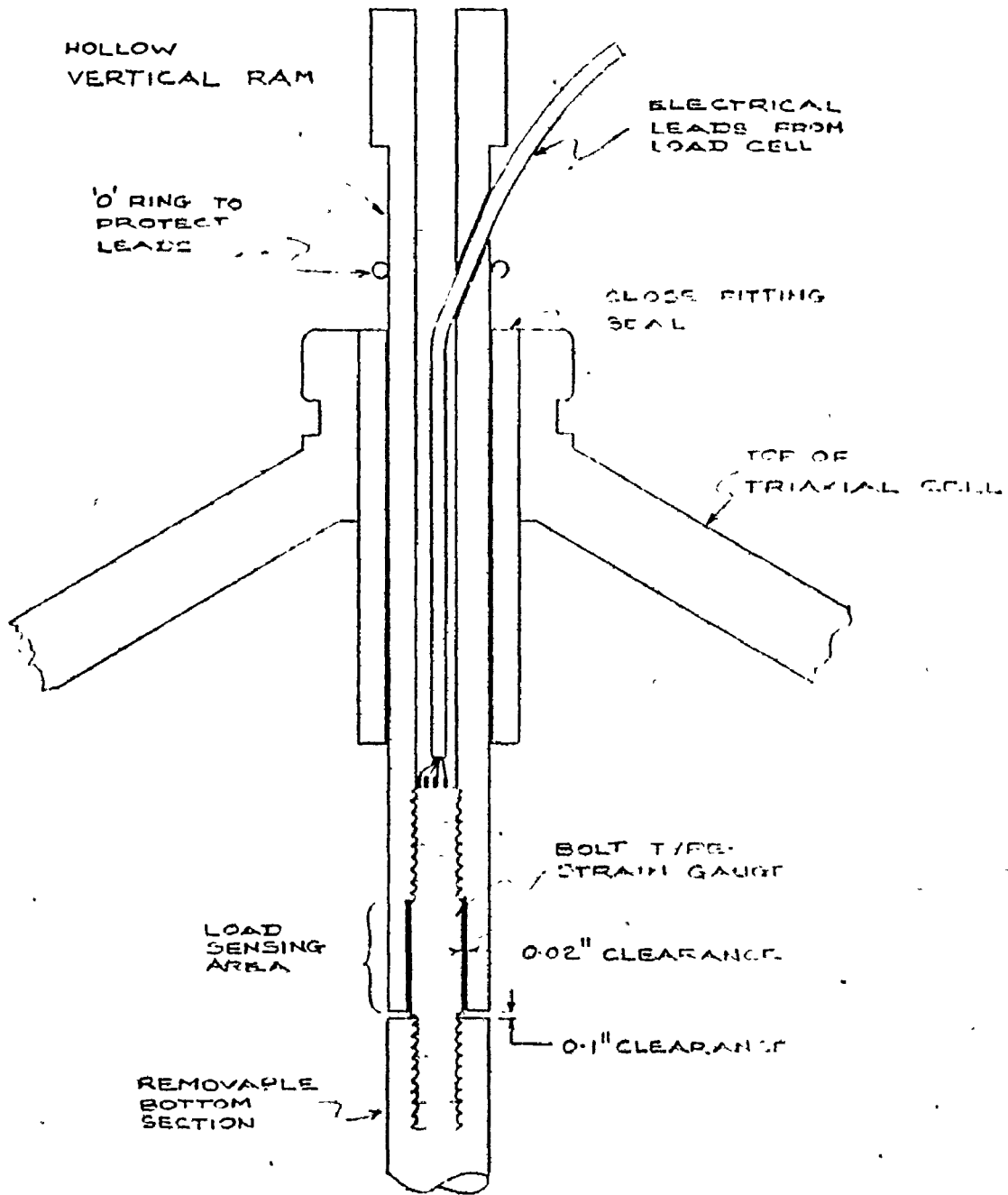


FIGURE 3-10 — MONITORING OF AXIAL LOAD

(cell pressures) were measured using a STATHAM (PA208TC-100-350) pressure transducer, mounted on the top of the triaxial cell. For the 100 psia range transducer used, the direct output signals were strong enough for the monitoring equipment so that no amplification was needed in this case.

3. Strain Gauge Output

Output signals from the strain gauge cantilever beams on both the resilient modulus and Poisson's ratio devices were found to be relatively low and had to be amplified before recording. Depending on the magnitude of the deformations being measured, the strain gauge signals were fed into the amplifier channel that provided the most suitable gain.

4. Specimen Temperature

The use of a mercury thermometer for measuring the specimen temperatures was found to be impractical due to physical constraints of the triaxial cell. Furthermore, since confining pressures were to be applied, this ruled out the possibility of placing any glass thermometer inside the cell. For this reason, a solid state temperature probe system was developed especially for the triaxial apparatus. A positive feature of this system was that the miniature transistor probe could be placed between the measuring collars close to the specimen. Comparisons of temperatures monitored, and using a probe implanted in the specimens, permitted determinations of times to temperature equilibrium. The design of this temperature probe circuitry is given in Figure B.4, APPENDIX B.

5. Data Acquisition Equipment

A photograph of the data acquisition system is given in Figure 3.11, showing the five major components:

- 1) a 5-channel amplifier/balancer unit;
- 2) a 6-channel light beam (SE3006) oscillographic recorder;
- 3) HEWLETT PACKARD (6204B) DC power supply units;
- 4) a digital voltmeter (FLUKE 8000A); and
- 5) a separate amplifier for the temperature probe.

The signal amplifier/balancer unit is used for boosting low level signals to a level that will give readily measurable light beam deflections on the oscillographic strip recorder. In addition to this, the unit is equipped for balancing of the amplified signals to prevent damage to the strip recorder by over shooting.

Much difficulty was encountered in the design of a suitable amplifier system. One major problem was the presence of electrical noise, which at one stage produced greater light beam deflections than the actual output signals. Difficulty was also experienced due to interaction between channels, which besides causing incorrect measurements, made balancing impossible. There was also the problem of obtaining adequate balancing range, and at the same time, having a fine enough adjustment on the potentiometers. The amplifier system eventually developed for this project is virtually noiseless with excellent balancing capabilities. It is also free of channel interaction, despite the fact that a common 12 volt power source was used for all five channels. Details of the electrical design of this amplifier are given in Figure B.3, APPENDIX B.

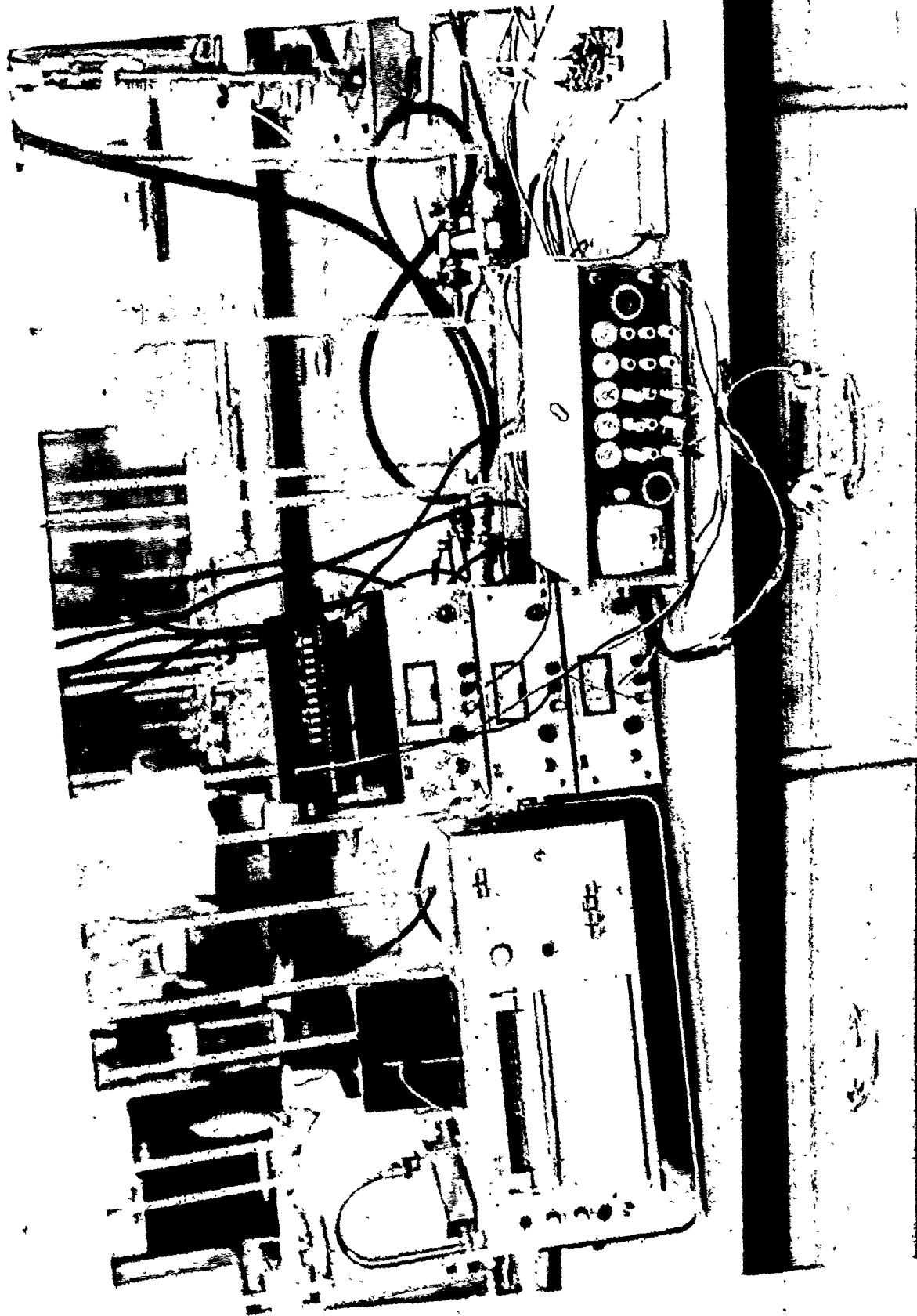


FIGURE 3.11: DATA ACQUISITION SYSTEM

The light beam oscillographic recorder used records analogue data by printing directly on light sensitive strip paper, and produces its own grid with 0.2 cm divisions. Measurements were made for each channel by counting the number of divisions created by a recorded deflection, and then multiplying the result by the appropriate calibration constant.

Three HEWLETT PACKARD power units were used for driving the data acquisition system. Two of the units were combined to produce a ± 6 volt supply for the amplifiers. In addition to the strain gauge cantilever beams, both the load cell and the temperature probe amplifier were also driven from this combined power source. The third unit was used to provide a 7 volt supply for the pressure transducer.

The digital voltmeter provided a convenient and accurate readout display for balancing voltages from the amplifier system. It was also used to monitor temperatures in conjunction with the temperature probe equipment.

3.2 Calibration of Equipment

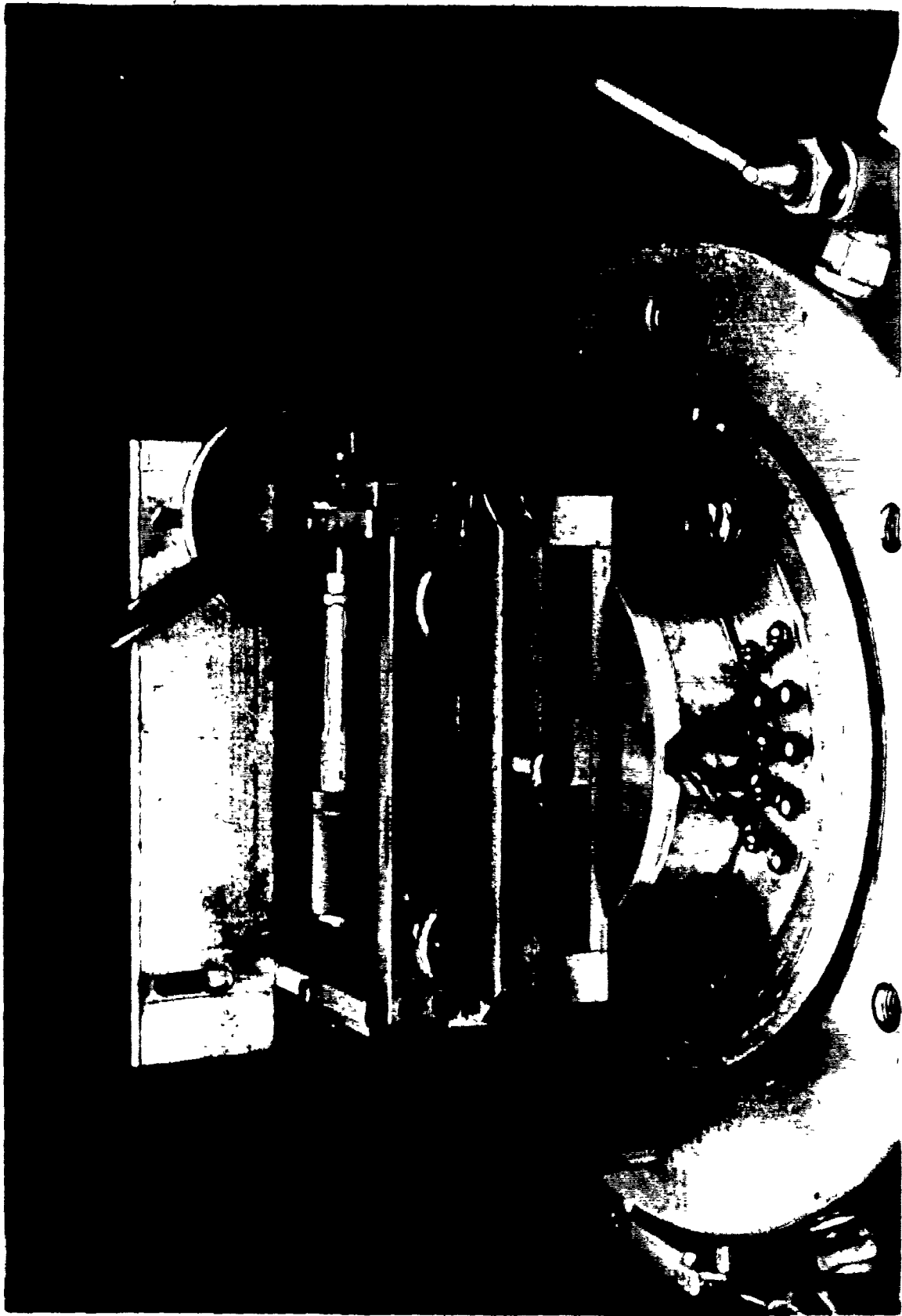
A fundamental consideration during the development of any equipment for materials testing is the accurate and simple calibration of all measuring devices. Before any measurements during testing could be made, the following components (already discussed in 3.1.7) had to be calibrated:

- 1) all strain gauge cantilever beams;
- 2) the load cell;
- 3) the pressure transducer; and
- 4) the temperature probe.

For this investigation, channels 1, 2 and 3 on the amplifier system were set to a gain of about 3, and channels 4 and 5 were turned to the maximum gain of 10. These settings were found to be approximately the amplifications required for the test programme, and were not changed during the course of this study.

1. Strain Gauge Cantilever Beams

Figure 3.12 shows the necessary special equipment used for calibrating the strain gauge cantilever beams on the resilient modulus collar. The micrometer screw is adjusted so that it just touches the screw on the cantilever beam, and the initial reading on the micrometer is taken. Next, connecting strain gauge number 1 to amplifier channel 1, the output is balanced, using the digital voltmeter (DVM). Oscillographic recorder channel 1 is then connected to amplifier channel 1, and the beam adjusted (by turning the galvanometer, located at the top of the oscillographic recorder) to about the 1 cm mark on the grid. After running a short strip of paper to record this initial position, the micrometer is then carefully rotated until the light beam on the oscillographic recorder is deflected to about the 14 cm grid mark. This is again recorded by running a short strip of paper from the oscillograph, after which the second reading on the micrometer is taken. The light beam is again adjusted to approximately the 1 cm mark, this time however, the balancing potentiometer on the amplifier unit is used. The process is repeated about fifteen times, from which a graph of micrometer deflection (inches) and



1-11-66

galvanometer deflection (divisions) is plotted, giving the calibration factor for cantilever beam number 1 on amplifier channel 1. The same procedure is then performed for cantilever beam number 2 using amplifier channel 2 and oscillograph channel 2.

If more amplification is needed, say for cantilever beam 1, the calibration is performed using amplifier channel 4 with recorder channel 1. Measurements are always performed, using the same cantilever beam, amplifier and channel number combination that was used for calibration. Besides avoiding confusion, this systematic approach avoids differences in calibration due to different sensitivity of various combinations. The same basic operation was conducted for the Poisson's ratio measuring collars.

2. Load Cell

Calibration of the load cell is performed in a standard WYKEHAM FARRANCE (T57) loading frame of the type used for soil testing. The piston containing the load cell is removed from the triaxial apparatus, and mounted vertically in the loading frame against a 500 lb. capacity proving ring. The idea is to load the system (connected in series), so that the oscillographic recorder galvanometer deflections can be equated to proving ring deflections, from which the load calibration constant is determined. The procedure of measuring galvanometer deflections is basically the same as in the case of the strain gauges.

3. Pressure Transducer

Calibration of the pressure transducer is performed

the tus set up as in a lar

no dynamic loads are applied and the air line connections are rearranged to bypass the electrical valve in the confining pressure system. In so doing, static pressures may be applied to the cell directly from the pressure tank fitted with an accurate pressure gauge. Due to the application of static pressures, the reservoir tank and triaxial cell must come to equilibrium at the same pressure.

Connecting the outlet leads from the transducer to the oscillographic recorder, the relationship between pressure gauge readings and galvanometer deflection may be determined.

4. Temperature Probe

The temperature probe system was designed for use with a digital voltmeter (DVM). The probe itself is actually a small transistor that is sensitive to temperature changes, which are read as millivolts on the DVM. Calibration is performed by taping the probe to an accurate mercury thermometer (0.1°C divisions), and then placing both in various temperature baths from approximately 0°C to 50°C. From this, a graph of millivolt readings and corresponding temperature readings is drawn, providing the necessary calibration chart for the temperature probe.

3.3 Sample Preparation

Asphaltic concrete specimens that were used in the resilient modulus investigation were prepared according to the Marshall method (21). The resulting briquettes were 4 inches (10.2 cm) in diameter by approximately 2-1/2 inches (6.4 cm) in thickness. However, the Poisson's ratio test required

specimens approximately three times as thick (2 inches, 20.3 cm). In this study, the latter specimens were conveniently produced by cementing three Marshall briquettes together, using emulsified asphalt as the bonding agent. Poisson's ratio tests were then performed on the middle briquette of this combination, taking advantage of the adjustable position of the measuring collars. In the next phase of the study, full size triaxial specimens prepared with a kneading compactor will be considered.

Before insertion into the triaxial cell, it was necessary to provide adequate protection of the specimen from the heat transfer oil. This was a critical step, since oil readily attacks asphaltic concrete. Various methods of sealing the specimen were investigated, however, only heat sealing in plastic bags proved successful for the resilient modulus specimens.

Prior to the sealing process, the specimen was given a thorough thin coating of emulsified asphalt to provide a sticky bond with the plastic bag. This was an essential procedure to exclude air pockets at critical points where monitoring equipment is attached. The specimen was then allowed to dry for one hour, and then carefully placed inside the plastic bag, with the specimen's axis perpendicular to the bottom of the plastic bag. A commercial heat sealer was then used to seal the open end of the bag as close as possible to the specimen. After, cutting a pinhole in a corner of the plastic bag, any air was then drawn out using a vacuum. The specimen was then placed in the cell of the

withdrawing as much air as possible, the open corner was finally pinched close, and quickly heat sealed.

Sealed specimens were left at least 24 hours, and then inspected prior to testing. If there was any indication of air getting into the bag, the plastic was removed, and the sealing process repeated. Plastic bags 0.004 inches thick (0.01 cm) were found to be adequate for the above procedure. The 8 in. high (20.3 cm) triaxial size specimens were sealed in the conventional "soil mechanics" manner using rubber membranes.

3.4 Equipment Operation

Having performed the necessary mounting procedures described in 3.1.2 or 3.1.3, the specimen is placed inside the triaxial cell, which is then positioned under the loading piston in the loading frame. All necessary external connections are then made as shown in Figure 3.13.

Next, the triaxial cell is filled with oil by opening the oil inlet valve, and applying a vacuum (7 to 10 in Hg) to the oil overflow chamber. When oil begins to enter this overflow chamber, the vacuum hose is disconnected, and the oil inlet valve is closed. The valve at the overflow chamber is left open to allow for volumetric changes of the oil within the cell during temperature changes between load applications.

Water (or glycol) is then circulated through the conducting coil in the triaxial cell from the temperature bath. This is allowed to circulate during the entire course of the experiment to stabilize the oil temperature for each desired



71

FIGURE 3.13: TRIAXIAL APPARATUS SHOWING FINAL CONNECTIONS BEFORE TESTING

measurement level.

The oscillographic recorder is then turned on, and the required channels are adjusted approximately to their respective positions on the strip chart grid. All electrical signal devices from the triaxial apparatus are then connected to their designated amplifier channels (if necessary), and balanced with the DVM. Connections are then made to the oscillographic recorder, and the galvanometers are again adjusted so that the light beams are placed at convenient grid locations.

The timers are then turned on, and the pressure reservoirs supplying both the confining pressure and axial piston systems are adjusted to the required levels. These adjusted levels are determined by the magnitude of the light beam deflections, but should be within the levels specified in 2.3.1. If necessary, adjustment of the pressure load equipment is made so that both load cell and pressure transducer outputs "peak" at the same instant. During the application of confining pressures, the oil overflow valve is closed. However, the valve must be reopened before changing cell temperatures to avoid damage to the triaxial apparatus.

It is evident from the procedures outlined in this chapter that considerable time is required in the preparation and testing of specimens using the triaxial equipment. In order to lessen the work load, it was found convenient to test one specimen from each mix design using the triaxial equipment, and to test the remaining specimens in the "simple" resilient modulus apparatus developed by Gonsalves. These

tested at ambient conditions and were found to correlate well with the specimen tested in the triaxial apparatus under the same temperature and stress conditions. The "simple" apparatus measures the resilient modulus under unconfined stress conditions only, however, this provides a quick and easy method of ensuring that the specimen tested in the triaxial apparatus is not "one of a kind". Measurement of the resilient moduli at different temperatures, using the "simple" apparatus, may be achieved by storing the specimen at the appropriate temperature level (using a temperature controlled oven or refrigerator) for at least three hours. The specimen is then removed quickly from the temperature controlled environment and tested in the device. The entire operation of mounting and testing each specimen takes only about 90 seconds. For this reason, errors due to changes in temperature will be small.

To ensure that both the "simple" and triaxial resilient modulus devices provided reliable measurements, a lucite sample similar to that used by Schmidt (6) was tested in both devices and the results were compared to Schmidt's results. Both devices produced results which were consistent with each other, and were found to be within 5 percent of Schmidt's results under similar conditions. The accuracy of the triaxial device was also checked by calculating the resilient moduli from the measured responses from the Poisson ratio device, and comparing these to the results found by using the indirect tensile test under the same conditions. Again, the resilient modulus as determined by both triaxial

Following the procedures outlined in this chapter, it is a straight forward process to obtain the measurements giving the M_R or v for any asphaltic concrete mix. In the next chapter, the experimental findings for measurement of specific asphaltic concrete mixes are detailed.

CHAPTER 4

EXPERIMENTAL FINDINGS.

4.1 Asphalt Mix Designs for Test Programme

Laboratory testing for both resilient modulus and Poisson's ratio determinations was performed on typical asphaltic concrete mixes meeting the City of Hamilton specifications. Both laboratory and field prepared (i.e. plant mix) specimens were used for this study in order to obtain a comparison between moduli for specimens from both sources. The asphaltic concrete mix designs examined were (1) HM-3; (2) HM-5; (3) steel slag (open hearth, OH-STELCO) and (4) type C. These designations refer to the gradation of the aggregate component having to meet certain limits as specified by the City of Hamilton. These gradation specification limits and physical requirements, along with the actual gradations and Marshall test results of the mixes examined, are given in Tables C.1 to C.5 of APPENDIX C. For all laboratory mixes, a single asphalt cement grade (85/100 penetration) was used, which was obtained exclusively from the Gulf Oil Company in Clarkson.

The testing programme focused mainly on investigating M_R characteristics using various percentages of asphalt cement (typically 5 to 7 percent) in the mixes. For all

| Mix Design | Specimen No. | Asphalt Content (% by wt) | Sample Temp. °C | Average Diametral Stress (psi) | Resilient Modulus | | |
|------------------------|--------------|---------------------------|-----------------|--------------------------------|------------------------------------|-------------|---------|
| | | | | | Mean M_R (ksi) ¹ x | Std. Dev. S | Range |
| HM-3 | 100 | 5 | 25.4 | 10.42 | 131 | 4.0 | 126-134 |
| | 100 | 5 | | 19.06 | 117 | 0.5 | 117-118 |
| | 100 | 5 | | 22.49 | 109 | 0.5 | 108-109 |
| | 102 | 6 | | 10.87 | 107 | 1.6 | 105-108 |
| | 102 | 6 | | 15.62 | 101 | 0.5 | 101-102 |
| | 102 | 6 | | 20.00 | 94 | 1.7 | 93- 96 |
| | 103 | 7 | | 11.51 | 95 | 1.7 | 93- 96 |
| | 103 | 7 | | 15.53 | 93 | 0.4 | 92- 93 |
| | 103 | 7 | | 19.40 | 91 | 0.6 | 90- 91 |
| STEEL SLAG (OH-STELCO) | 300 | 5 | 19.1 | 14.88 | 737 | 18.5 | 711-755 |
| | 300 | 5 | | 21.58 | 689 | 8.9 | 678-694 |
| | 300 | 5 | | 26.09 | 656 | 12.0 | 641-669 |
| | 300 | 5 | | 29.93 | 617 | 4.5 | 615-627 |
| | 302 | 5.5 | | 14.40 | 469 | 9.1 | 452-477 |
| | 302 | 5.5 | | 21.27 | 436 | 7.1 | 426-445 |
| | 302 | 5.5 | | 25.43 | 419 | 8.1 | 409-434 |
| | 302 | 5.5 | | 30.12 | 399 | 6.6 | 391-408 |
| | 304 | 6 | | 13.87 | 438 | 5.7 | 433-447 |
| | 304 | 6 | | 20.60 | 411 | 10.4 | 399-427 |
| | 304 | 6 | | 24.91 | 385 | 6.6 | 375-394 |
| | 304 | 6 | | 28.83 | 275 | 6.8 | 366-382 |
| | 306 | 6.5 | | 13.69 | 299 | 7.1 | 290-309 |
| | 306 | 6.5 | | 20.26 | 280 | 3.9 | 274-285 |
| | 306 | 6.5 | | 24.79 | 269 | 5.6 | 262-275 |
| | 306 | 6.5 | | 28.95 | 262 | 5.0 | 256-267 |

1: 8 readings were taken for each diametral stress level

TABLE 4.1: RESILIENT MODULI OF HM-3 AND STEEL SLAG (OH-STELCO) MIXES FOR VARIOUS DIAMETRAL STRESS LEVELS

mined by the use of a linear regression analysis by the method of least squares. The method is based on the general equation for a straight line:

$$y = mx + c \quad (4.1)$$

where

$$m = \frac{\Sigma xy - \frac{\Sigma x \Sigma y}{n}}{\Sigma x^2 - \frac{(\Sigma x)^2}{n}} \quad (4.2)$$

and $c = \bar{y} - m\bar{x} \quad (4.3)$

where $\bar{y} = \frac{\Sigma y}{n} \quad (4.4)$

$$\bar{x} = \frac{\Sigma x}{n} \quad (4.5)$$

n = number of paired observations

An advantage of using this method is that a third value, the coefficient of determination (r^2), may be found. This is defined by the relationship:

$$r^2 = \frac{\left[\Sigma xy - \frac{\Sigma x \Sigma y}{n} \right]^2}{\left[\Sigma x^2 - \frac{(\Sigma x)^2}{n} \right] \left[\Sigma y^2 - \frac{(\Sigma y)^2}{n} \right]} \quad (4.6)$$

The value of r^2 lies between 0 and 1 and will indicate how closely the equation fits the experimental data. The closer r^2 is to 1, the better the fit. The necessary data inputs are paired values of x and y , or in our specific case, corresponding value of diametral stress level (σ_{DM}), and mean M_R , respectively.

The results using equations (4.1) to (4.6) are summarized in Table 4.2, and are observed to fit the straight line equations reasonably well. However, it should be noted that the above relationships become meaningless as the diametral

| Mix Design | Specimen No. | Asphalt Content (% by wt) | Sample Temp. | m ksi/psi | c ksi | r ² |
|------------------------|--------------|---------------------------|--------------|-----------|--------|----------------|
| HM-3 | 100 | 5 | 25.4 | -0.1686 | 149.91 | 0.99 |
| | 102 | 6 | | -0.1370 | 122.29 | 0.99 |
| | 103 | 7 | | -0.0496 | 100.84 | 1.00 |
| STEEL SLAG (OH-STELCO) | 300 | 5 | 19.1 | -0.8293 | 856.03 | 0.99 |
| | 302 | 5.5 | | -0.4803 | 532.11 | 1.00 |
| | 304 | 6 | | -0.4593 | 498.83 | 0.99 |
| | 306 | 6.5 | | -0.2630 | 331.31 | 0.99 |

TABLE 4.2: FITTED STRAIGHT LINE EQUATIONS FOR HM-3 AND STEEL SLAG (OH-STELCO) MIXES

stress level approaches zero. Figure 4.1 gives a graphical presentation of the M_R -diametral stress level relationship for both types of specimens tested.

4.3 Effect of Varying Temperature on M_R

The results obtained in this study relating the dependence of M_R on temperature are presented in graphical form (M_R against temperature) in Figures 4.2 through 4.7. Resilient moduli used in these figures are mean values taken from a number of axial load pulses for each temperature at zero confining pressure. Although not strictly correct, Poisson's ratio for all calculations was assumed to be a constant of 0.35. The observed curves are in agreement with previous research on this temperature dependence (6, 29), and confirm the fact that temperature is the main variable influencing the M_R . The curves are seen to follow a certain characteristic pattern for laboratory prepared samples, and this is particularly noticeable in the case of the steel slag specimens. For each mix type, differences are due mainly to vertical shifting of the curves, for different asphalt contents. For field specimens from asphalt plants that were compacted in the laboratory, often after reheating, a straight line was observed to provide the best fit in most cases. This phenomenon is probably due to slight hardening of the asphalt binder as these samples were reheated before being compacted into briquettes. Consequently, all HM-5 specimens that were prepared from field mixes were found to display a straight line pattern on the semi-log plot.

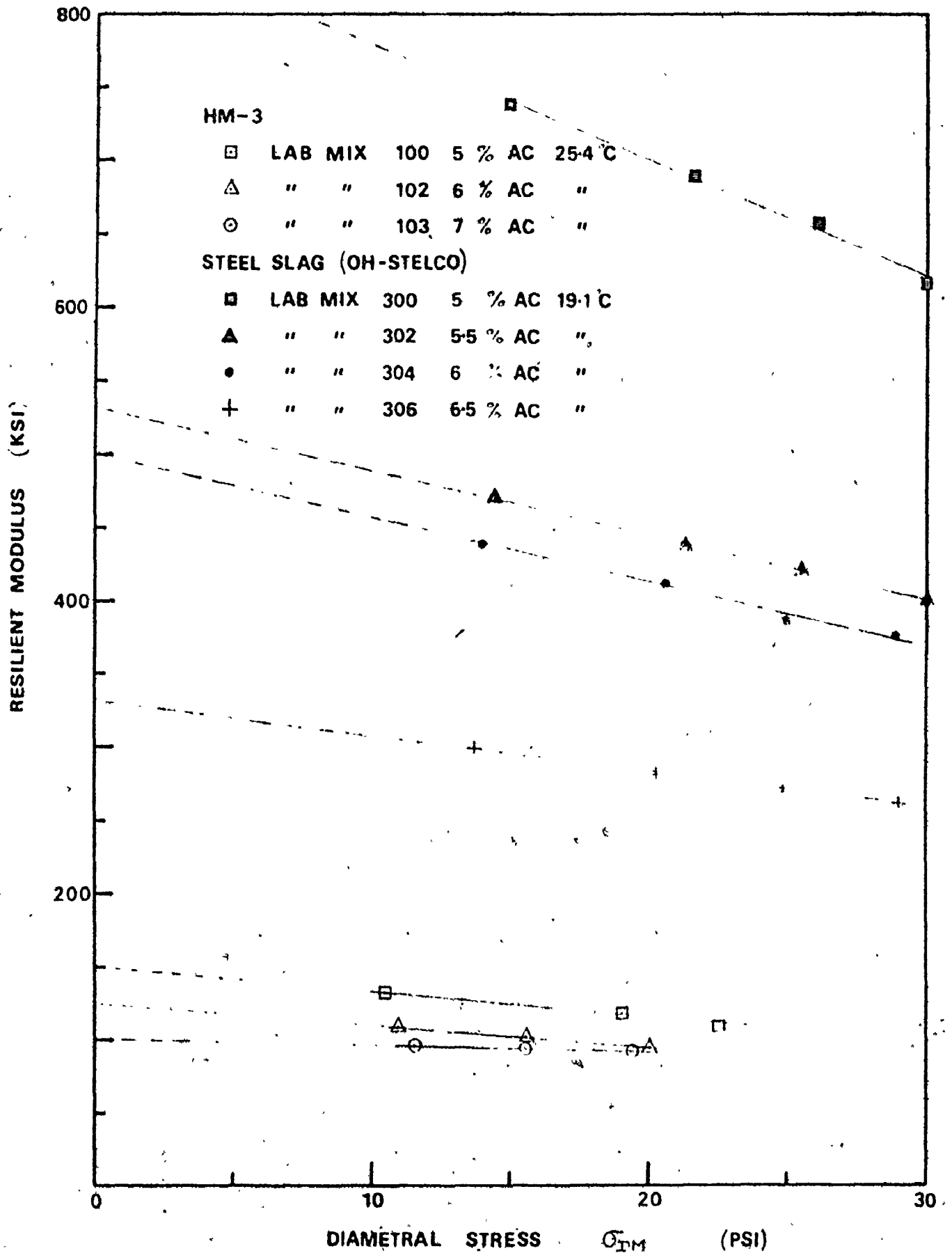


FIGURE 4.1 — M_R - DIAMETRAL STRESS RELATIONSHIP

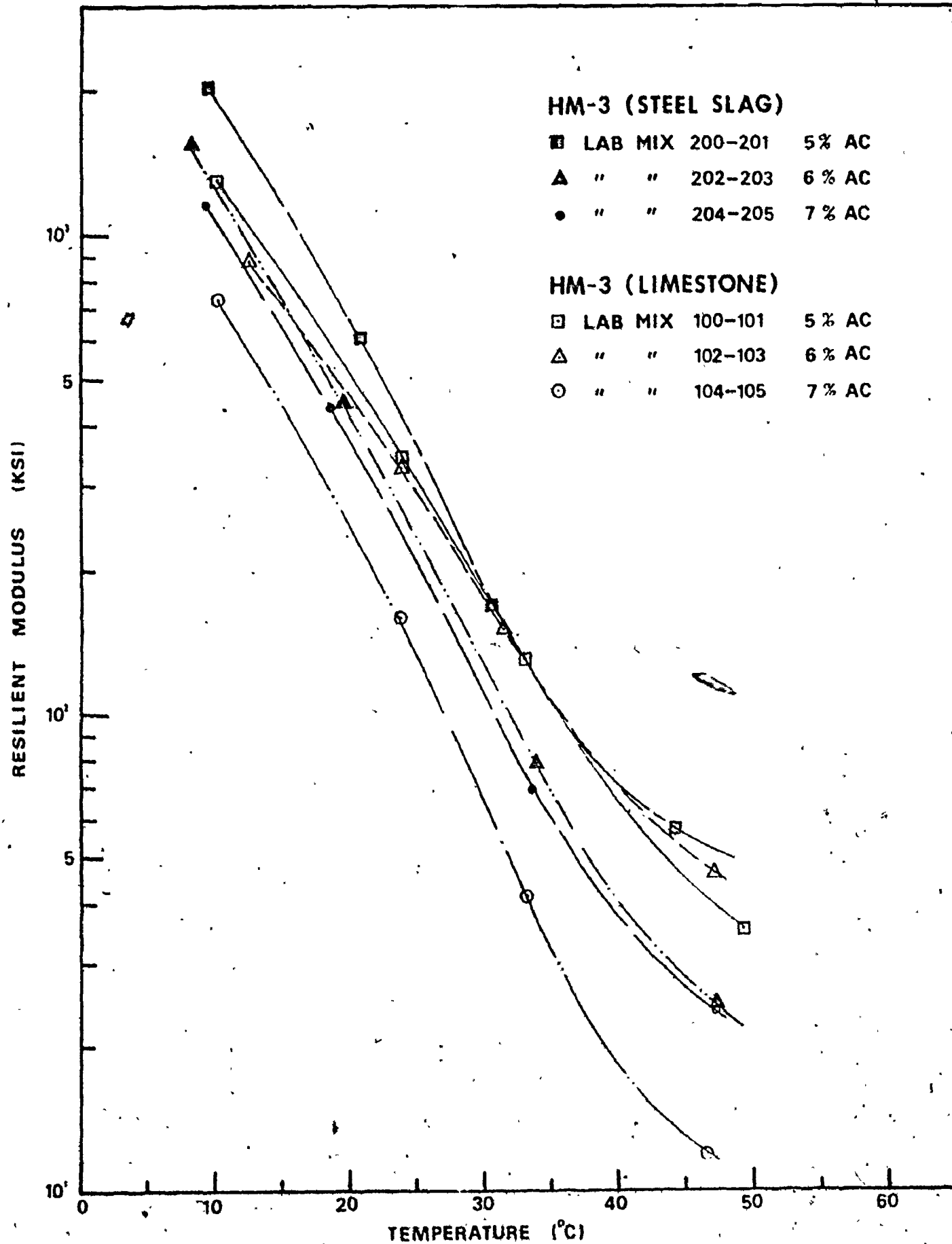


FIGURE 4.2: RELATIONSHIP BETWEEN M_R AND TEMPERATURE

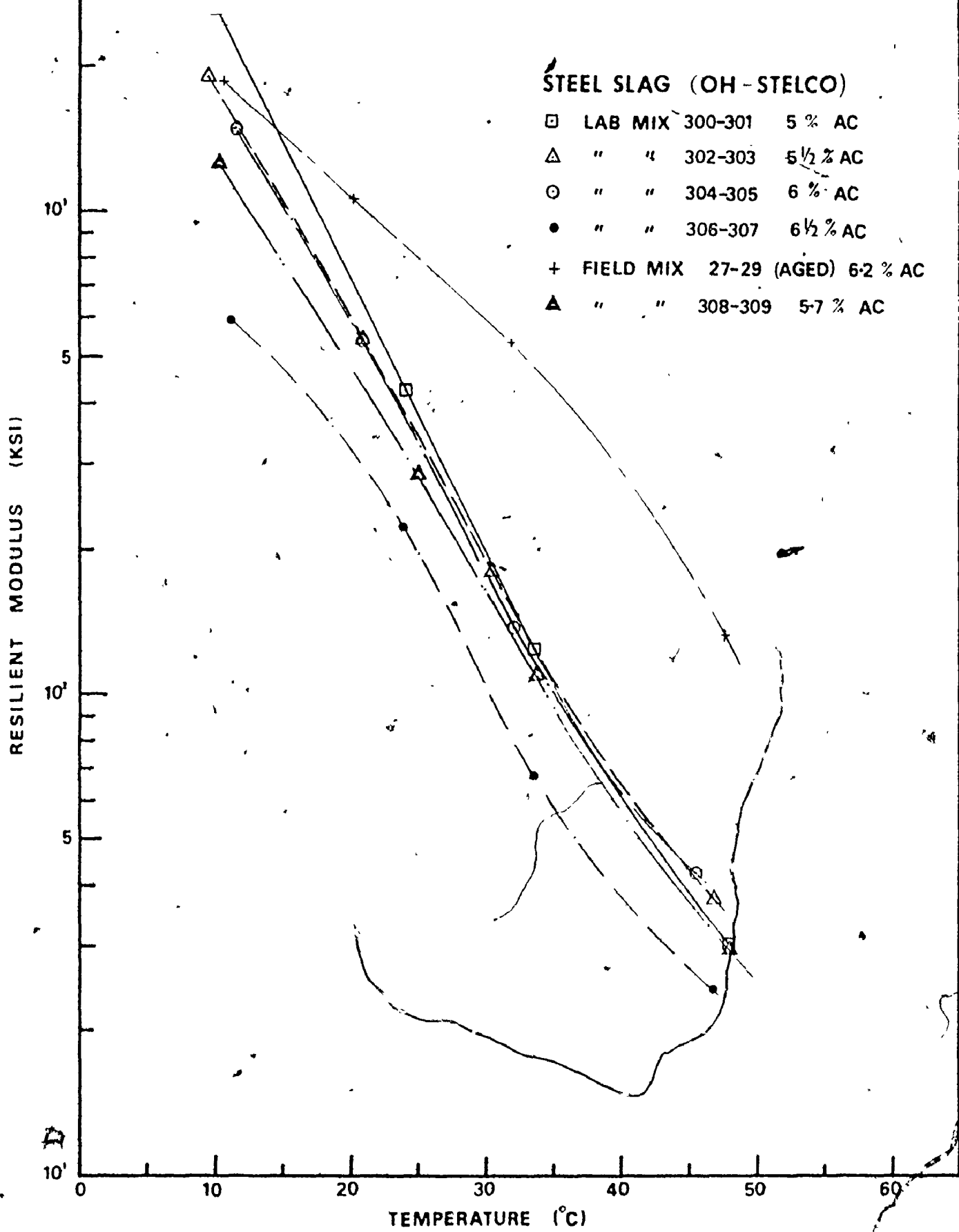


FIGURE 4.3: RELATIONSHIP BETWEEN M_R AND TEMPERATURE FOR STEEL SLAG (OH-STELCO) MIXES

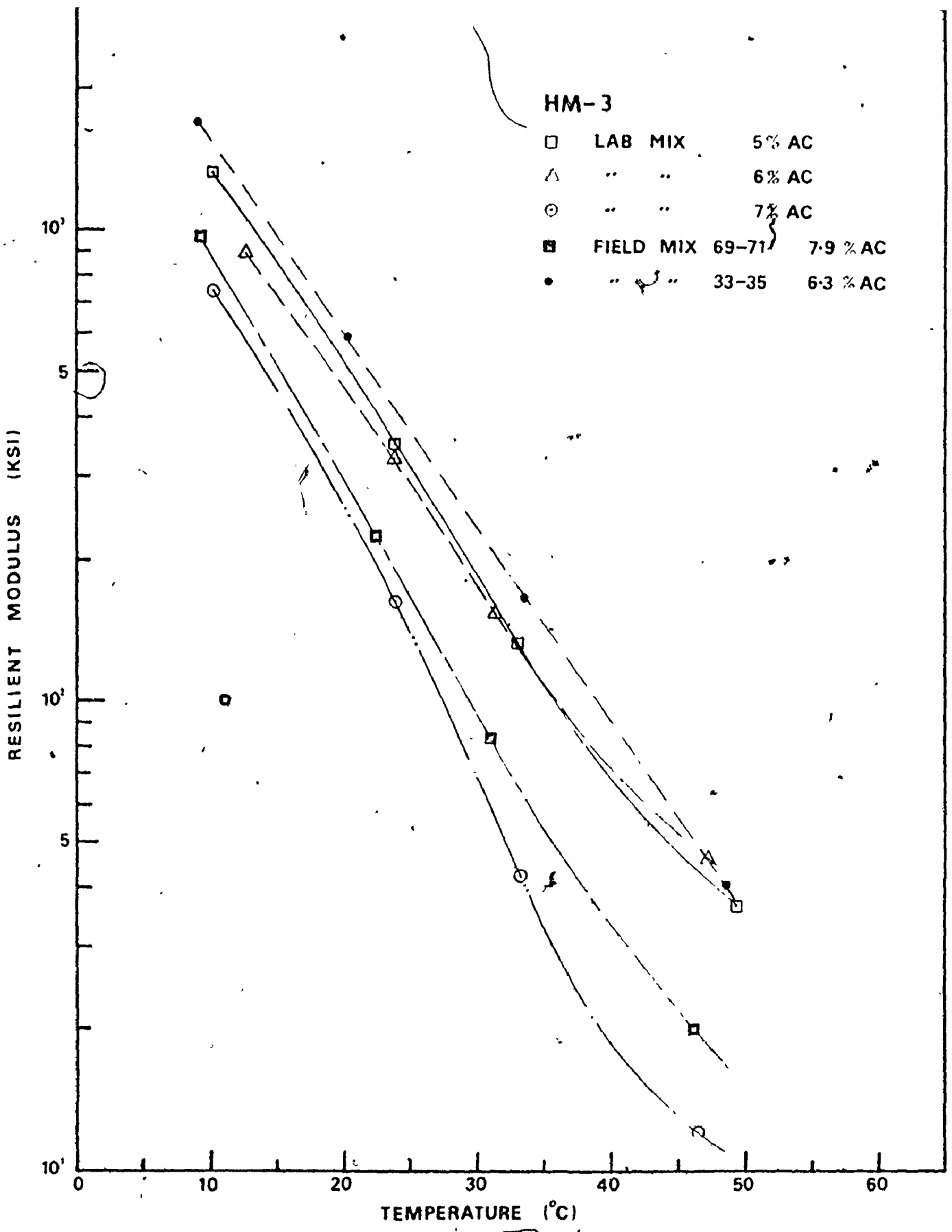


FIGURE 4.4: RELATIONSHIP BETWEEN M_R AND TEMPERATURE FOR HM-3 MIXES

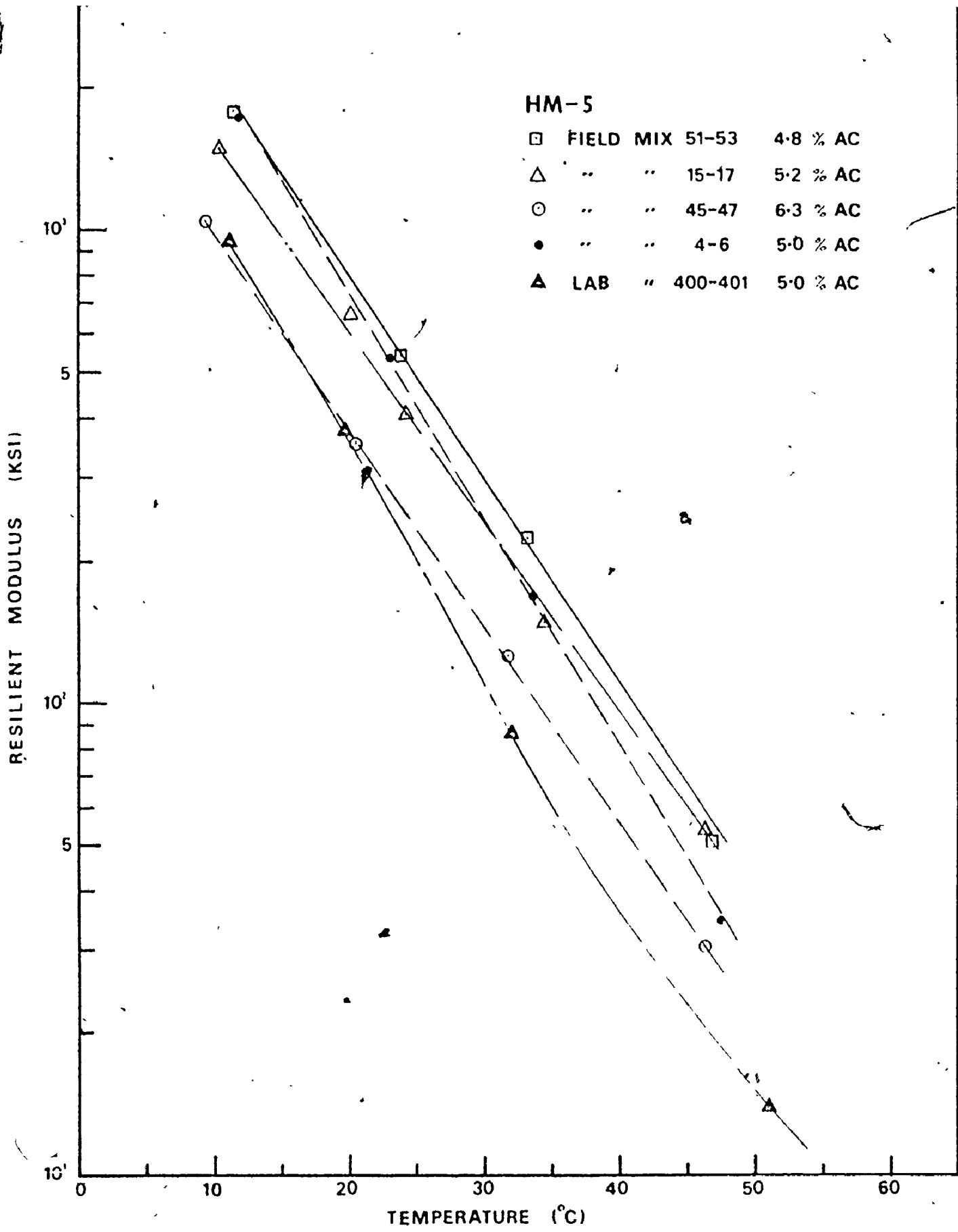


FIGURE 4.5: RELATIONSHIP BETWEEN M_R AND TEMPERATURE FOR HM-5 MIXES

TYPE C FIELD MIX 6.6% AC

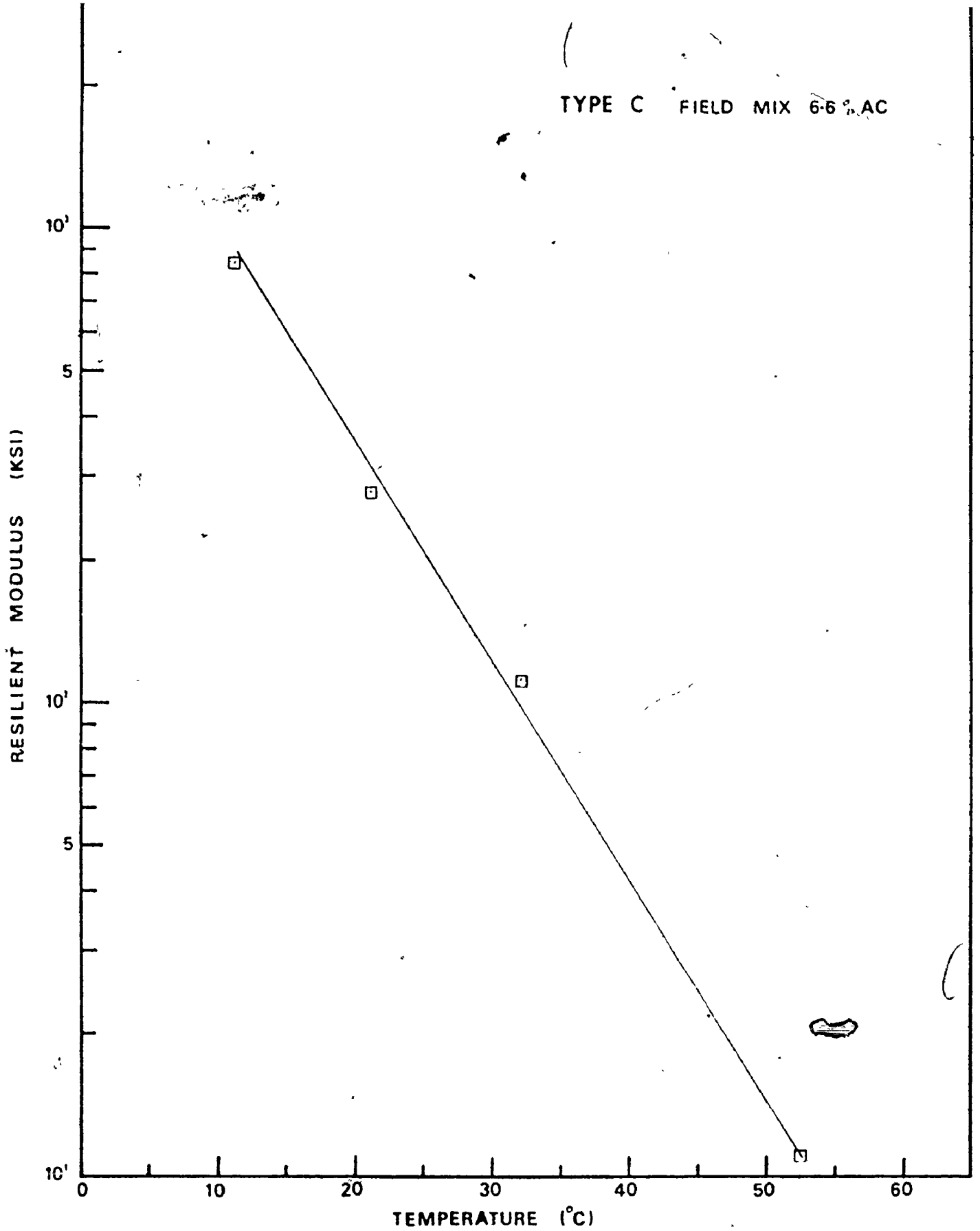


FIGURE 4.6: RELATIONSHIP BETWEEN M_R AND TEMPERATURE FOR TYPE C FIELD MIX

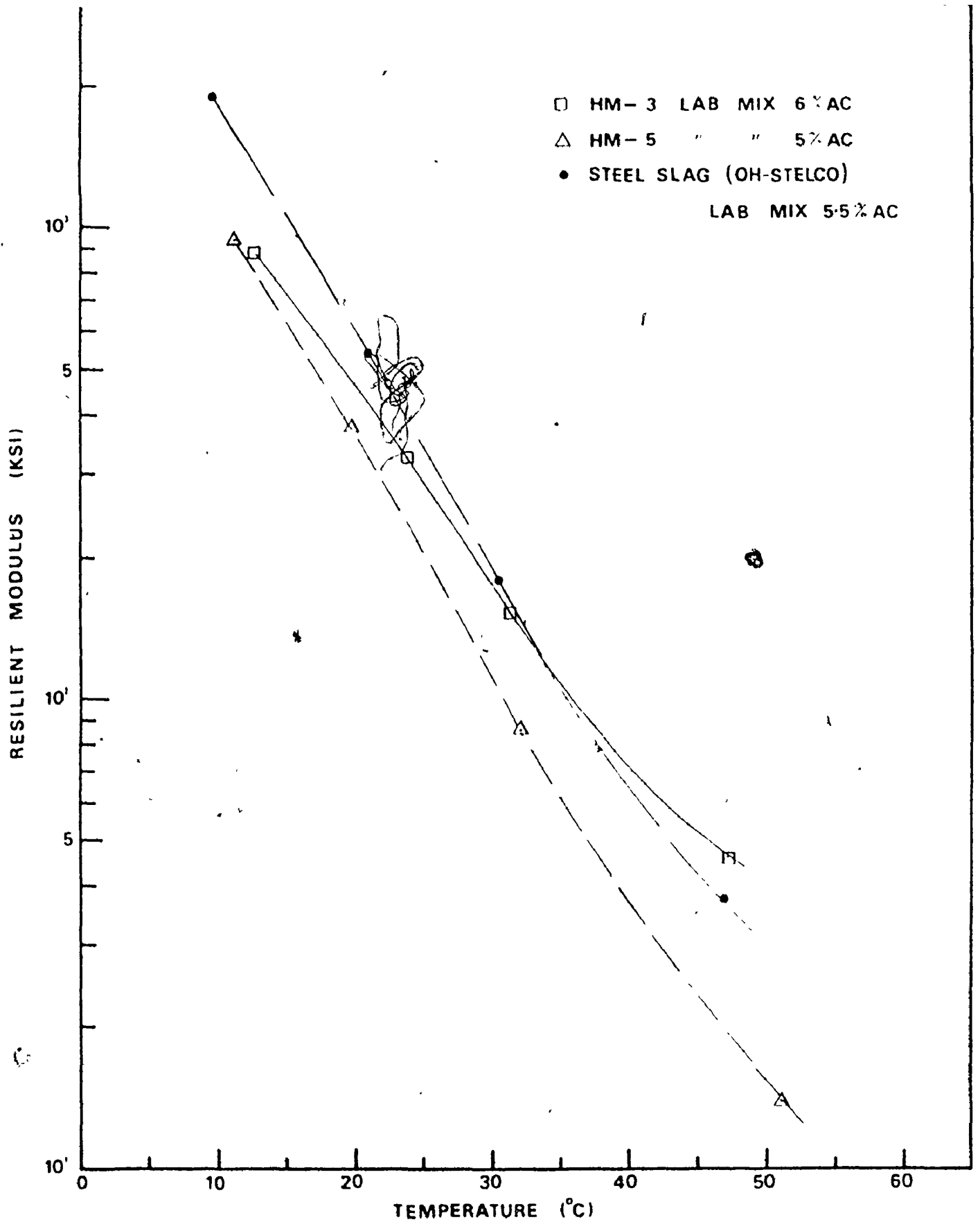


FIGURE 4.7: COMPARISON OF M_R -TEMPERATURE RELATIONSHIP FOR HM-3, HM-5, AND STEEL SLAG (OH-STELCO) MIXES FOR ASPHALT CONTENTS CLOSE TO MAXIMUM MARSHALL DESIGNS

Another typical characteristic of reheated specimens, as anticipated, is that they displayed greater M_R values than the freshly prepared specimens.

As previously indicated, in order to compare the characteristics due to different aggregate materials, steel slag was graded to approximate the median of the HM-3 specifications. Figure 4.2 shows that steel slag asphaltic concrete mixes produced higher resilient moduli throughout the temperature range (10 to 50°C) for 5 and 7% asphalt cement content compared to regular HM-3 mix (limestone aggregate) at the same asphalt contents. However, for 6% asphalt cement, regular aggregate was found to have higher M_R values at temperatures above 16°C. This phenomenon is probably due to differences in optimum asphalt contents. It should be pointed out that HM-3 using steel slag is about 1.32 times as dense as regular mixes (Table C.2), and thus contains 32% more asphalt per unit volume at the same asphalt content.

It is logical that material properties should be controlled by volumetric proportions of asphalt to aggregate. In this respect, 5% asphalt in HM-3 (steel slag) mixes should be equivalent to 6.6% asphalt in regular HM-3 mix. However, as indicated by Figure 4.2, 5% asphalt cement content for steel slag mixes had much higher M_R values than any combination for regular mixes. These results seem to indicate that the Shell nomograph method is only approximate, as aggregate characteristics do contribute significantly to the modulus of the total mix. This accentuates the need for materials

characterization if reliable numbers are to be employed in flexible pavement structural design methods.

Figure 4.3 shows the M_R -temperature relationship for unadjusted gradation open hearth steel slag (STELCO) asphalt concrete mixes. The curves for the laboratory prepared mixes, ranging from 5 to 6-1/2% asphalt cement content give a good indication of the effects of using different asphalt cement contents. However, the results show only fair correlation with the field plant mixes compacted in the laboratory, for the same aggregate gradation. Also included in this figure are results from tests conducted on an aged steel slag specimen (1 year old), which was taken from an existing pavement. As indicated by the curve, the temperature susceptibility for the aged sample was very different from that of freshly made samples. This shows the importance of considering aging effects on asphaltic concrete if proper evaluation of existing pavements is to be made. This highlights another fertile area for future research.

Figures 4.4 to 4.6 give the M_R -temperature relationships for typical HM-3, HM-5 and type c mixes, respectively. In general, it is seen that field plant mixes compacted in the laboratory, especially in the case of HM-5, gave higher resilient moduli values than laboratory prepared mixes. As previously indicated, this is due to hardening of the asphalt binder, as the field plant mixes were subjected to various levels of reheating prior to being compacted into briquettes. Figure 4.7 gives a comparison of the M_R -temperature relationship for laboratory prepared HM-3, HM-5, and unadjusted steel

slag (OH-STELCO) asphaltic concrete mixes at asphalt cement contents close to that of the optimum Marshall design (as used in the field). A typical series of calculations for M_R values under different temperature and stress conditions is presented in Table C.7 (APPENDIX C).

4.4 Effect of Varying Confining Pressure on M_R

Figures 4.8 and 4.9 are plots of M_R against the dimensionless ratio, $\sigma_{CON}/(\sigma_{DM}-\sigma_{CON})$, for HM-3 and unadjusted steel slag (OH-STELCO) laboratory asphaltic concrete mixes at different temperatures. This dimensionless ratio was chosen since, as expected, the effect of pulsating confining pressure was found to depend on the diametral stress level which was applied simultaneously with the confining pressure. This effect is shown in Figure 4.10, which gives the plot of M_R against actual pulsating confining pressure, σ_{CON} , for different $(\sigma_{DM}-\sigma_{CON})$ stress levels on sample No. 45 (HM-5 field mix). Figures 4.8 and 4.9 are presented in order to summarize experimental measurements in graphical form. However, due to the crowded appearance of these figures, it is difficult to make any clear observations from them, apart from the closely parallel, linear relationship on the semi-log scale.

In order to compare the effects of pulsating confining pressure on different mix designs at the same asphalt content (5% by weight), plots of M_R against $\sigma_{CON}/(\sigma_{DM}-\sigma_{CON})$ for HM-3, HM-3 (steel slag), HM-5, and unadjusted steel slag (OH-STELCO) were made on the same graph, as shown in Figure 4.11. The figure shows that the resilient moduli of different asphaltic

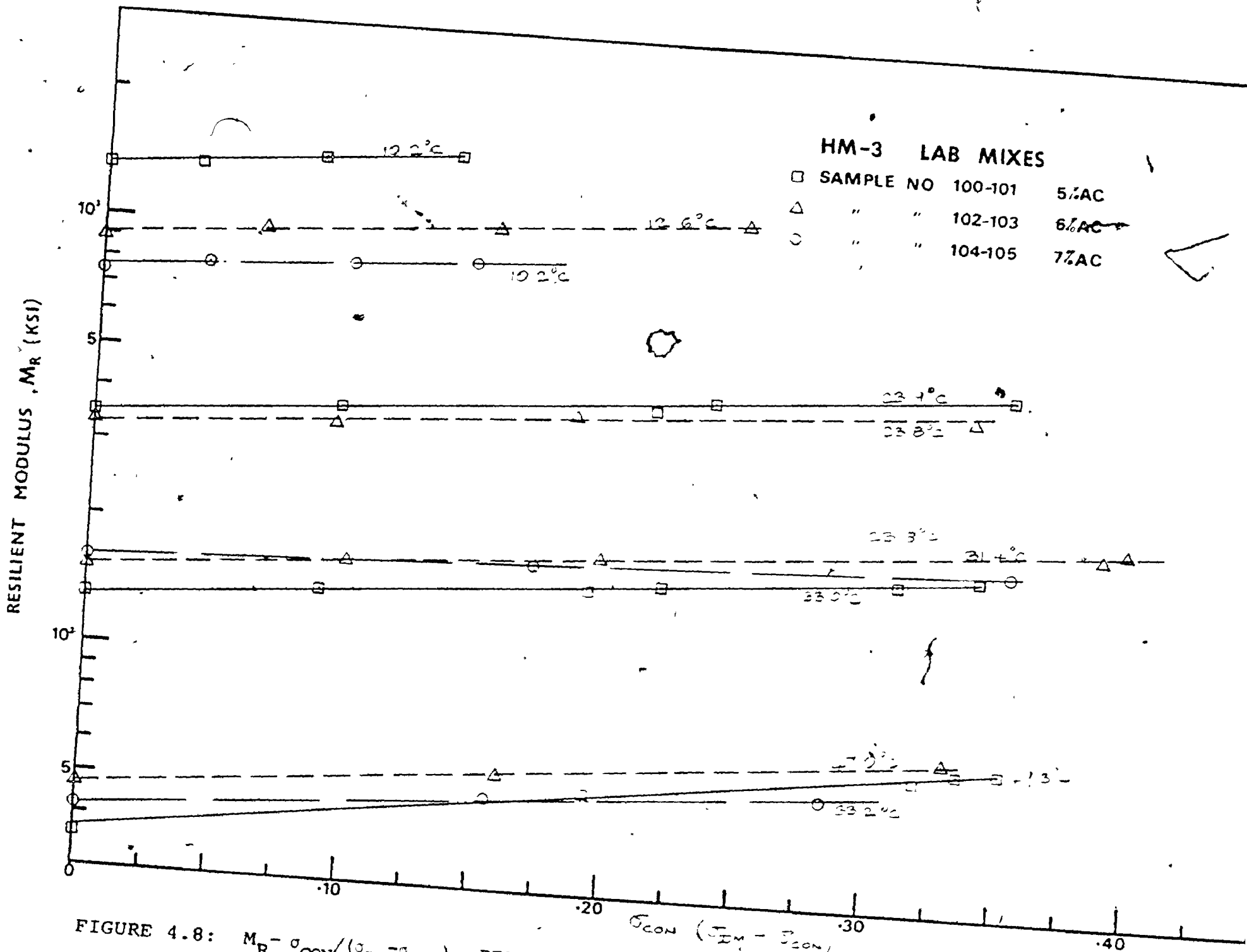


FIGURE 4.8: $M_R - \sigma_{CON} / (\sigma_{DM} - \sigma_{CON})$. RELATIONSHIP FOR HM-3 LAB MIXES

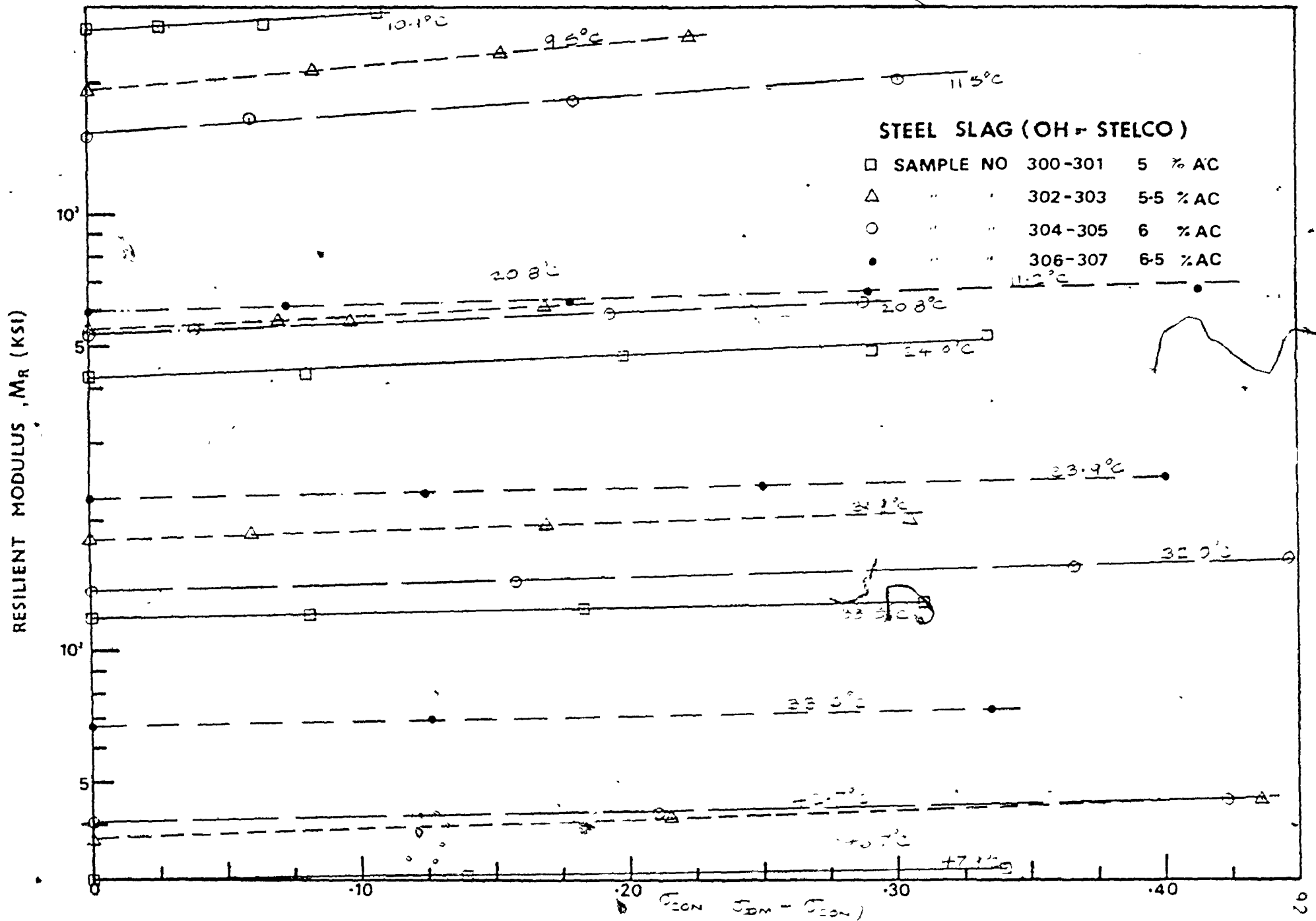


FIGURE 4.9: $M_R - \sigma_{CON} / (\epsilon_{DM} - \epsilon_{CON})$ RELATIONSHIP FOR STEEL SLAG (OH-STELCO) LAB MIXES

SAMPLE NO 45

$$(\sigma_{DM} - C_{CON}) = 3.56 \text{ PSI}$$

7.58 PSI

11.66 PSI

RESILIENT MODULUS (KSI)

0

1

2

3

4

σ_{CON} (PSI)

FIGURE 4.10 — M_R - CONFINING PRESSURE RELATIONSHIP FOR HM-5 MIX

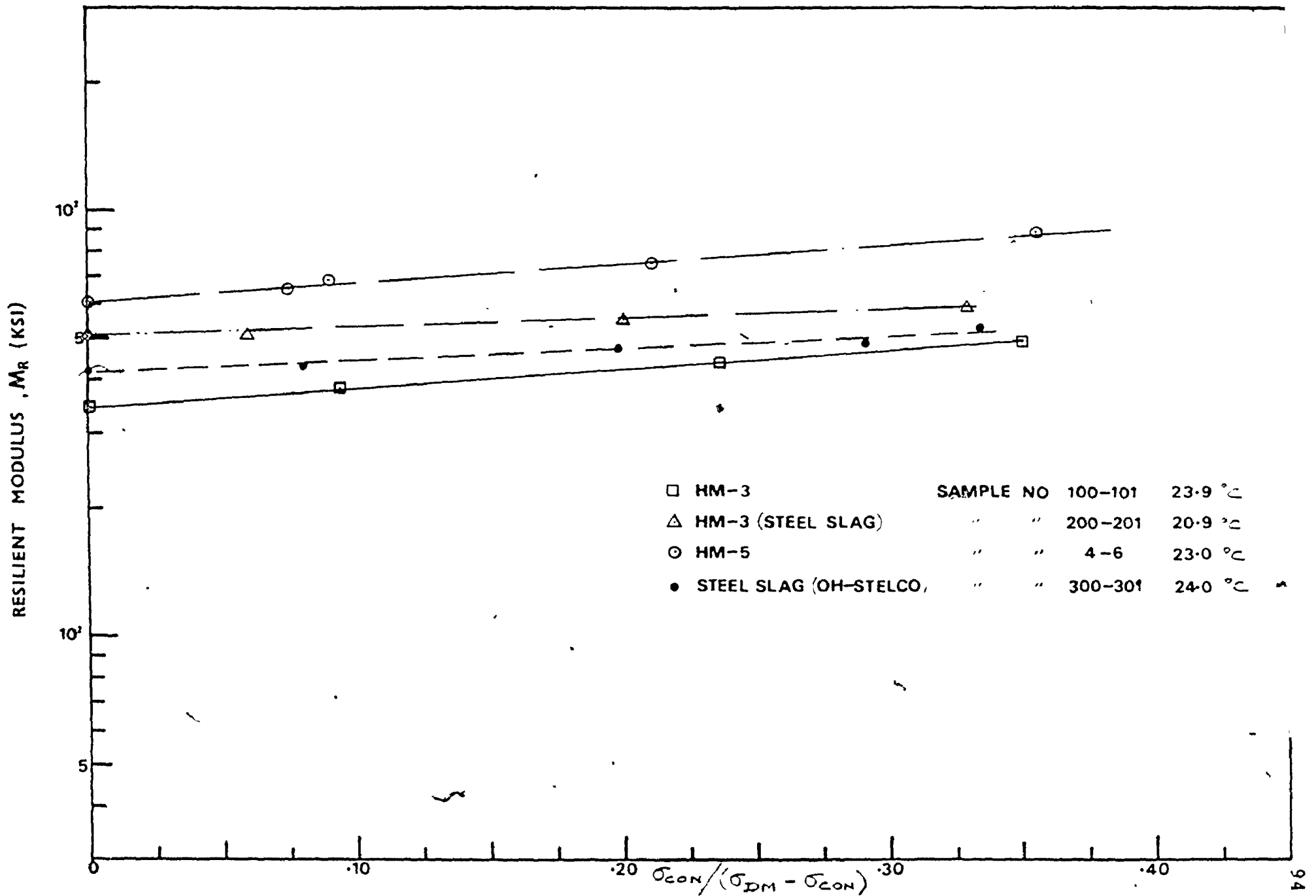


FIGURE 4.11: $M_R - \sigma_{CON} / (\sigma_{DM} - \sigma_{CON})$ FOR HM-3, HM-3 (STEEL SLAG), HM-5, AND STEEL SLAG (OH-STELCO) AT 5% AC

concrete mixes are affected to different extents when subjected to similar confining pressures.

4.5 Effect of Varying Temperature on Dynamic ν

The relationship between dynamic Poisson's ratio and temperature for HM-3 and steel slag (OH-STELCO) asphaltic concrete mixes, containing 5% asphalt cement each, is presented in Figure 4.12. Due to the limited time allotted for this study, results from only two specimens were obtained, although a great deal of time was spent in perfecting the equipment, and also in developing techniques for obtaining reliable measurements. However, results from both samples were in reasonable agreement (despite the difference in materials), showing that ν varies from about 0.24 at 10°C (50°F) to 0.46 at approximately 42°C (108°F).

4.6 Effect of Varying Confining Pressure on Dynamic ν

Investigation of the influence of confining pressure on the dynamic Poisson's ratio was carried out for a steel slag (OH-STELCO) asphaltic concrete mix, containing 5% asphalt cement. From this test, it was observed that by increasing the confining pressure, there was very little increase in ν , and for all practical purpose, this influence could be assumed to be negligible. However, more tests are required in order to confirm this observation. A typical series of calculations for determining ν under different confining pressures is given in Table C.8 (APPENDIX C).

These experimental results can be readily incorporated into linear elastic flexible pavement analysis computer

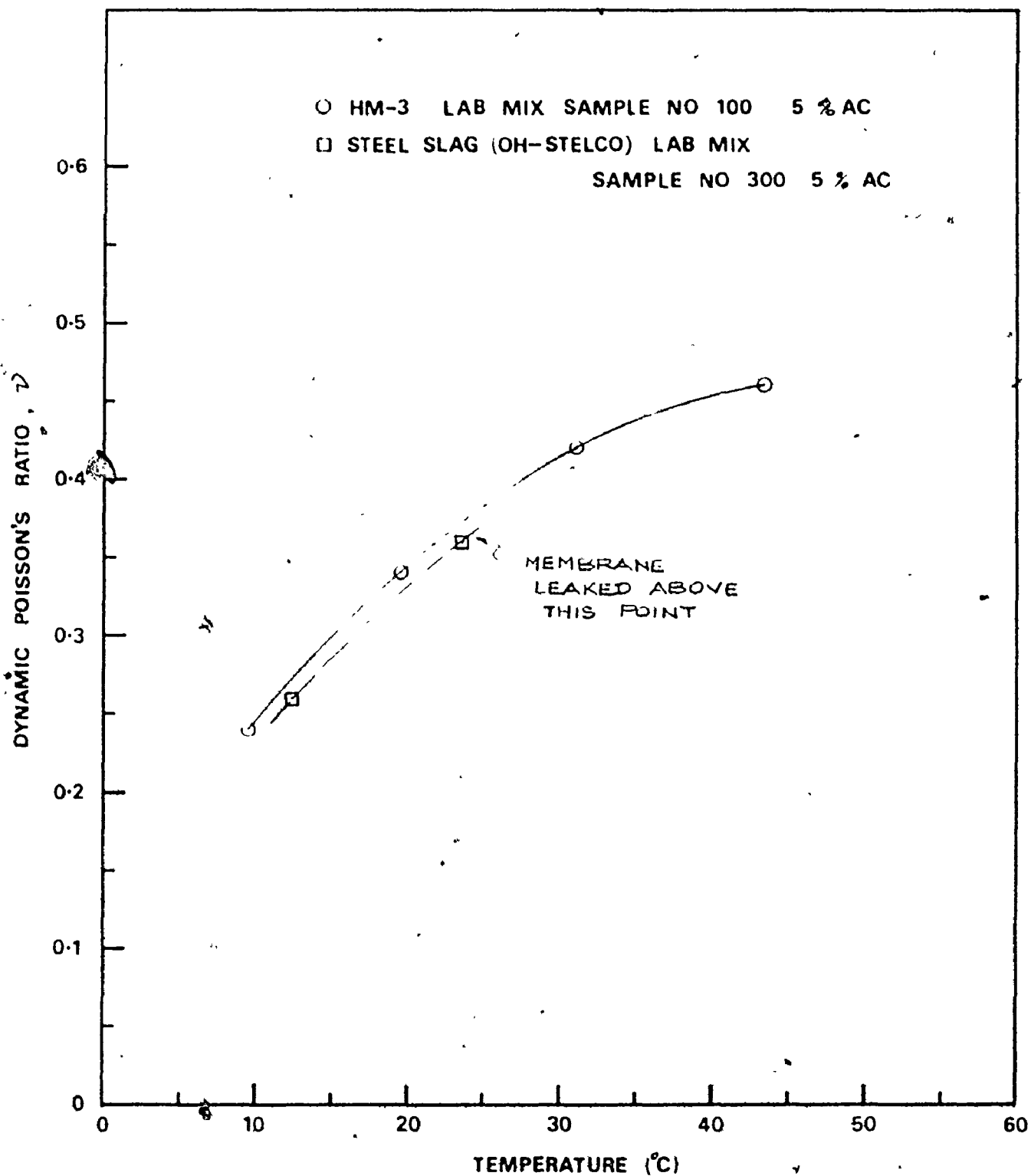


FIGURE 4.12: RELATIONSHIP BETWEEN DYNAMIC POISSON'S RATIO AND TEMPERATURE .

programmes in order to study material influences on optimization of design. In the next chapter the use of typical values of asphaltic concrete M_R and v is examined to demonstrate the advantages of utilizing the structural analysis approach to flexible pavement design.

CHAPTER 5

INFLUENCE OF ASPHALTIC CONCRETE M_R AND v ON RATIONAL FLEXIBLE PAVEMENT DESIGNS

5.1 Preliminary Design Considerations

In this chapter, two representative flexible pavement structures are examined in order to determine the difference in thickness of the asphaltic concrete layer(s), which might result from employing different mixes. In order to provide realistic numbers, the environmental and subgrade conditions of the Ontario Ministry of Transportation and Communication Brampton Test Road (19) are adopted. For design purposes, it is convenient to determine a single temperature to represent the effect of seasonal temperature variations, and this is taken when the combined pavement structure is at its weakest condition. This condition for the Brampton Test Road has been shown to occur in June, where the mean maximum air temperature is 21.1°C (70°F) and the pavement surface temperature is 29.4°C (85°C) (19). Assuming a total asphaltic concrete thickness of about 6 ins. (15.24 cm), the temperature at mid depth is estimated to be 29°C (84°F) from Figure 5.1.

For this example, two pavement structures are examined:

- 1) a pavement consisting of a wearing course (HM-3) 2-1/2 ins.

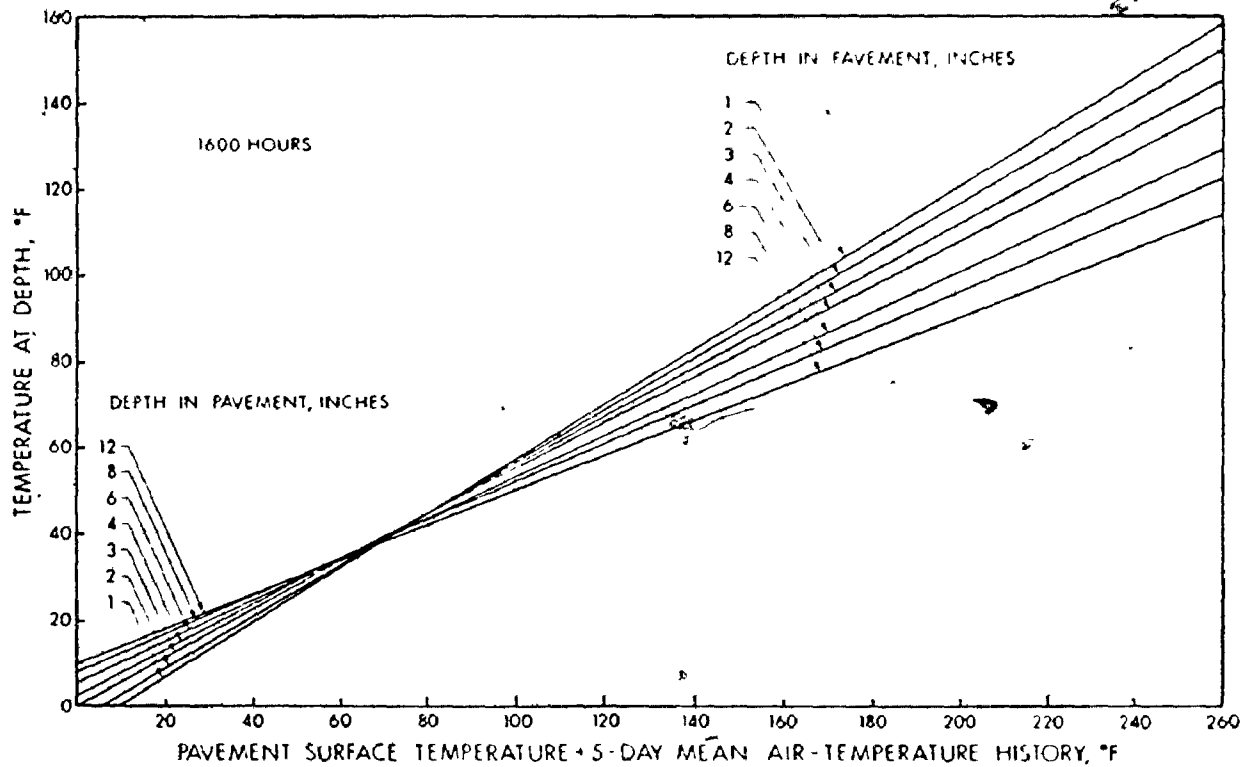


FIGURE 5.1: TEMPERATURE PREDICTION GRAPH FOR PAVEMENT GREATER THAN 2 INCHES THICK (after ref. 19)

(6.35 cm) thick; an asphalt base course (HM-5) of thickness to be determined; and a granular subbase, 20 ins. (50.80 cm) thick; and

- 2) a pavement consisting of a full depth steel slag asphaltic concrete course of thickness to be determined; and a granular base course, 20 in. (50.80 cm) thick.

Other necessary input data and assumptions are as follows:

Load: Two 4,500 lb. (20 kN) circular loads of radius 4.23 in. (10.74 cm), spaced 12 in. (30.5 cm) apart, centre to centre. This is representative of the dual tires on the standard 18 kip (80 kN) axle.

Traffic: Assume 10^6 accumulated 18 kip standard axle loads over a design period of 20 years.

Subgrade: $M_R = 20,000$ psi (137.9 MN/m²) (Brampton Test Road (19));

$$\nu = 0.43 \text{ (Brampton Test Road (19))}.$$

Unbound Granular Layer: $M_R = 2.5 \times M_R$ for subgrade (5);

$$\nu = 0.3 \quad (5).$$

Asphaltic Concrete Layer(s):

$$M_R = 200,000 \text{ psi (1379 MN/m}^2\text{) for HM-3}$$

$$= 130,000 \text{ psi (896 MN/m}^2\text{) for HM-5}$$

$$= 240,000 \text{ psi (1655 MN/m}^2\text{) for steel slag}$$

$$\nu = 0.41$$

The above values for asphaltic concrete were estimated from the results of the previous chapter. These results are representative of typical M_R values at 29°C (84°F), for the optimum Marshall design of the asphaltic concrete mixes as determined from laboratory prepared specimens. These values

are obviously somewhat less than those from the field that were subjected to various temperature levels. The value for v was estimated from Figure 4.12 for 29°C (84°F), and was assumed to be the same for all three mixes.

5.2 Limiting Stress and Strain Conditions

5.2.1 Tensile Strain at Bottom of Lowest Asphalt Cement Bound Layer

The fatigue criteria for the tensile strain at the bottom of the lowest asphalt cement bound layer, as discussed in Chapter 1, is dependent on the mix variables. These mix variables include aggregate type and grading, asphalt cement type and content, degree of mix compaction, and percentage of air voids (27, 28). Clearly, it is almost impossible to obtain the fatigue strain criteria for a particular mix, in view of the numerous combinations of the above variables. Also, due to the deficiencies of the laboratory fatigue tests conducted to date, little has been done to correlate laboratory results to the actual field behaviour of pavements (30). However, until better design limits are developed, laboratory derived criteria must be used.

Research by Pell and Brown (27) has indicated that the two factors which appear to be of primary importance to flexible pavement fatigue are binder content and voids content. For mixes with similar asphalt cement contents, the aggregate type and asphalt cement grade have a negligible effect on the strain-life relationship. In view of the above observations, the limiting strain criterion for asphaltic

concrete, with voids between 3 to 5% was interpolated from results given by Pell and Brown (27). For a fatigue life of 10^6 applications of the standard 18 kip (80 kN) axle load, a tensile strain, ϵ_h , of 10^{-4} was found to be appropriate. This value is in close agreement with the limiting strain at 10^6 load repetitions from results due to Monismith (43).

5.2.2 Compressive Strain at Top of the Subgrade

The permissible vertical compressive strains at the top of the subgrade are the maximum values to which the subgrade can be subjected without significant permanent deformation occurring. In the absence of any fundamental or laboratory data, the criteria developed by Dormon and Metcalf (29) has been adopted for this study. Based on this method, the limiting compressive strain in the subgrade, ϵ_z , for 10^6 standard axle load applications, was found to be 6.5×10^{-4} .

5.2.3 Horizontal Tensile Stress at the Bottom of the Unbound Layer

As indicated in Chapter 1, the tensile stress at the bottom of the unbound base or subbase layer, σ_h , is restricted to a maximum value of 0.5 times the vertical stress plus the horizontal overburden pressure at the point concerned. The horizontal overburden pressure is assumed to be equal to the vertical overburden pressure (ie $k_0=1$) for compacted granular material. The vertical stress is determined along with the induced strains at the designated points using the BISTRO computer programme.

5.3 Computer Runs Comparing Designs for Various Mixes

Several runs were made, using the BISTRO computer programme, in order to determine the optimum asphalt layer thicknesses of the two pavement structures cited above. The final designs are summarized in Table 5.1, from which it is seen that a saving of 1-1/2 in. (3.81 cm) of asphaltic concrete is obtained by the second design, using a material of higher M_R .

This example serves to demonstrate the economic advantage of utilizing the structural analysis approach to flexible pavement design. This is contrasted with empirical methods which do not allow for the optimization of design for more efficient use of materials.

| Pavement Structure | Layer | Material | Thickness ins. (cm) | Design Stress or Strain Value | Computed Stress or Strain Value |
|--------------------|-----------|---------------|---------------------|------------------------------------|-------------------------------------|
| 1 | surfacing | HM-3 | 2.5 (6.35) | σ -- | -- |
| | base | HM-5 | 5.5 (13.97) | $\epsilon_h = 10^{-4}$ | $\epsilon_h = 0.96 \times 10^{-4}$ |
| | subbase | crushed stone | 20 (50.80) | $\sigma_h = 3.67 \text{ psi}$ | $\sigma_h = 2.89 \text{ psi}$ |
| | subgrade | cohesive soil | ∞ | $\epsilon_z = -6.5 \times 10^{-4}$ | $\epsilon_z = -1.38 \times 10^{-4}$ |
| 2 | surfacing | steel slag | 6.5 (16.51) | $\epsilon_h = 10^{-4}$ | $\epsilon_h = 1.00 \times 10^{-4}$ |
| | base | crushed stone | 20 (50.80) | $\sigma_h = 3.65 \text{ psi}$ | $\sigma_h = 3.06 \text{ psi}$ |
| | subgrade | cohesive soil | ∞ | $\epsilon_z = -6.5 \times 10^{-4}$ | $\epsilon_z = -1.47 \times 10^{-4}$ |

TABLE 5.1: FINAL ANALYSIS FOR HYPOTHETICAL DESIGN EXAMPLES

CHAPTER 6

CONCLUSIONS

Laboratory equipment capable of providing reliable measurements of material properties for asphaltic concrete mixes, under variable stress and temperature conditions has been developed. The basic material properties obtained by these measurements are the resilient modulus (M_R) and dynamic Poisson's ratio (ν), which are necessary inputs for the elastic analysis of flexible pavement structures. Due to the variable traffic and environmental conditions to which pavements are subjected, it was necessary to investigate these effects on the material properties.

Tests conducted on asphaltic concrete mixes, using the diametral tension resilient modulus test method, have indicated temperature to be the main parameter affecting the resilient modulus. For asphaltic concrete, a decrease of 10°C (18°F) was found to cause increases in M_R of more than three times the original value. The temperature susceptibility of any particular mix is dependent on the asphalt cement content, aggregate gradation, and actual aggregate employed. In addition, aging or hardening of the asphalt cement plays an important role in the M_R -temperature relationship. Reheating of asphaltic concrete samples taken from the field (in order to make Marshall specimens) causes significant hardening,

reflected by unusually high resilient moduli.

Changes in diametral stress level (using the diametral tension method) affects the resilient modulus to a moderate degree, depending on the mix variables, and possibly the specimen temperature. This relationship between resilient modulus and diametral stress level is approximately inverse and linear. Pulsating confining pressures also affect the resilient modulus as determined by the diametral tension resilient modulus test method. The resilient modulus increases approximately logarithmically with increasing pulsating confining pressure, with approximately the same slope, regardless of temperature. The results seem to indicate that different mix designs are affected to different extents when subjected to similar confining pressures.

The dynamic Poisson's ratio increases with temperature from about 0.24 at 10°C (50°F) to approximately 0.46 at 42°C (108°F). This observation is based on tests conducted on only two specimens, however, the results are consistent with the expected behaviour of asphaltic concrete under static loading conditions. Confining pressure is found to have little or no effect on the dynamic ν , based on the results of tests conducted on one specimen. However, this will have to be verified by more tests in the future.

Although the experimental work reported in this study relates only to asphaltic concrete mixes, tests were also conducted on lime stabilized materials with very promising results. Indeed, the dynamic testing using the developed equipment is not restricted to asphaltic concrete materials

may be examined, provided that proper sampling and freezing techniques are employed. This is a possible consideration for future phases of this continuing research. Future research should also focus on testing asphaltic concrete cores from existing pavement structures to examine the aging effects on both resilient modulus and dynamic Poisson's ratio. It is also required that similar techniques be extended to obtain samples from pavements constructed from emulsified asphalts. It is anticipated that future studies will include the investigation of fatigue effects using the same, or a slightly modified version of the equipment. In addition, the triaxial apparatus will be transferred over to the MTS system to examine the effects of using precise servo controlled loadings of different waveforms.

Although further research is required on the triaxial apparatus, it is clear from the results of this study that the "simple" unconfined apparatus developed in earlier studies is quite adequate for commercial use. In the design of this equipment, the policy of keeping cost to a minimum was strictly adhered to. In view of the current trend towards the rational approach to flexible pavement design, it is hoped that the "simple" apparatus, or similar relatively inexpensive equipment will be made readily available to small laboratories specializing in materials testing.

REFERENCES

1. Warren, H., and W. L. Dieckmann, "Numerical Computation of Stresses and Strains in a Multiple-Layered Asphalt Pavement System", California Res. Corp., Richmond, California, September, 1963.
2. Peutz, M. G. F., A. Jones, and H. P. M. Van Kempen, "Computer Program Bistrolayered Systems Under Normal Surface Loads", Shell-Laboratorium, Amsterdam.
3. DeJong, D. L., M. G. F. Peutz, and A. R. Korswagen, "Computer Program Bistar-Layered Systems Under Normal and Tangential Surface Loads", Shell-Laboratorium, Amsterdam, External Report, AMSR.0006.73.
4. The Asphalt Institute, "Computer Program Supplement to Full-Depth Asphalt Pavements for Air Carrier Airports", Manual Series No. 11A(MS-11A).
5. Brown, S.F., and P.S. Pell, "A Fundamental Structural Design Procedure for Flexible Pavements", Proc. Third Int. Conf. on the Struct. Des. of Asp. Pvs., London, England, 1972.
6. Schmidt, R.J., "A Practical Method for Measuring the Resilient Modulus of Asphalt-Treated Mixes", H.R.B. Record, No. 404, 1972.

7. Schmidt, R.J., "Effect of Temperature, Freeze-Thaw, and various Moisture Conditions on the Resilient Modulus of Asphalt-Treated Mixes", T.R.B. Record, No. 515, 1974.
8. Hondros, G., "The Evaluation of Poisson's Ratio and The Modulus of Materials of a Low Tensile Resistance by the Brazilian (indirect tensile) Test with Particular Reference to Concrete", Australian Journal of Applied Science, Vol. 10, No. 3, September, 1959.
9. Hudson, W.R., and T.W. Kennedy, "An Indirect Tensile Test for Stabilized Materials", Center for Highway Research, Res. Report No. 98-1, Austin, Texas, January, 1968.
10. Hadley, W.O., W.R. Hudson, and T.W. Kennedy, "An Evaluation of Factors Affecting the Tensile Properties of Asphalt-Treated Materials", Centre for Highway Research, Res. Report No. 98-2, Austin, Texas, March, 1969.
11. Hadley, W.O., W.R. Hudson, and T.W. Kennedy, "Evaluation and Prediction of the Tensile Properties of Asphalt-Treated Materials", Centre for Highway Research, Res. Report No. 98-9, Austin, Texas, May 1971.
12. Kennedy, T.W., and W.R. Hudson, "Tensile Properties of Subbases for Use in Rigid Pavement Design", Centre for Highway Research, Res. Report No. 98-14F, Austin, Texas, February 1973.

13. Thompson, M.R., "The Split-Tensile Strength of Lime-Stabilized Soils", Lime Stabilization, H.R.B. Record, No. 92, 1965.
14. Breen, J.J., and J.E. Stephens, "Split Cylinder Test Applied to Bituminous Mixtures at Low Temperatures", Journal of Materials, Vol. 1, No. 1, A.S.T.M., March 1966.
15. Vila, J.M., and R.L. Terrel, "Influence of Accelerated Climatic Conditions on Split Tension Deformations of Asphalt Concrete", Proc. Assoc. Asph. Paving Technologists, 1975.
16. Carniero, F.L.L.B., and A. Barcellus, "Concrete Tensile Strength", Bulletin No. 13, International Assoc. of Testing and Res. Laboratories for Materials and Structures, Paris, March 1953.
17. Akazawa, T., "Tension Test Method for Concrete", Bulletin No. 16, International Assoc. of Testing and Res. Laboratories for Materials and Structures, Paris, November 1953.
18. Schmidt, R.J., and P.E. Graf, "The Effect of Water on the Resilient Modulus of Asphalt Treated Mixes", Proc. Assoc. Asph. Paving Technologists, Cleveland, Ohio, 1972.
19. Haas, R.C.G., N.I. Kamel, and J. Morris, "Brampton Test Road: An Application of Layer Analysis to Pavement Design", M.T.C. Report No. RR182, November 1972.
20. Highway Research Board, "Review of Existing Theories and Methods of Pavement Design", Hwy. Res. Circular, No. 112, October 1970.

21. The Asphalt Institute, "Mix Design Methods for Asphalt Concrete and Other Hot-Mix Types", Manual Series No. 2 (MS-2), 4th Ed., March 1974.
22. Oglesby, C.H., Highway Engineering (3rd Ed.), John Wiley & Sons, Inc., New York, 1975, pp 205-206.
23. Finn, F.N., K. Nair, and C. L. Monismith, "Applications of Theory in the Design of Asphalt Pavements", Proc. Third Int. Conf. on the Structure Des. of Asph. Pvts., London, England, 1972.
24. Carey, W.N., and P.E. Irick, "The Pavement Servicibility-Performance Concept", H.R.B. Bulletin, No. 250, 1960.
25. Shell International Petroleum Company Limited, "Shell Design Charts for Flexible Pavements", London 1963.
26. Yoder, E.J., and M.W. Witczak, "Asphalt Mix Stiffness (Shell Nomograph)", Principles of Pavement Design (2nd Ed.), John Wiley & Sons, Inc., New York, 1975.
27. Pell, P.S., and S.F. Brown, "The Characteristics of Materials for the Design of Flexible Pavement Structures", Proc. Third Int. Conf. on the Struct. Des. of Asph. Pvts., London, England, 1972.
28. Pell, P.S., and K.E. Cooper, "The Effect of Testing and Mix Variables on the Fatigue Performance of Bituminous Materials", Proc. Assoc. Asph. Paving Technologists, 1975.

29. Dormon, G.M., and C.T. Metcalf, "Design Curves for Flexible Pavements Based on Layered System Theory", H.R.B. Record, No. 71, 1964.
30. Morris, J., "The Prediction of Permanent Deformation in Asphalt Concrete Pavements", The Transport Group, University of Waterloo, Waterloo, Ontario, September, 1973.
31. Sargious, M., "Load Equivalency Factors for Highway Flexible Pavements", Pavements and Surfacing for Highways and Airports, Applied Science Publishers Ltd., London, 1975.
32. Timoshenko, S., and J.N. Goodier, "Stresses in a Circular Disk", Theory of Elasticity (2nd Ed.), McGraw-Hill, New York, 1951.
33. Frocht, M.M., Photoelasticity, Vol. 2, John Wiley & Sons, Inc., New York, 1957.
34. Brown, S.F., "Improved Framework for Predicting Permanent Deformation in Asphalt Layers", T.R.B. Record, No. 537, 1975.
35. Bowles, J.E., "Load Induced Pressures", Foundation Analysis and Design, McGraw-Hill Book Co., New York, 1968.
36. Brown, S.F., "Determination of Young's Modulus for Bituminous Materials in Pavement Design", H.R.B. Record, No. 431, 1973.
37. Barksdale, R.G., "Compressive Stress Pulse Times in Flexible Pavements for Use in Dynamic Testing", H.R.B. Record, No. 345, 1971.

38. Bergan, A.T., and C.L. Monismith, "Some Fatigue Considerations in the Design of Asphalt Concrete Pavements", Dept. of Civil Engineering, University of Saskatchewan, Saskatoon, November, 1972.
39. Seed, H.B., F.G. Mitry, C.L. Monismith, and C.K. Chan, "Prediction of Flexible Pavement Deflections from Laboratory Repeated Load Tests", H.R.B., N.C.H.R.P., No. 35, 1965.
40. Bergan, A.T., and C.L. Monismith, "Characterization of Subgrade Soils in Cold Regions for Pavement Design Purposes", H.R.B. Record, No. 431, 1973.
41. Benkleman, A.C., "Analysis of Flexible Pavement Deflection and Behaviour Data", H.R.B. Bulletin, No. 210, 1959.
42. Emery, J.J., and W.G. Heslop, "A Comparison of Flexible Pavement Behaviour under Dual and Flotation Tires for Static and Moving Loads", 48th Annual Convention of the Canadian Good Roads Assoc., Vancouver, 1967.
43. Yoder, E.J., and M.W. Witczak, "Materials Characterization", Principles of Pavement Design (2nd Ed.), John Wiley & Sons, Inc., New York, 1975.

```

1      PROGRAM TST (INPUT,OUTPUT,TAPE5=INPUT,TAPE6=OUTPUT)
2      DIMENSION A(20),B(20)
3      READ(R,1)C,RAD
4      *****WHERE C = WIDTH OF STRIP,RAD = RADIUS OF SPECIMEN *****
5      1 FORMAT(2F10.5)
6      R = C/2
7      *****WHERE R = DISTANCE FROM CENTRE OF DISK *****
8      DR = C/2
9      DELA = C/2
10     DELB = C/2
11     ALPHA = C/(2.0+RAD)
12     SIN = SIN(2.0*ALPHA)
13     COS = COS(2.0*ALPHA)
14     TH = TAN(ALPHA)
15     I = 1
16     J = C
17     3 I = I+1
18     J = J-1
19     TOPA = (1.0-(R**2)/(RAD**2))
20     BOTA = 1.0+2*(R**2)/(RAD**2)+COS*(R**4)/(RAD**4)
21     TOPB = (1.0-(R**2)/(RAD**2))
22     BOTB = (1.0+(R**2)/(RAD**2))
23     A(I) = (TOPA/BOTA)*SIN*DR
24     B(J) = (ATAN((TOPB/BOTB)+TH))*DR
25     DELA = DELA + A(I)
26     DELB = DELB + B(J)
27     R = R + C/2
28     IF(R.GT. RAD)GOTO-
29     GOTO 3
30     WRITE(6,5)C,RAD
31     5 FORMAT(1H ,*WIDTH OF STRIP = *,1X,F10.5,14 ,*RADIUS = *,1X,F10.5)
32     WRITE(6,2)DELA,DELB
33     2 FORMAT(1H ,*DELA = *,1X,F12.3,14 ,*DELB = *,1X,F12.8)
34     STOP
35     END

```

APPENDIX A

COMPUTER PROGRAMME FOR CALCULATING DELA & DELB



APPENDIX B

ELECTRICAL CIRCUIT DIAGRAMS

MINI TYPE EA 06-125RZ - 350
(OPTION W) STRAIN GAUGE

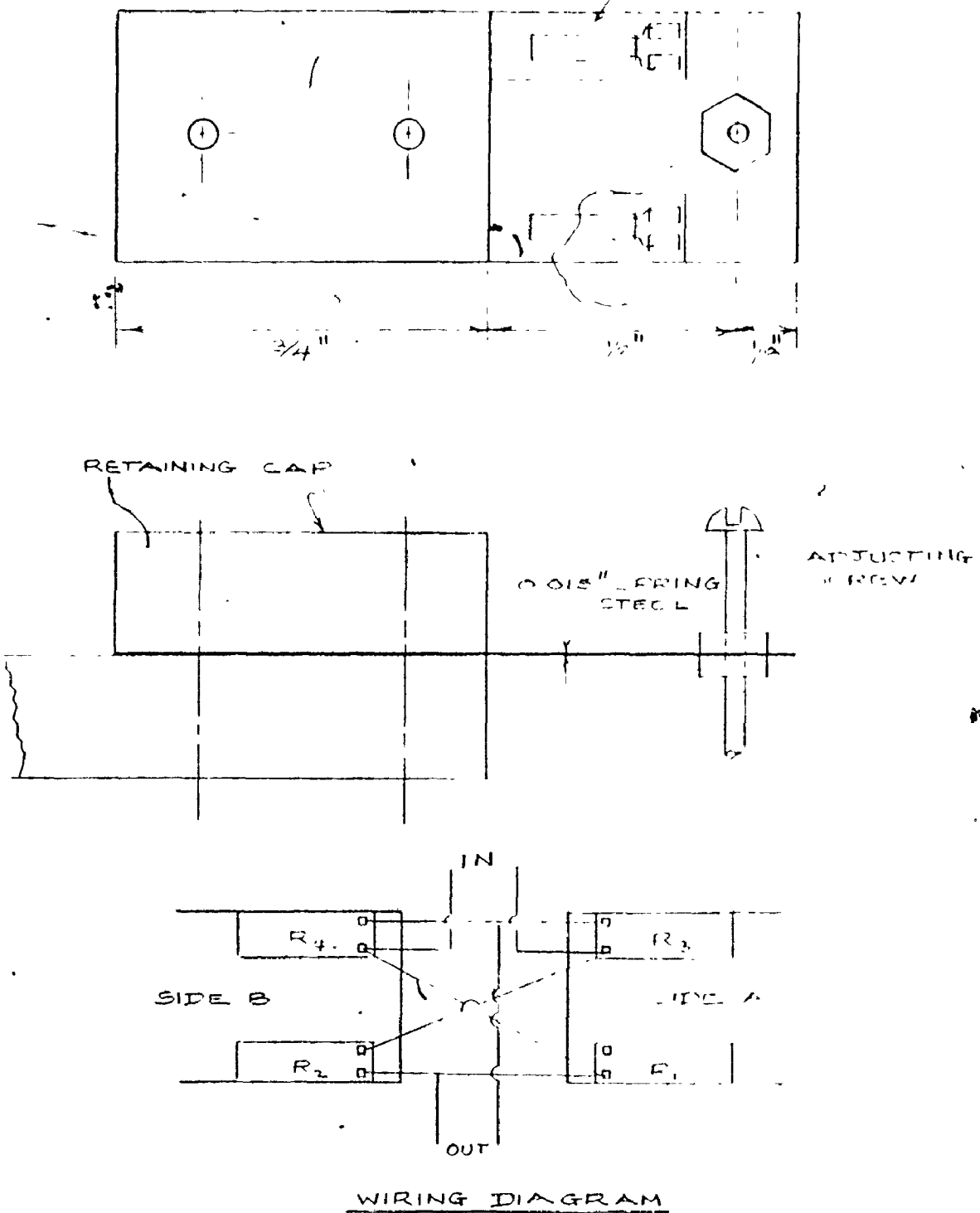


FIGURE B.1: TYPICAL STRAIN GAUGE CANTILEVER BEAM

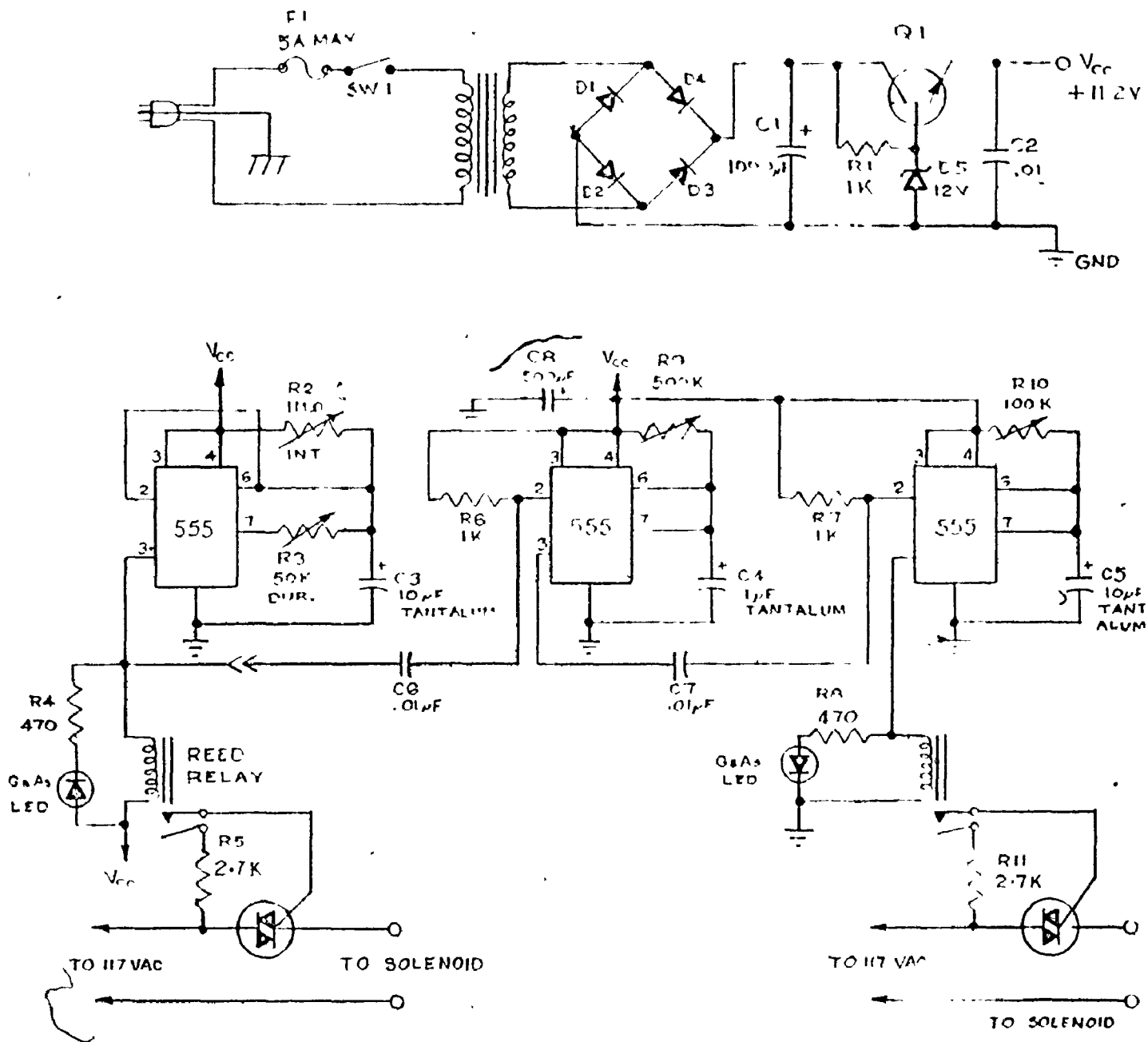


FIGURE B.2: CIRCUIT DIAGRAM FOR MAIN AND PHASE LAG TIMERS

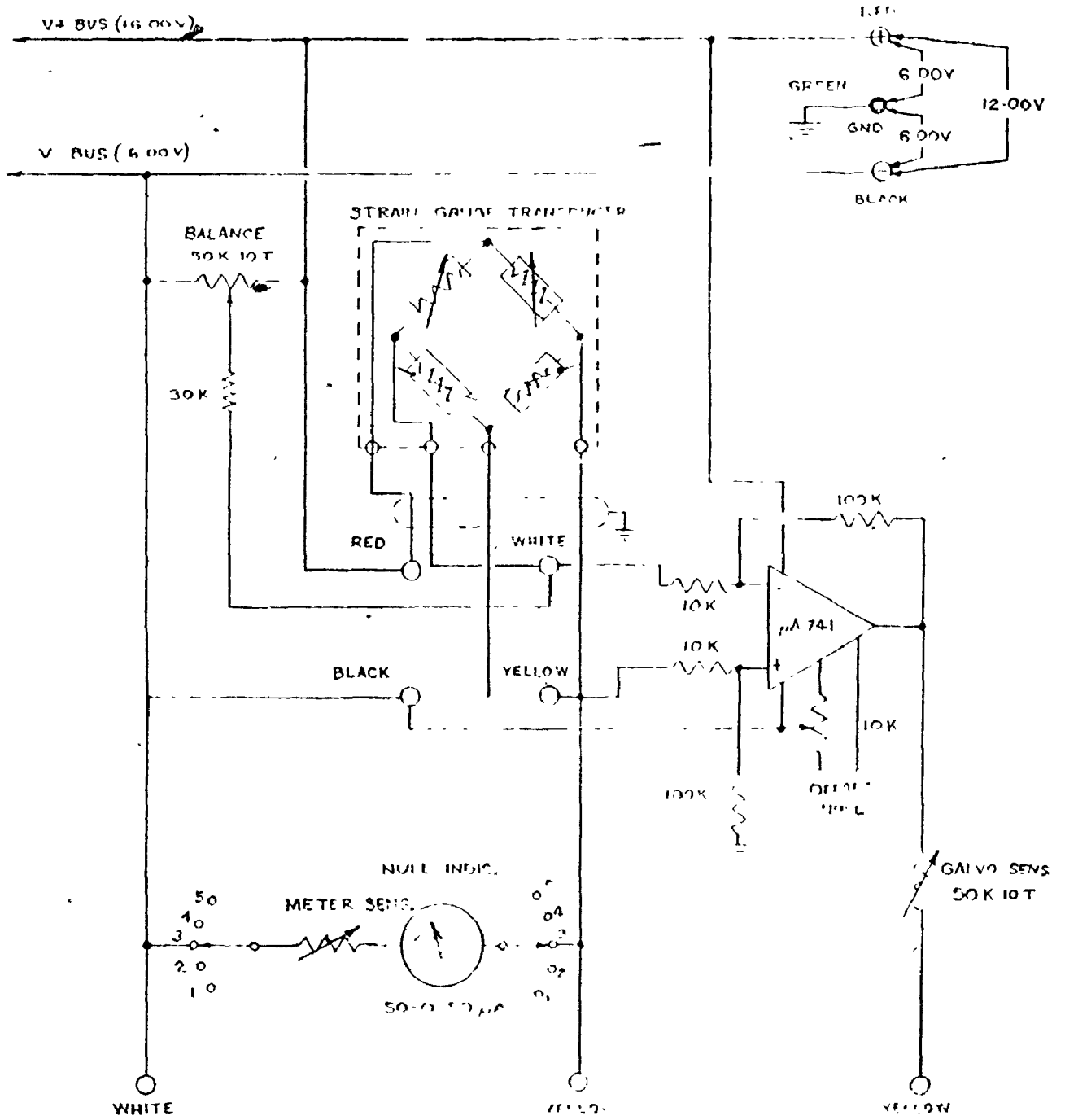


FIGURE B.3: DIAGRAM OF TYPICAL AMPLIFIER CIRCUIT FOR 5-CHANNEL AMPLIFIER

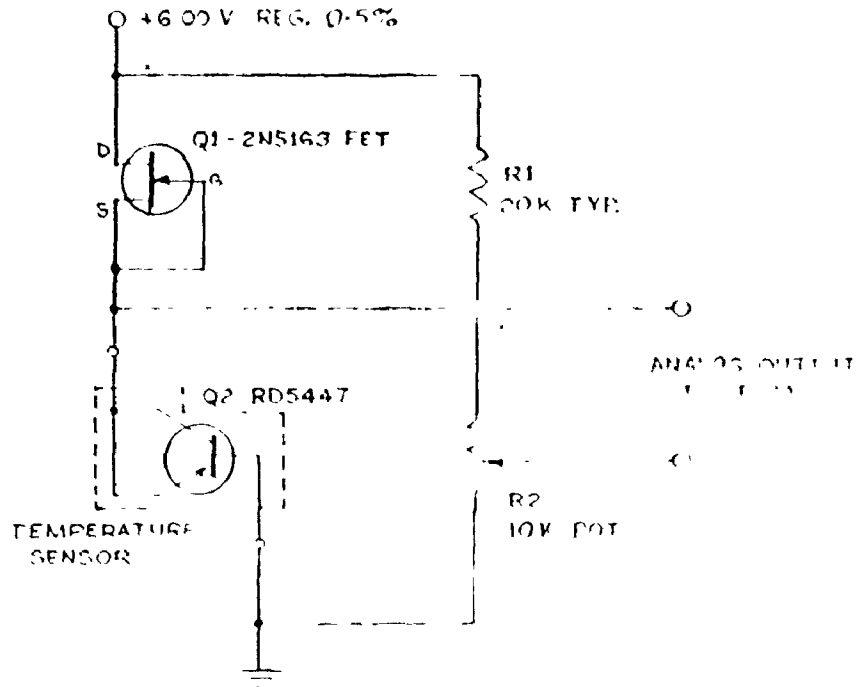


FIGURE B.4: CIRCUIT DIAGRAM FOR TEMPERATURE PROBE AMPLIFIER

APPENDIX C

TESTING PROGRAMME AND PHYSICAL CHARACTERISTICS
OF ASPHALTIC CONCRETE MIXES

GRADATION FOR MIXES (% Passing)

| Specimen No. Sieve Size (Tyler) | 100-101 | 102-103 | 104-105 | 33-35 | 69-71 | HM-3 Spec. |
|---------------------------------------|--------------------------|---------|---------|-------|-------|---------------|
| 3/8 | 100 | 100 | 100 | 100 | 100 | 100 |
| 4 | 84.3 | 84.3 | 84.3 | 85.4 | 88.2 | 75-100 |
| 8 | 65.3 | 65.3 | 65.3 | 60.2 | 56.7 | 50- 80 |
| 16 | 52.0 | 52.0 | 52.0 | 39.4 | -- | -- |
| 30 | 33.1 | 33.1 | 33.1 | 27.2 | -- | -- |
| 50 | 13.6 | 13.6 | 13.6 | 19.5 | 16.4 | 5- 20 |
| 100 | 5.3 | 5.3 | 5.3 | 13.3 | -- | -- |
| 200 | 2.9 | 2.9 | 2.9 | 5.5 | 4.5 | 0- 5 |
| Property of Mixture | Physical Characteristics | | | | | |
| Marshall Stability (lbs) | 2203 | 2106 | 1754 | 4403 | 2081 | 1200 min. |
| Flow Index (0.01") | 10.19 | 10.46 | 10.55 | 17 | 15.94 | 7 - 16 |
| VMA (% Vol) | -- | -- | -- | 17 | -- | 18 min. |
| Density (lb/cu ft) | 152.7 | 150.7 | 147.0 | 152.0 | 149.5 | -- |
| Voids (% Vol) | 1.8 | 2.4 | 3.4 | 2.5 | 1.4 | 2 - 4 |
| % AC | 5 | 6 | 7 | 6.3 | 7.9 | 5 - 10 |

TABLE C.1: GRADATION AND PHYSICAL PROPERTIES
OF HM-3 MIXES

GRADATION FOR MIXES (% Passing)

| Specimen No. Sieve Size (Tyler) | 200-201 | 202-203 | 204-205 | HM-3 Spec. |
|--|--------------------------|---------|---------|---------------|
| 3/8 | 100 | 100 | 100 | 100 |
| 4 | 80.7 | 80.7 | 80.7 | 75-100 |
| 8 | 65.8 | 65.0 | 65.0 | 50- 80 |
| 16 | 41.2 | 41.2 | 41.2 | -- |
| 30 | 25.4 | 25.4 | 25.4 | -- |
| 50 | 12.5 | 12.5 | 12.5 | 5- 20 |
| 100 | 8.5 | 8.5 | 8.5 | -- |
| 200 | 3.9 | 3.9 | 3.9 | 0- 5 |
| Property of Mixture | Physical Characteristics | | | |
| Marshall stability (lbs) | 4633 | 4040 | 2780 | 1200 min. |
| Flow Index ¹¹ (0.01 ¹¹) | 12.73 | 16.85 | 15.20 | 7- 16 |
| VMA (% Vol) | 21.7 | 21.6 | 22.9 | 18 min. |
| Density (lb/cu. ft.) | 193.8 | 196.6 | 195.6 | -- |
| Voids (% Vol) | 6.8 | 3.4 | 1.8 | 2- 4 |
| % AC | 5 | 6 | 7 | 5- 10 |

TABLE C.2: GRADATION AND PHYSICAL PROPERTIES
OF HM-3 (STEEL SLAG) MIXES

Gradation for Mixes (% Passing)

| Specimen No. Sieve Size (Tyler) | 300-301 | 302-303 | 304-305 | 306-307 | 308-309 | 27- 29 | Steel Slag Spec. |
|---------------------------------------|--------------------------|---------|---------|---------|---------|--------|------------------|
| 1/2 | 97.7 | 97.7 | 97.7 | 97.7 | 97.4 | 98.3 | 100 |
| 3/8 | 89.9 | 89.9 | 89.9 | 89.9 | 89.7 | 79.7 | 98-100 |
| 4 | 65.2 | 65.2 | 65.2 | 65.2 | 65.3 | -- | 75- 95 |
| 8 | 45.1 | 45.1 | 45.1 | 45.1 | 44.3 | 53.3 | 55- 80 |
| 16 | 30.8 | 30.8 | 30.8 | 30.8 | 31.1 | 32.2 | 35- 60 |
| 30 | 21.3 | 21.3 | 21.3 | 21.3 | 22.3 | 19.7 | 20- 45 |
| 50 | 16.3 | 16.3 | 16.3 | 16.3 | 15.6 | 11.6 | 10- 30 |
| 100 | 11.5 | 11.5 | 11.5 | 11.5 | 11.0 | 7.2 | 5- 15 |
| 200 | 6.2 | 6.2 | 6.2 | 6.2 | 7.0 | 4.9 | 0- 10 |
| Property of Mixture | Physical Characteristics | | | | | | |
| Marshall Stability (lbs) | 5360 | 4417 | 3430 | 2900 | | 4000 | 3500 min. |
| Flow Index (0.01") | 19.25 | 19.29 | 23.10 | 24.55 | | 22 | 8- 16 |
| VMA (% Vol) | -- | -- | -- | -- | | 20.9 | 20 min. |
| Density (lb/cu.ft.) | 189.2 | 189.7 | 187.7 | 184.7 | | 184 | -- |
| Voids (% Vol) | 3.1 | 2.4 | 1.6 | 1.2 | | 3.4 | 3- 5 |
| % AC | 5 | 5.5 | 6 | 6.5 | | 6.2 | 5- 7 |

TABLE C.3: GRADATION AND PHYSICAL PROPERTIES OF STEEL SLAG (OH-STELCO) MIXES

Gradation for Mixes (% Passing)

| Specimen No. Sieve Size (Tyler) | 4-6 | 15-17 | 18-20 | 45-47 | 51-53 | 400-401 | HM-5 Spec |
|---------------------------------------|--------------------------|-------|-------|-------|-------|---------|-----------|
| 1 | 100 | -- | -- | | -- | 100 | 100 |
| 3/4 | 92.6 | -- | -- | 99.4 | 98.8 | 97.4 | 90-100 |
| 5/8 | 81.3 | -- | -- | -- | -- | 92.0 | -- |
| 1/2 | 65.8 | -- | -- | -- | -- | 77.0 | -- |
| 3/8 | 58.3 | -- | -- | 64.9 | 72.3 | 62.9 | 60-80 |
| 4 | 51.5 | -- | -- | 51.3 | 53.4 | 50.4 | 35-65 |
| 8 | 44.9 | -- | -- | 39.8 | 37.0 | 45.6 | 20-50 |
| 16 | 37.2 | -- | -- | -- | 8.5 | 37.6 | -- |
| 30 | 26.1 | -- | -- | -- | -- | 23.9 | -- |
| 50 | 13.1 | -- | -- | 11.3 | -- | 9.8 | 3-20 |
| 100 | 7.7 | -- | -- | -- | -- | 3.8 | -- |
| 200 | 4.8 | -- | -- | 4.9 | 3.2 | 2.0 | 2- 8 |
| Property of Mixture | Physical Characteristics | | | | | | |
| Marshall Stability (lbs) | 2915 | 3513 | 4400 | 3600 | 3012 | 3082 | 1200 min. |
| Flow Index (0.01") | 16.24 | 14.5 | 15 | 18 | 13.1 | 13.3 | 8-16 |
| VMA (% Vol) | 14.6 | -- | 15 | 16 | 14.6 | 16.3 | 20 min. |
| Density (lb/cu.ft.) | 155.4 | 152.0 | 152.3 | 155 | 152 | 149.8 | -- |
| Voids (% Vol) | 2.2 | 1.6 | 2.8 | 1.3 | 3.4 | 4.4 | 3- 5 |
| % AC | 5.0 | 5.2 | 5.2 | 6.3 | 4.8 | 5.0 | 5- 7 |

TABLE C.4: GRADATION AND PHYSICAL PROPERTIES OF HM-5 MIXES

Gradation for Mixes (% Passing)

| Specimen No. Sieve Size (Tyler) | 10-12 | Type C Spec. |
|---------------------------------------|--------------------------|--------------------|
| 1/2 | | 100 |
| 3/8 | | 98-100 |
| 4 | | 75- 95 |
| 8 | | 55 - 80 |
| 16 | | 35- 60 |
| 30 | | 20- 45 |
| 50 | | 10- 30 |
| 100 | | 5- 15 |
| 200 | | 0- 10 |
| Property of Mixture | Physical Characteristics | |
| Marshall Stability (lbs) | 1685 | 500 min. |
| Flow Index (0.01") | 9.88 | 7-12 |
| VMA (% Vol) | -- | 18-25 |
| Density (lb/cu.ft) | 141.3 | -- |
| Voids (% Vol) | 6.2 | 2-8 |
| % AC | 6.6 | 6-10 |

TABLE C.5: PHYSICAL PROPERTIES OF
TYPE C MIX

| Mix Design | Specimen No. | Source | Asphalt Content (% by wt) | Tests Performed | | | | |
|------------------------|------------------|----------------|---------------------------|-----------------------|--------------------------|--------------------------|-----------------------|--------------------------|
| | | | | M_R | | | σ | |
| | | | | Temperature Variation | Diametral Load Variation | σ_{CON} Variation | Temperature Variation | σ_{CON} Variation |
| HM-3 | 100,101 | Lab | 5 | x | x | x | x | |
| | 102,103 | Lab | 6 | x | x | x | | |
| | 104,105 | Lab | 7 | x | x | x | | |
| | 33-35 | Field | 6.3 | x | | | | |
| | 69-71 | | 7.9 | x | | | | |
| HM-3 (steel slag) | 200,201 | Lab | 5 | x | | x | | |
| | 202,203 | Lab | 6 | x | | | | |
| | 204,205 | Lab | 7 | x | | | | |
| Steel Slag (OH-STELCO) | 300,301 | Lab | 5 | x | x | x | x | x |
| | 302,303 | Lab | 5.5 | x | x | x | | |
| | 304,305 | Lab | 6 | x | x | x | | |
| | 306,307 | Lab | 6.5 | x | x | x | | |
| | 308-309 27-29 | Field Field | 5.7 6.2 | x x | | | | |
| HM-5 | 4-6 | Field | 5.0 | x | | | | |
| | 15-17 | Field | 5.2 | x | | | | |
| | 18-20 | Field | 5.2 | x | | | | |
| | 45-47 | Field | 6.3 | x | | | | |
| | 51-53 | Field | 4.8 | x | | | | |
| | 400-401 | Lab | 5.0 | x | | | | |
| Type C | 10-12 | Field | 6.6 | x | | | | |

TABLE C.6: TESTING PROGRAMME FOR VARIOUS ASPHALT MIXES

SAMPLE THICKNESS, $t = 2.33$ in.

| Temp. (°C) | Vertical Ram Load | | Confining Pressure | | Strain Gauges | | Assumed Poisson's Ratio ν | Resilient Modulus M_R (ksi) |
|---------------|--------------------------------|----------------------------|--------------------------------|--------------------------------|-----------------------|-----------------------|--|-------------------------------------|
| | Galvo Deflection (divs.) | Converted Load (lbs) | Galvo Deflection (divs.) | Converted Pressure (psi) | δ_1 (divs.) | δ_2 (divs.) | | |
| 24.0 | 18.7 | 110.2 | 0 | 0 | 21.8 | 16.8 | 0.35 | 437 |
| | 18.9 | 111.4 | 0 | 0 | 23.3 | 17.5 | | 418 |
| | 18.5 | 109.0 | 0 | 0 | 22.4 | 16.6 | | 429 |
| | 18.0 | 106.1 | 2.4 | 0.99 | 19.5 | 15.0 | | 471 |
| | 18.4 | 108.4 | 2.4 | 0.99 | 19.1 | 15.2 | | 484 |
| | 18.4 | 108.4 | 2.4 | 0.99 | 19.8 | 15.0 | | 478 |
| | 18.0 | 106.1 | 3.5 | 1.45 | 18.7 | 14.6 | | 488 |
| | 18.0 | 106.1 | 3.5 | 1.45 | 18.8 | 14.5 | | 488 |
| | 18.0 | 106.1 | 3.5 | 1.45 | 18.7 | 14.7 | | 487 |

$$M_R = \frac{P \text{ (lbs)}}{t [(\delta_1)(C_1) + (\delta_2)(C_2)]} [0.99416\nu + 0.26417] \quad \text{where } C_1 = 1.69 \times 10^{-6} \text{ ins/div}$$

$$C_2 = 1.75 \times 10^{-6} \text{ ins/div}$$

TABLE C.7: TYPICAL CALCULATIONS FOR FINDING M_R

TEMPERATURE = 23.6°C

DIAMETER OF SPECIMEN, D = 4 in.

AVERAGE DISTANCE BETWEEN COLLARS A & B, x = 4.07 in.

| GALVANOMETER DEFLECTIONS (Divisions) | | | | | | Converted Deviator Load P (lbs) | Converted Confining Pressure σ_{CON} (psi) | Poisson's Ratio ν |
|--------------------------------------|---|-------------------|------------|--------------------|------------|--|--|-----------------------------|
| Deviator Load P | Confining Pressure σ_{CON} | Strain Gauges | | | | | | |
| | | Axial Deformation | | Radial Deformation | | | | |
| | | δ_1 | δ_2 | δ_3 | δ_4 | | | |
| 47.1 | 0 | 20.5 | 44.7 | 6.5 | 3.8 | 277.5 | 0 | 0.36 |
| 47.1 | 0 | 20.3 | 44.6 | 6.4 | 4.1 | 277.5 | 0 | 0.36 |
| 47.1 | 0 | 20.2 | 44.5 | 6.1 | 3.9 | 277.5 | 0 | 0.35 |
| 47.1 | 7.7 | 20.5 | 45.2 | 6.1 | 3.5 | 277.5 | 3.19 | 0.33 |
| 47.1 | 7.6 | 20.5 | 45.0 | 6.1 | 3.5 | 277.5 | 3.15 | 0.33 |
| 47.1 | 7.7 | 20.5 | 45.0 | 6.3 | 3.6 | 277.5 | 3.15 | 0.34 |

$$\nu = \left[\frac{(\delta_3)(C_3) + (\delta_4)(C_4)}{D} \right] \left[\frac{2x}{(\delta_1)(C_1) + (\delta_2)(C_2)} \right]$$

where $C_1 = 7.22 \times 10^{-6}$ ins/div
 $C_2 = 5.61 \times 10^{-6}$ ins/div
 $C_3 = 7.16 \times 10^{-6}$ ins/div
 $C_4 = 6.14 \times 10^{-6}$ ins/div

TABLE C.8: TYPICAL CALCULATIONS FOR
FINDING ν